Quantum Criticality at a Conductance Plateau Transition in a Quantum Wire

Quantenkritisches Verhalten am Plateau-Übergang im Quantendraht

Diploma Thesis

by

Matthias Sitte

Institute of Theoretical Physics, Department of Physics
Faculty of Mathematics and Natural Sciences
University of Cologne

June 2008

Abstract

In this thesis, we present a theoretical study of interacting spinless electrons in a two-band quantum wire. While the lower band is described as a Luttinger liquid with gapless density excitations, the upper band is modelled in terms of fermions at the bottom of the band. In addition to the usual density-density interaction between the two bands, we investigate the possibility of transferring of pairs of electrons from one subband to the other.

We perform a renormalization group analysis around the strong coupling fixed point, calculating the self-energy and vertex corrections. We then consider the renormalization of the theory with complementary renormalization conditions. As a main result, we find that the interactions between the two bands can lead to a modification of the dispersion relation.

Finally, we focus on the thermodynamical properties of the model. A calculation of the specific heat coefficient is presented in both the non-interacting and interacting system. It is shown that in the presence of interactions the activation of the second band, and the subsequent quantum phase transition, strongly influences the thermodynamics.

Contents

Chapter 1

Introduction

1.1 Motivation

Over the past decades, experiments have provided evidence that strong correlations and dimensionality are a central ingredient to the understanding of the physical properties in certain classes of materials. Among them are the heavy fermion compounds, the high-T_c superconductors, organic materials, semiconductor heterostructures, and quantum wires.

In three dimensions, strongly correlated electrons are a well studied problem. Their theoretical description by Fermi liquid theory is approximate but well understood. It is based on the phenomenological picture of quasi-particles which evolve out of the bare particles of a Fermi gas upon adiabatically switching on interactions between the bare particles. These quasi-particles are in one-to-one correspondence with the bare particles and carry the same quantum numbers. The electron-electron interaction then renormalizes the kinematic parameters of the quasi-particles such as the effective mass, and thermodynamic properties such as the specific heat. Moreover, the quasi-particles obtain a finite lifetime which diverges as the Fermi surface is approached.

However, the picture of quasi-particles breaks down in one dimesion due to the special topology of the Fermi surface which now is a set of two distinct Fermi points. The elementary excitations are rather bosonic collective charge and spin fluctutations dispersing with different velocities. An incoming electron decays into a charge and a spin excitation which then spatially separate in time. This spin-charge separation obviously violates the assumption of Fermi liquids that the quasi-particles carry the same quantum numbers as the bare particles such as momentum and spin. This makes it impossible to describe one-dimensional systems by Fermi liquid theory. Finally, the correlations between these excitations are anomalous and show up as interaction-dependent non-universal power laws whereas in normal metals these correlations are characterized by universal power laws.

1.2 Experimental Evidence for Luttinger Liquid Physics

In this section, we briefly list some systems which are good candidates for Luttinger liquid physics: quantum wires, carbon nanotubes, and fractional quantum Hall edge states. In all these cases, the electron motion is effectively one-dimensional. However, regarding Luttinger liquid physics, the interpretation of the experiments remains controversial.

1.2.1 Quantum Wires

Natural candidates for one-dimensional electron systems are quantum wires. These can be made, for example, by applying a gate voltage to a two-dimensional electron gas formed at the inversion layers of heterostructures, such as the interface of GaAs and AlGaAs. The gate voltage leads to discrete transverse modes, and the electron motion is effectively one-dimensional. However, it is hard to fabricate quantum wires which are sufficiently clean since backscattering from impurities destroys the collective modes [1].

Typical quantum wire experiments measure the dc conductance. However, note that in most of the cases, the conductance probes the physics of the Fermi-liquid leads rather than the Luttinger liquid behavior of the quantum wire.

1.2.2 Carbon Nanotubes

Carbon nanotubes are relatively new systems and their low-temperature behavior is predicted to be governed by Luttinger liquid theory.

A carbon nanotube is a graphene sheet rolled up in a cylindrical structure with a diameter of only a few nanometers and a length up to several micrometers. The remarkable electronic properties of carbon nanotubes emerge from the special band structure of graphite. The electron wavelength around the circumference of a nanotube is quantized due to periodic boundary conditions, leading to discrete wavelengths. Because of the quantization of circumferential modes, the electronic states split into one-dimensional bands which, for single-walled carbon nanotubes, are separated on the scale of 1 eV. In metallic carbon nanotubes only two subbands cross the Fermi energy so that they can be regarded as one-dimensional quantum wires even at room temperature [2].

1.2.3 Edge States in Fractional Quantum Hall Systems

Finally, the edge states in fractional quantum Hall systems are a good candidate for Luttinger liquid physics.

In the classical Hall effect, electrons moving in a magnetic field generate a potential difference V transverse to the current I. In the quantum Hall effect, the

transverse resistance V/I exhibits plateaus upon varying the magnetic field. These plateaus appear for particular filling factors ν at a resistance $\hbar/(\nu e^2)$. The filling factor ν takes integer values for the integer quantum Hall effect and fractional values for the fractional quantum Hall effect.

Edge states in the integer quantum Hall effect are described by one-dimensional chiral Fermi liquids [3]. The chirality can be understood semi-classically in terms of skipping Landau orbits at the boundaries, with opposite directions for opposite edges. Due to the spatial separation between left and right moving excitations, backscattering from impurities is supressed. In the case of fractional plateaus, Wen [4, 5] has conjectured that the edge states are Luttinger liquids. However, this prediction has not yet been confirmed unambigously.

1.3 Outline

In this thesis, we consider a model of spinless electrons in a quantum wire with two subbands of transverse quantization. Here, we study the quantum phase transition where the second subband becomes activated. It was shown by Meyer *et al.* [6] that this conductance plateau transition is preempted by the formation of an inter-band pairing state which, in the limit of infinitely strong density-density interaction between the two bands, is supposed to be of Ising type. We perform a perturbative analysis around this strong coupling limit using renormalization group methods. As a result, we show that the critical Ising mode induces superconducting fluctuations in the Luttinger liquid of the filled first band. This is reflected in a logarithmically strong attractive interaction and a reduction of the corresponding velocity. Finally, we discuss possible consequences like a fluctuation-induced first order transition preempting Ising criticality.

Chapter 2 presents a brief overview of Landau's theory of Fermi liquids and discusses its breakdown in one dimension. An extensive introduction of the Abelian bosonization technique and its applications to one-dimensional systems is also given.

Chapter 3 presents the Hamiltonian description of the model of interacting spinless electrons in a two-band quantum wire. In addition to the usual inter-band density-density interaction, the transfer of pairs of electrons between the two bands is discussed.

Chapter 4 presents the general ideas of renormalization group methods. In a perturbative approach to the strong coupling limit, the leading-order self-energy corrections as well as the vertex corrections are calculated. The renormalization of the theory and solutions of the resulting β functions are discussed.

Chapter 5 presents a brief survey of quantum phase transitions and quantum critical points. Regarding our model, the specific heat coefficient is calculated, and the results are compared with predicitions from scaling theory.

Chapter 2

Interacting Fermions in One Dimension

Many elementary textbooks on condensed matter physics begin with a discussion of the non-interacting electron gas, explaining the characteristics of conduction electrons in metals. Although some oversimplified assumptions are made such as neglecting interactions between electrons or the effect of ions in a solid, this picture of free electrons explains many important phenomena like the conductivity of metals. Moreover, the theory of free electrons is but the simplest of all theories in condensed matter physics.

However, the naive picture of the non-interacting Fermi gas is far from being complete. The most successful attempt to establish a more realistic theory was introduced by Landau in a series of articles [7, 8, 9] aimed at explaining the properties of liquid ^{3}He. This theory, which is commonly referred to as *Fermi liquid theory*, is motivated by phenomenology and is based on the assumption that characteristic particle excitations of the real system carry the same quantum numbers as the particles in the non-interacting Fermi gas. This *a priori* assumption has proven well in a large number of systems, and Fermi liquid theory has thus been one of the most influencing theories in condensed matter physics.

In this chapter, we present the central ideas of Landau's theory of Fermi liquids in Sec. 2.1, and the breakdown of Fermi liquid theory in one dimension in Sec. 2.2. Readers familiar with Fermi liquid theory may safely skip this section since they will not need it for the rest of the thesis. On the other hand, in one-dimensional systems, the low-energy properties are generically described by Luttinger liquid theory in terms of bosonic excitations. This theory, based on the Tomonaga-Luttinger model, and the bosonization technique are summarized in Sec. 2.3. Finally, in Sec. 2.4, we discuss a few models whose low-energy physics can be described by the Tomonaga-Luttinger model.

2.1 Fermi Liquid Theory

Fermi liquid theory begins with the observation that macroscopic properties of real systems often involve only excitations of the system on energy scales that are small compared to the Fermi energy. The state of the system can thus be described in terms of its ground state and its low-lying elementary excitations, the so-called *quasi-particles*. A normal Fermi liquid is defined as a system in which the non-interacting ground state (the Fermi gas) evolves continuously, that means without any symmetry-breaking process, into the interacting ground state, and there is a one-to-one correspondence between the bare particles of the original system and the quasi-particles of the interacting system. Note that the principle of adiabatic continuity is an *a priori* hypothesis which has to be verified at the end of the day.

The theory of Fermi liquids essentially describes the physics of quasi-particles. A quasi-particle with momentum $|\mathbf{k}| > k_F$ is defined as the difference between an interacting system with an added fermion with momentum $\mathbf{k}$ and a system without such an addition, and similarly a quasi-hole is obtained by starting with hole state. When a particle is added to an interacting system, its propagation is distorted by the self-energy cloud which arises from interactions between the particle and its surrounding neighbors. A quasi-particle, that is a bare particle and its self-energy cloud, is an independent entity and constitutes an elementary excitation of the interacting system. Since the quasi-particles evolve from the non-interacting Fermi gas, they carry the same quantum numbers but their dynamical properties are renormalized by interactions.

With the help of the one-to-one correspondence between the bare particles and the quasi-particles we can describe the physics of the quasi-particles by mapping it onto the physics of the bare ones. To this end, let us consider an eigenstate of the interacting system, characterized by its momentum distribution function $n^0_{\mathbf{k}}$. Excitations of the system are measured by the deviation in the momentum distribution $n_{\mathbf{k}}$ function from the ground state:

$$\delta n_{\mathbf{k}} = n_{\mathbf{k}} - n^0_{\mathbf{k}} \tag{2.1}$$

At low temperatures only low-lying states in the vicinity of the Fermi surface are excited. Under such conditions, the quasi-particle damping is usually negligible.

In a non-interacting system, the relation between the energy of a given state and the corresponding distribution function is simply a linear relation,

$$E_0 = \sum_{\mathbf{k}} n^0_{\mathbf{k}} \epsilon_{\mathbf{k}} \tag{2.2}$$

with $\epsilon_{\mathbf{k}}$ the single-particle energy. Upon switching on interactions, the relation between the state energy, E, and the quasi-particle distribution function, $n_{\mathbf{k}}$, becomes much more complicated and in general cannot be specified explicitly. If, however,

$n_{\mathbf{k}}$ is sufficiently close to the ground state distribution function $n^0_{\mathbf{k}}$, i.e. for small $\alpha = N^{-1}\sum_{\mathbf{k}}|\delta n_{\mathbf{k}}|$, we can carry out a Taylor expansion of the free energy:

$$F = F_0 + \sum_{\mathbf{k}} \delta n_{\mathbf{k}} \xi_{\mathbf{k}} + \frac{1}{2}\sum_{\mathbf{k},\mathbf{k}'} \delta n_{\mathbf{k}} \delta n_{\mathbf{k}'} f(\mathbf{k},\mathbf{k}') + \mathcal{O}(\delta n^3) \tag{2.3}$$

where $\xi_{\mathbf{k}} = \epsilon_{\mathbf{k}} - \mu$ is the energy relative to the chemical potential. Eq. (2.3) is the core of the phenomenological theory of Fermi liquids. The most important feature is the quadratic term describing interactions between quasi-particles. The coefficient $f(\mathbf{k},\mathbf{k}')$ is the interaction energy between quasi-particles of momentum $\mathbf{k}$ and $\mathbf{k}'$.

Let us now consider a state of the system with a certain distribution of excited quasi-particles $\delta n_{\mathbf{k}'}$. Adding an extra quasi-particle with momentum $\mathbf{k}$, its free energy is equal to

$$\tilde{\xi}_{\mathbf{k}} = \xi_{\mathbf{k}} + \sum_{\mathbf{k}'} \delta n_{\mathbf{k}'} f(\mathbf{k},\mathbf{k}') \tag{2.4}$$

If the momentum $\mathbf{k}$ is close enough to the Fermi surface, both terms have the same order of magnitude. The free energy of a quasi-particle thus depends on the state of the system through its interaction energy with other excited quasi-particles. This inter-dependence arises from the quadratic interaction term in Eq. (2.3) and leads to a modification of the quasi-particle's transport properties.

So far, the core features of Fermi liquid theory have been presented only at zero temperature. Of course these ideas can be generalized to finite temperatures. Applying Landau's theory of Fermi liquids to a number of macroscopic properties such as specific heat, compressibility, sound wave velocity, spin susceptibility, and so on, one can characterize a system at equilibrium. For more details on thermodynamical properties see e.g. [10, 11, 12].

Finally, let us consider the application of Fermi liquid theory to electrons in metals. In a system of non-interacting electrons which move in a periodic potential of a crystalline solid the single-particle eigenstates are Bloch waves. These eigenstates are characterized by two quantum numbers, a band index n and a wave vector $\mathbf{k}$, the latter lying in the first Brillouin zone of the crystal. The ground state of an N-electron system is obtained by filling up the N lowest Bloch states. The Fermi surface which lies in the first Brillouin zone inherits the symmetry of the lattice and will in general be anisotropic. By using the principle of adiabatic continuity we can establish a one-to-one correspondence between the eigenstates of the real system and those of the non-interacting system. In the same manner, we can define quasi-particles by adding one particle with quantum numbers $(n,\mathbf{k})$ to the non-interacting system and then switch on interactions adiabatically. Due to momentum conservation the resulting quasi-particle will have the same quantum numbers as the original Bloch wave, namely a band index and a momentum $\mathbf{k}$ in the first Brillouin zone. The quasi-particle thus has the same characteristics as a Bloch wave, and one

can define a Fermi surface for the interacting system. Because of the quasi-particle damping due to particle interactions, the concept of quasi-particles is valid only in the vicinity of the Fermi surface. This is a major difference from the non-interacting system where Bloch waves are defined over the entire first Brilouin zone. However, for most practical purposes this restriction is unimportant because $T_F \gg T$. The fraction of excited quasi-particles always remains very small, so that we can neglect quasi-particle damping.

In the abscence of interactions, a Bloch wave has an energy $\epsilon_{n\mathbf{k}}$ and a velocity equal to $v_{\mathbf{k}} = \nabla_{\mathbf{k}}\epsilon_{n\mathbf{k}}$. Let us now switch on interactions. In the interacting system, the quasi-particles have an energy $\epsilon_{n\mathbf{k}}$ equal to the first derivative of the energy functional. We can define a quasi-particle velocity in the same way as before. However, due to the influence of the periodic lattice and the Coulomb interaction between electrons the velocity is renormalized compared to the bare single-particle velocity. In the case of a nearly isotropic Fermi surface we can write

$$|\mathbf{v}_{\mathbf{k}_F}| = \frac{\hbar|\mathbf{k}_F|}{m^*} \tag{2.5}$$

where the *effective mass* m^* contains the combined influence of the periodic lattice field and electron interactions. However, since the Fermi surface of a metal is in general not isotropic, the interaction between quasi-particles, $f(\mathbf{k}, \mathbf{k}')$, depends on the direction of both $\mathbf{k}$ and $\mathbf{k}'$. Having the anisotropy of the Fermi surface in mind, it is obvious that a comparison between theory and experiment is not easy and can be fruitful only in the case of nearly isotropic Fermi surfaces. Another complication arises from the long-range character of Coulomb interaction between electrons. Here we note that the above considerations work quite well provided one regards $f(\mathbf{k}, \mathbf{k}')$ as the screened quasi-particle interaction. Finally, not only do the electrons interact with each other, they interact as well with the lattice vibrations (phonons) of the crystal. One must therefore consider to what extent the phenomena are influenced by this further electron interaction.

To conclude, note that Landau's theory of Fermi liquids has been described to great extent in many articles and condensed matter textbooks. For some review of Fermi liquid theory and related subjects see e.g. [10, 11, 12].

2.2 Breakdown of Fermi Liquid Theory in One Dimension

The principle of adiabatic continuity is an *a priori* hypothesis in Fermi liquid theory which requires some verification. Although it works for repulsive interactions in three dimensions, it fails for attractive interactions where a phase transition to superconductivity takes place. Moreover, it cannot be justified for repulsive interactions in one dimension, the case of interest in this thesis. Here, we briefly discuss

the breakdown of Fermi liquid theory in one dimension. The first discussion is rather handwaving, while the second one computes perturbative corrections in the electron-hole susceptibility.

It is very easy to see that in one dimension interactions between electrons have drastic effects compared to higher dimensions. In high dimension, the quasi-particles are nearly free whereas the individual electrons themselves are strongly coupled. On the other hand, in one dimension, an electron that tries to propagate has to "push" its neighbors aside because of electron-electron interactions. Hence, no individual motion is possible, and any individual excitation has to become a collective one. This is obviously a major difference between one and higher dimensions and clearly makes it impossible to have a Fermi liquid theory work in one dimension. The situation gets even more complicated for fermions with spin. Because only collective excitations can exist, it implies that a single fermionic excitation has to split into a collective charge excitation and a collective spin excitation. These excitations have in general different velocities, so the electron "breaks up" into two elementary excitations. This interaction effect, known as *spin-charge separation*, is a hallmark of interacting electrons in one dimension. To conclude, even on a qualitative level the physical properties of the one-dimensional electron gas must be very different from those of the free electron gas in higher dimensions.

On a more formal level, if one would attempt to treat the electron-electron interaction perturbatively some correlation functions such as the density-density correlation function would appear in the perturbation theory. In linear response theory, such correlations measure the response of the electron gas to an applied external potential:

$$\mathcal{H}_{\text{ext}} = \int d^d x \int dt\, V(x,t)\rho(x,t) \tag{2.6}$$

The susceptibility that measures the response is given by (see e.g. [12])

$$\chi(\mathbf{q},\omega) = \frac{1}{V}\sum_{\mathbf{k}} \frac{n_F(\xi_{\mathbf{k}}) - n_F(\xi_{\mathbf{k}+\mathbf{q}})}{\omega + \xi_{\mathbf{k}} - \xi_{\mathbf{k}+\mathbf{q}} + i0^+} \tag{2.7}$$

where V is the volume of the system and n_F the Fermi occupation factor. Let us focus on the static susceptibility $\chi(\mathbf{q}, \omega = 0)$. Normally, the static susceptibility is well-behaved and goes to a constant in the dc-limit, $\omega \to 0$. One recovers then that $\chi(\mathbf{q} \to \mathbf{0}, \omega = 0)$ is proportional to the density of states at the Fermi level, $\nu_0 = \nu(\xi = 0)$. Usually, the compressibility is defined with a potential $V(x,t) = -\mu$, so with the above conventions χ is negative. For finite $\mathbf{q}$ its behavior is controlled by the momentum dependence of $\xi_{\mathbf{k}}$. When $\mathbf{k}$ is on the Fermi surface one has $\xi_{\mathbf{k}} = 0$, and if one can find a wavevector $\mathbf{Q}$ sucht that both $\xi_{\mathbf{k}}$ and $\xi_{\mathbf{k}+\mathbf{Q}}$ are zero, one gets a singularity in the susceptibility. In high dimensions, this occurs in general only for a very few points. Moreover, because of the integration over $\mathbf{k}$ the singularity is smoothed out by the integration measure which is equal to $d^d k \sim k^{d-1}\, dk\, d\Omega$. The

only way to have a stronger singularity is to have a nesting property for the Fermi surface, that is, to find a wavevector $\mathbf{Q}$ such that for a finite domain of momenta $\mathbf{k}$ the energy satisfies the relation $\xi_{\mathbf{k}} = -\xi_{\mathbf{k}+\mathbf{Q}}$. In this domain, the real part of the particle-hole susceptibility (2.7) becomes

$$\mathrm{Re}\,\chi(\mathbf{Q}, \omega = 0) = -\frac{1}{V}\sum_{\mathbf{k}} \frac{\tanh(\beta\xi_{\mathbf{k}}/2)}{2\xi_{\mathbf{k}}} \tag{2.8}$$

where $\beta = 1/(k_B T)$ is the inverse of the temperature. Assuming that the density of states is approximately a constant close to the Fermi level, the real part of the susceptibility χ is dominated by a logarithmic divergence. But in high dimension it is in general impossible to satisfy this nesting property, except on isolated points. Thus, the susceptibility χ itself cannot diverge, but its derivatives are in general singular.

However, in one dimension the nesting property is always satisfied. Close to the Fermi points, one can linearize the dispersion relation to obtain

$$\begin{aligned} \xi_k &\simeq v_F(k - k_F) \qquad \text{for } k \approx k_F \\ \xi_k &\simeq v_F(-k - k_F) \qquad \text{for } k \approx -k_F \end{aligned} \tag{2.9}$$

It is thus easy to see that

$$\xi_{k+Q} = -\xi_k \quad \text{for } Q = 2k_F \tag{2.10}$$

In one dimension, there is perfect nesting, regardless of the precise form of the dispersion relation. Since the susceptibility diverges at the nesting vector $Q = 2k_F$, one can expect that any perturbation in the theory will be divergent at this wavevector. This usually indicates that the ground state of the interacting system is quite different from the one started from, i.e. the non-interacting ground state. No matter how weak the interactions are, they cannot be treated in perturbation theory. Moreover, the properties of one-dimensional interacting fermions are fundamentally different from the free electron ones. A theoretical description of interacting electrons in one dimension has thus to be completely different from Landau's theory of Fermi liquids.

2.3 The Tomonaga-Luttinger Model

In the previous section, we have seen that Fermi liquids in one dimension are very special in that there are no fermionic quasi-particles, and their elementary excitations are rather bosonic collective charge and spin fluctuations with different velocities. An electron decays into such charge and spin excitations which then separate with time.

The reason for this peculiar properties is the topology of the Fermi surface which produces both singular particle-hole response and severe conservation laws. In a one-dimensional system, the Fermi surface is simply a set of points $\pm k_F$, and one has perfect nesting with a wavevector $Q = 2k_F$. This produces a singular particle-hole response at $2k_F$ in the particle-hole susceptibility leading to the breakdown of Fermi liquid theory in one dimension. On the other hand, the disjoint Fermi surface gives a well-defined dispersion to the low-energy particle-hole excitations, and these excitations can be taken as building blocks upon which a description of the low-energy physics in one dimension is constructed.

The aforementioned properties are generic for any one-dimensional system but particularly prominent in a one-dimensional model of interacting fermions proposed by Luttinger [13] and Tomonaga [14] and solved exactly by Mattis and Lieb [15]. The notion of a *Luttinger liquid* was coined by Haldane [16] to describe the universal low-energy properties of gapless one-dimensional quantum systems, and to emphasize that an asymptotic description, that means in the low-energy limit $q \to 0$ and $\omega \to 0$, can be based on the Luttinger model in the same way as the Fermi liquid theory in higher dimension is based on the free Fermi gas.

Let us now start with a formal derivation of a way to describe the low-energy properties of one-dimensional systems. The method we present here is known as *Abelian bosonization* and is a very useful tools in one dimension. We introduce this method in a two-step way: First, we present a model on which this method is essentially exact and which allows us to derive exact formulas that can be used for other models as well. Later, we present a physical interpretation of the bosonization formulas that allows to make contact to other systems and to show the universality of the model.

Of course, the technique of Abelian bosonization has been subject of many reviews and textbooks. For some reviews of interacting fermions in one dimension see e.g. [17, 18, 19].

2.3.1 Particle-Hole Excitations and Their Spectrum

Before turning to the mathematical formulation of the model, let us consider an outstanding property of one-dimensional systems first. An important component of the excitations of the electron gas are particle-hole excitations where an electron is taken from below the Fermi level and promoted above. Since one annihilates a particle with momentum k and creates another one with momentum $k + q$, the momentum of the excitation is well fixed and equal to q. In contrast, the energy of such an excitation depends in general on both k and q. Looking at the energy of the particle-hole excitations as function of q, one finds in general a continuum of energies. In high dimensions, for $q < 2k_F$ one can create particle-hole pairs with arbitrary

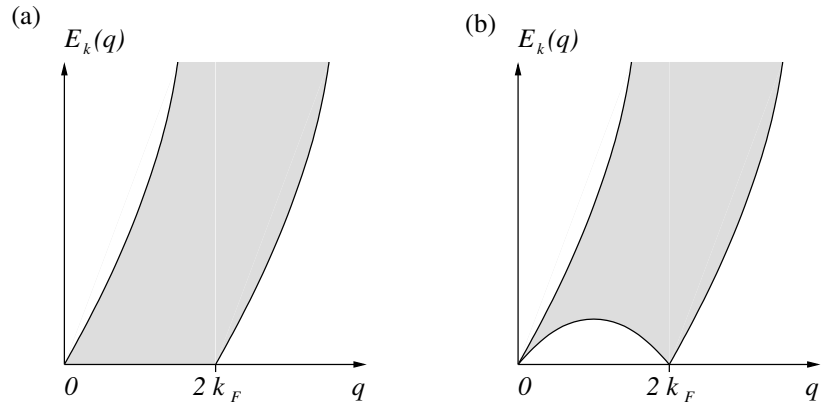

Figure 2.1: (a) Particle-hole spectrum for two- and three-dimensional systems. (b) Particle-hole spectrum for one-dimensional systems. (Figure taken from [17].)

low energy by destroying a particle just below the Fermi surface at one point and creating a particle just above the Fermi surface at another point. The particle-hole spectrum is thus a continuum extending to zero for all momentum vectors q smaller than $2k_F$, as shown in Fig. 2.1 (a). However, in one dimension, the Fermi surface is reduced to two points, and the only way to get a low-energy excitation is to destroy and create pairs of particles close to the Fermi surface. The only places where the particle-hole energy can be zero are for $q = 0$ and $q = 2k_F$. The resulting particle-hole spectrum is shown in Fig. 2.1 (b). In one dimension, contrary to higher dimensions, the particle-hole excitations thus have both a well-defined momentum and energy.

Let us focus on the particle-hole excitations with momentum $q = 0$ for the moment. At small q the energy of a particle-hole excitation is given by

$$E_k(q) = \xi_{k+q} - \xi_k \tag{2.11}$$

where ξ_k and ξ_{k+q} is the energy of an occupied (unoccupied) state relative to the chemical potential, respectively. If we consider the standard quadratic dispersion

$$\xi_k = \frac{k^2}{2m} - \mu \quad \text{with} \quad \mu = \frac{k_F^2}{2m} \tag{2.12}$$

with $k \in [k_F - q, k_F]$, the average value $E(q)$ of $E_k(q)$ and the dispersion $\delta E(q)$ are given by

$$E(q) = \frac{k_F q}{m} = v_F q \tag{2.13}$$

$$\delta E(q) = \frac{q^2}{m} = \frac{E(q)^2}{m v_F^2} \tag{2.14}$$

One obtains the same results when expanding the energy ξ around k_F to second order. Regardless of the precise form of the dispersion relation ξ_k, these results

show that the average energy $E(q)$ of a particle-hole excitation depends only on its momentum q and that the dispersion in energy $\delta E(q) \sim E(q)^2$ vanishes much faster than the average energy $E(q)$, provided ξ_k has a finite slope at the Fermi level. This means that in one dimension the particle-hole excitations are well-defined, i.e. they are particles with well-defined momentum and energy whose lifetime becomes longer and longer when the energy goes to zero. This is the same situation as for the quasi-particles in a Fermi liquid. Because these excitations are made of fermionic annihilation and creation operators they are of bosonic nature. These bosonic quasi-particles are the key ingredient to solving one-dimensional interacting fermions.

2.3.2 Representation of Excitations in the Spinless Model

Let us start with spinless fermions. As mentioned above, the particle-hole excitations of the system have a nearly linear spectrum, with a well-defined momentum and energy. In order to make this relation perfect we replace the original model by a model with a purely linear spectrum which is called the *Tomonaga-Luttinger model*, as shown in Fig. 2.2. To get a total independence of the energy of the particle-hole excitation $E_k(q)$ on the initial momentum k for all values of q it is necessary to extend the energy spectrum down to $-\infty$. This forces us to introduce two new species of fermions, namely left and right-moving fermions. The Hamiltonian of such a one-dimensional system reads

$$\mathcal{H} = \sum_{r=R,L} \sum_{k} v_F(rk - k_F) c^\dagger_{rk} c_{rk} \tag{2.15}$$

where $r = +1$ for right-moving fermions and $r = -1$ for left-moving fermions. Eq. (2.15) is the one-dimensional equivalent of a Dirac Hamiltonian. Similarly, the Fermi sea where all states below the chemical potential, i.e. all states with momentum k and energy $\xi_k < 0$, are filled is replaced by a Dirac sea where the infinite number of states with negative energy $\xi_{rk} < 0$ are filled.

The energy of particle-hole excitations of this model is now given by

$$E_{rk}(q) = \xi_{r,k+q} - \xi_{rk} = v_F(r(k+q) - k_F) - v_F(rk - k_F) = v_F rq \tag{2.16}$$

and is totally independent on k. The particle-hole excitations are thus well-defined excitations with well-defined momentum q and energy $E_r(q) = v_F rq$. This leads to the particle-hole spectrum as shown Fig. 2.3 (b).

Let us rewrite the Tomonaga-Luttinger liquid in terms of the particle-hole excitations. Because we have introduced an infinite number of occupied states in Eq. (2.15), we have to be careful in defining operators such as the density operator, particle number operator, and so on, to avoid infinite quantities which are ill-defined. For that purpose we define the *normal ordering* of a product of operators $: AB \cdots :$ with respect to a specific vacuum $|0\rangle$. In a normal ordered product, the annihilation

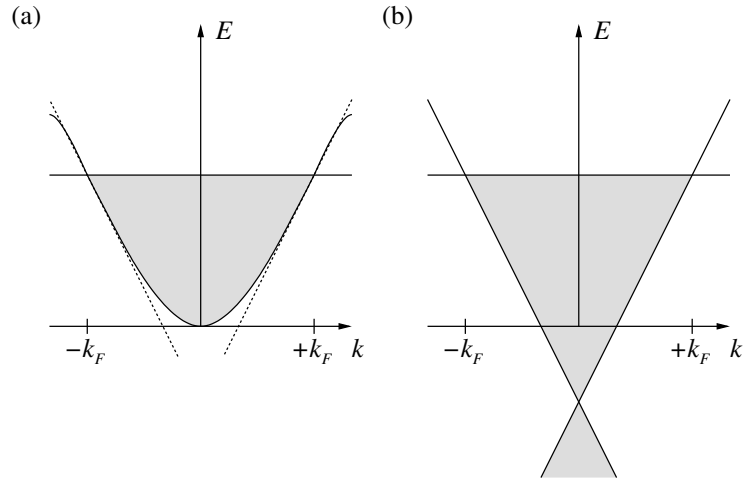

Figure 2.2: (a) The original model with band curvature. (b) A model of fermions with a linear spectrum which is now extended to all values of k, leading to an infinite number of negative energy states. (Figure taken from [17].)

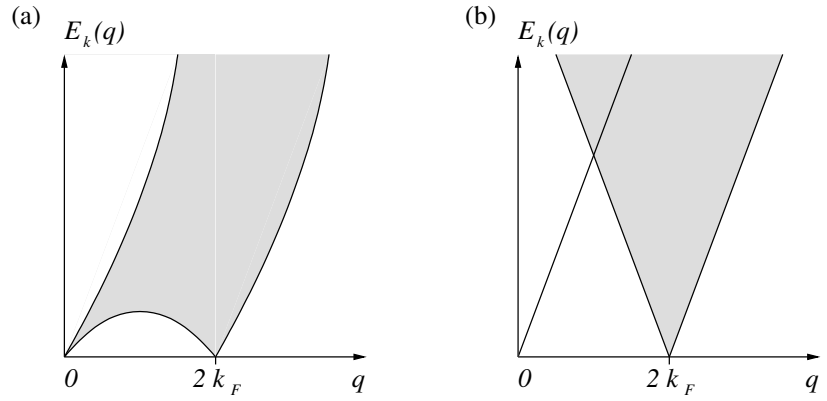

Figure 2.3: Particle-hole spectrum (a) for one-dimensional systems and (b) for the Tomonaga-Luttinger model (2.15). (Figure taken from [17].)

operators with respect to a given vacuum state are put on the right and the creation operators on the left. For two operators A and B which are linear combinations of annihilation and creation operators, normal ordering the product of operators is equivalent to subtracting the average value in the vacuum:

$$: AB := AB - \langle 0|AB|0\rangle \tag{2.17}$$

This normal ordering recipe is all we need to know. The normal ordered density is thus defined as

$$: \rho_r(x) :=: \psi_r^\dagger(x)\psi_r(x) : \tag{2.18}$$

where we introduced the notation $\psi_r(x)$ and $\psi_r^\dagger(x)$ for annihilating and creating a right-moving ($r = R$) or left-moving ($r = L$) fermion at point x, respectively. The

Fourier component $\rho_r(p)$ of the density is defined by

$$: \rho_r(x) := \frac{1}{L} \sum_p : \rho_r(p) : e^{ipx} \tag{2.19}$$

This is leads to ($p \neq 0$)

$$: \rho_r(p) := \sum_k c^\dagger_{r,k-p} c_{rk} \tag{2.20}$$

while for $p = 0$

$$N_r =: \rho_r(p=0) := \sum_k \left(c^\dagger_{rk} c_{rk} - \langle 0 | c^\dagger_{rk} c_{rk} | 0 \rangle \right) \tag{2.21}$$

defines the particle number operator N_r for each species. As usual $\rho^\dagger(p) = \rho(-p)$ since the electron density $\rho(x)$ is a real quantity. The subtraction of the average value for $p = 0$ ensures that the matrix elements of the density operator are finite. It is straightforward to calculate the commutator of the density operators. However, because of the infinite number of occupied states the bare density operators contain infinity and one has to take care when changing variables within the commutator. For periodic boundary conditions, this leads to (see e.g. [17])

$$[\rho_r(p), \rho^\dagger_{r'}(p')] = \delta_{rr'} \delta_{pp'} \frac{rpL}{2\pi} \tag{2.22}$$

Eq. (2.22) shows that because of the infinite number of occupied states the density operators have commutation relations similar to those of bosonic operators. One thus recovers that density fluctuations behave as bosonic annihilation and creation operators. Note that for the Tomonaga-Luttinger model (2.15) this is an exact result. Since

$$\begin{aligned} \rho_L(p<0)|0\rangle &= 0 \\ \rho_R(p>0)|0\rangle &= 0 \end{aligned} \tag{2.23}$$

these density operators can be identified with the destruction operators for bosons. We thus define bosonic creation and annihilation operators as ($p \neq 0$)

$$b^\dagger_p = \left(\frac{2\pi}{L|p|} \right)^{1/2} \sum_r \Theta(rp) \rho^\dagger_r(p) \tag{2.24}$$

$$b_p = \left(\frac{2\pi}{L|p|} \right)^{1/2} \sum_r \Theta(rp) \rho_r(p) \tag{2.25}$$

where $\Theta(x)$ is the Heaviside step function.

Let us now use these bosonic operators to express fermionic operators in the new basis, especially the Hamiltonian (2.15). Using the commutation rules of the boson operators, and assuming that the basis generated by the bosonic operators $b_p, b^\dagger_p$ is complete, it is easy to check from the commutation relations that the Hamiltonian that would satisfy the same commutation rules is given by

$$\mathcal{H} = \sum_{p \neq 0} v_F |p| b^\dagger_p b_p + \frac{\pi v_F}{L} \sum_r N_r^2 \tag{2.26}$$

Eq. (2.26) shows that the kinetic energy which is normally quadratic in fermionic operators can also be rewritten in a quartic term of fermionic operators. This result is crucial because it shows that the interaction between fermions which is usually quartic in fermion operators can be easily incorporated into the model, keeping the bosonic Hamiltonian quadratic and thus solvable in a simple way.

Rather than working in terms of the bosonic operators $b_p, b_p^\dagger$ it is usually more convenient to introduce two new fields $\phi(x)$ and $\theta(x)$ which are defined by

$$\phi(x) = -(N_R + N_L)\frac{\pi x}{L} - \frac{i\pi}{L}\sum_{p\neq 0}\frac{1}{p}\, e^{-\alpha|p|/2 - ipx}(\rho_R^\dagger(p) + \rho_L^\dagger(p)) \tag{2.27}$$

$$\theta(x) = (N_R - N_L)\frac{\pi x}{L} + \frac{i\pi}{L}\sum_{p\neq 0}\frac{1}{p}\, e^{-\alpha|p|/2 - ipx}(\rho_R^\dagger(p) - \rho_L^\dagger(p)) \tag{2.28}$$

Using Eqs. (2.24) and (2.25) we can rewrite these fields:

$$\phi(x) = -(N_R + N_L)\frac{\pi x}{L} - \frac{i\pi}{L}\sum_{p\neq 0}\left(\frac{L|p|}{2\pi}\right)^{1/2}\frac{1}{p}\, e^{-\alpha|p|/2 - ipx}(b_p^\dagger + b_{-p}) \tag{2.29}$$

$$\theta(x) = (N_R - N_L)\frac{\pi x}{L} + \frac{i\pi}{L}\sum_{p\neq 0}\left(\frac{L|p|}{2\pi}\right)^{1/2}\frac{1}{|p|}\, e^{-\alpha|p|/2 - ipx}(b_p^\dagger - b_{-p}) \tag{2.30}$$

Here, α introduces a momentum cutoff of the order of $1/\alpha$, and thus a finite bandwidth to our model. In a strict sense, one should take the limit $\alpha \to 0$ only after having calculated all observables one is interested in.

The fields ϕ and θ obey simple commutation rules. Using the bosonic commutation rules for $b_p, b_p^\dagger$ one easily obtains

$$[\phi(x), \theta(x')] \approx i\frac{\pi}{2}\,\mathrm{sign}(x' - x) \tag{2.31}$$

which becomes valid in the limit $L \to \infty$ and then $\alpha \to 0$ (see e.g. [17]). Similarly,

$$\begin{aligned}[\phi(x), \partial_x\theta(x')] &= i\pi\delta(x' - x)\\ [\partial_x\phi(x), \theta(x')] &= i\pi\delta(x' - x)\end{aligned} \tag{2.32}$$

Eq. (2.32) shows that the conjugate momentum $\pi_\phi(x)$ to the field $\phi(x)$ is simply given by

$$\pi_\phi(x) = \frac{1}{\pi}\partial_x\theta(x) \tag{2.33}$$

which gives using Eq. (2.30)

$$\pi_\phi(x) = \frac{(N_R - N_L)}{L} + \frac{1}{L}\sum_{p\neq 0}\left(\frac{L|p|}{2\pi}\right)^{1/2}\mathrm{sign}(p)e^{-\alpha|p|/2 - ipx}(b_p^\dagger - b_{-p}) \tag{2.34}$$

Using Eqs. (2.27) and (2.28) one obtains

$$\partial_x\phi(x) = -\pi(\rho_R(x) + \rho_L(x)) \tag{2.35}$$

$$\partial_x\theta(x) = \pi(\rho_R(x) - \rho_L(x)) \tag{2.36}$$

$\partial_x\phi$ is thus the $q = 0$ part of the density fluctuations at point x. $\partial_x\theta$ is simply the current operator in a one-dimensional system. Finally, with the help of Eqs. (2.29) and (2.30) the Hamiltonian (2.26) can be rewritten in terms of the fields ϕ and θ

$$\mathcal{H} = \frac{v_F}{2\pi}\int dx\big[(\partial_x\theta)^2 + (\partial_x\phi)^2\big] \tag{2.37}$$

where we used the convention $\hbar = 1$. Since the particle number operators for each species N_r are normal ordered and thus have finite matrix elements, the corresponding terms vanish in the limit $L \to \infty$.

Single-particle creation and annihilation operators can be defined in a similar way. To this end, let us consider operators $\psi_r(x), \psi_r^\dagger(x)$ for each species $r = R, L$ which destroy or create a particle at point x, respectively. From the commutation rules with the bosonic operators we can guess an operator that would produce the same commutation rules. In terms of the fields ϕ and θ this single-particle operator is (see e.g. [17])

$$\psi_r(x) = \eta_r \lim_{\alpha\to 0}\frac{1}{\sqrt{2\pi\alpha}} e^{ir(k_F-\pi/L)x} e^{i(\theta(x)-r\phi(x))} \tag{2.38}$$

In the limit $L \to \infty$, the single-particle operator becomes

$$\psi_r(x) = \eta_r \lim_{\alpha\to 0}\frac{1}{\sqrt{2\pi\alpha}} e^{irk_F x} e^{i(\theta(x)-r\phi(x))} \tag{2.39}$$

Introducing the operators η_r, the so-called *Klein factors*, allows us to make the mapping between the fermion basis and the boson basis rigorous [16, 18]. The construction of the operators η_r is tedious but one establishes an exact operator identity. For a proof that the bosonic space plus operators η is a complete Hilbert space see e.g. [18].

Finally, let us have a look at the physical interpretations of the formulas derived above. First we notice from Eq. (2.35) that the field ϕ is obviously related to the density of particles. Adding a particle at point x_0 manifests itself as a kink in the ϕ field because $\delta\rho(x) \sim \delta(x - x_0)$. Since

$$1 = \int_{-\infty}^{x>x_0} dx'\,\rho(x') = -\frac{1}{\pi}\big[\phi(x) - \phi(-\infty)\big] \tag{2.40}$$

one sees immediately that the step in the ϕ field is quantized and is a measure of the total number of particles in the system. Conversely, any kink-link excitation of the ϕ field can be interpreted as a particle in the system. This interpretation carries over to the single-particle operator (2.39). Since $\pi_\phi(x) = \partial_x\theta(x)/\pi$ is the canonically conjugate momentum of the ϕ field, the operator creating a particle at point x, i.e. a kink of amplitude π in ϕ, is given by

$$\exp\left\{-\frac{i}{\hbar}\int_{-\infty}^{x} dx'\,\pi_\phi(x)\right\} = \exp\left\{-\frac{i}{\hbar}\big[\theta(x) - \theta(-\infty)\big]\right\} \tag{2.41}$$

Note that the phase $\theta(-\infty)$ can be safely dropped since in physical operators this phase always appears multiplied by an integer number. Of course, one has to introduce an operator that changes the global number of particles by one which actually is the Klein factor η.

2.3.3 Interactions

After we have established a mapping between the system of non-interacting fermions and the bosons, we can have a look at the effect of interactions between fermions. For spinless fermions a typical interaction reads

$$\mathcal{H}_{\text{int}} = \frac{1}{2}\int dx\, dx'\, V(x-x')\rho(x)\rho(x') = \frac{1}{2L}\sum_{k,k',q} V(q) c^\dagger_{k+q} c^\dagger_{k'-q} c_{k'} c_k \tag{2.42}$$

The range of the interaction $V(x-x')$ is usually finite in one dimension due to screening provided by nearby gates or the surrounding medium. Since we are interested in the properties in the long-range limit, we can approximate the finite interaction range to a local one. This means that the most important interaction processes are the ones that are close to the Fermi surface or, equivalently, all momenta have to be close to the Fermi points $\pm k_F$. The fact that the Fermi surface is reduced to a set of two disjoint points allows us to decompose the interaction into three different sectors, as shown in Fig. 2.4. The first process g_4 couples only fermions on the same side of the Fermi surface. The second process g_2 couples fermions from one side of the Fermi surface with fermions on the other side. However, each species remains on the same side after the interaction. This is commonly referred to as *forward scattering*. Finally, the last process g_1 corresponds to a $2k_F$ scattering (*backscattering*) where fermions exchange sides. Note that for spinless fermions the g_2 and g_1 processes are identical because the outgoing particles are indistinguishable.

Since we now have two species of fermions, the left-moving and the right-moving fermions, we first have to define the density operator. Starting from the single-

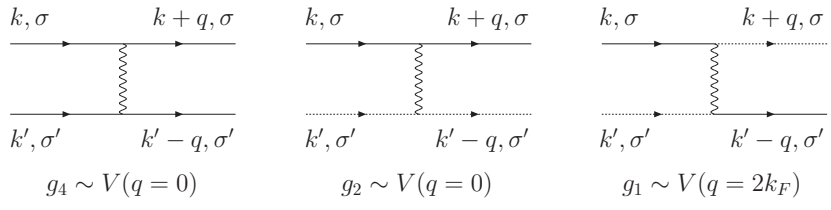

Figure 2.4: Decomposition of the interaction processes into three sectors. The solid (dashed) line is for right (left) going fermions and a wavy line indicates the interaction V. For spinful fermions each interaction can take two values, either $g_\parallel$ if the spins σ and σ' are equal or $g_\perp$ if the spins are opposite. For a description of the interaction processes see the main text. (Figure taken from [17].)

particle operator,

$$\psi(x) = \frac{1}{L}\sum_k e^{ikx} c_k \tag{2.43}$$

we can decompose the sum into momenta close to $\pm k_F$:

$$\psi(x) \simeq \frac{1}{L}\left[\sum_{|k|<\Gamma} e^{ik_F x} e^{ikx} c_k + \sum_{|k|<\Gamma} e^{-ik_F x} e^{ikx} c_k\right] \equiv \psi_R(x) + \psi_L(x) \tag{2.44}$$

where Γ is a momentum cutoff such that $v_F\Gamma$ is of the order of the bandwidth. The density operator thus becomes

$$\rho(x) = \psi^\dagger(x)\psi(x) = \psi_R^\dagger(x)\psi_R(x) + \psi_L^\dagger(x)\psi_L(x) + [\psi_R^\dagger(x)\psi_L(x) + \text{h.c.}] \tag{2.45}$$

The first two terms correspond to the $q = 0$ part of the density, where particles are excited on the same side of the Fermi surface. The last two terms are the $q = 2k_F$ excitations where a fermion is transferred from one side of the Fermi surface to the other.

For spinless fermions we only have to consider the g_2 and g_4 processes. The g_4 process can be written in the boson language as

$$\frac{g_4}{2}\psi_r^\dagger(x)\psi_r(x)\psi_r^\dagger(x)\psi_r(x) = \frac{g_4}{2}\rho_r(x)\rho_r(x) = \frac{g_4}{2}\frac{1}{(2\pi)^2}\left[\partial_x\phi(x) - r\partial_x\theta(x)\right]^2 \tag{2.46}$$

The sum of the two processes leads to the g_4 interaction Hamiltonian,

$$\mathcal{H}_4 = \frac{g_4}{(2\pi)^2}\int dx\left[(\partial_x\phi)^2 + (\partial_x\theta)^2\right] \tag{2.47}$$

In a similar way, the g_2 process becomes

$$g_2\psi_R^\dagger(x)\psi_R(x)\psi_L^\dagger(x)\psi_L(x) = g_2\rho_R(x)\rho_L(x) = \frac{g_2}{(2\pi)^2}\left[(\partial_x\phi(x))^2 - (\partial_x\theta(x))^2\right] \tag{2.48}$$

and the g_2 interaction Hamiltonian reads

$$\mathcal{H}_2 = \frac{g_2}{(2\pi)^2}\int dx\left[(\partial_x\phi)^2 - (\partial_x\theta)^2\right] \tag{2.49}$$

Obviously, the Hamiltonian remains quadratic in the presence of interactions, and the net effect of interactions between fermions can be absorbed in two parameters. We can rewrite the quadratic Hamiltonian as ($\hbar = 1$)

$$\mathcal{H} = \frac{uK}{2\pi}\int dx\left[(\partial_x\theta)^2 + \frac{(\partial_x\phi)^2}{K^2}\right] \tag{2.50}$$

where u has the dimension of a velocity, and K is a dimensionless parameter, the so-called *Luttinger liquid parameter*. We thus have

$$uK = v_F\left(1 + \frac{g_4}{2\pi v_F} - \frac{g_2}{2\pi v_F}\right) \tag{2.51}$$

$$\frac{u}{K} = v_F\left(1 + \frac{g_4}{2\pi v_F} + \frac{g_2}{2\pi v_F}\right) \tag{2.52}$$

or

$$u = v_F \left[\left(1 + \frac{g_4}{2\pi v_F} \right)^2 - \left(\frac{g_2}{2\pi v_F} \right)^2 \right]^{1/2} \tag{2.53}$$

$$K = \left(\frac{1 + g_4/(2\pi v_F) - g_2/(2\pi v_F)}{1 + g_4/(2\pi v_F) + g_2/(2\pi v_F)} \right)^{1/2} \tag{2.54}$$

Note that quite generally $K < 1$ for repulsive interaction and $K > 1$ for attractive interactions. The parameters u and K totally characterize the low-energy properties of any massless one-dimensional system. Note that one can absorb the factor K in the Hamiltonian (2.50) by rescaling the fields,

$$\phi(x) \to \sqrt{K}\phi(x), \quad \theta(x) \to \frac{1}{\sqrt{K}}\,\theta(x) \tag{2.55}$$

which preserves the commutation relations. The rescaled Hamiltonian is thus equal to Eq. (2.37) but with renormalized velocity u instead of v_F. In terms of the bosonic Hamiltonian, the rescaling of the fields is equivalent to a Bogoliubov transformation which diagonalizes the interaction of the bosons containing terms such as bb and $b^\dagger b^\dagger$. The rescaling of fields is simply much easier to perform than the Bogoliubov transformation of bosons.

2.3.4 Spinful Fermions and Spin-Charge Separation

Let us now turn to a model of fermions with spin. Similar to the fields ϕ and θ we introduce two sets of fields $(\phi_\uparrow, \theta_\uparrow)$ and $(\phi_\downarrow, \theta_\downarrow)$ for each spin species separately. To ensure proper anti-commutation relations between the fermion species, we have to introduce corresponding Klein factors $\eta_\uparrow$ and $\eta_\downarrow$ for each spin species. The kinetic part of the Tomonaga-Luttinger Hamiltonian is obviously equal to

$$\mathcal{H}_{\text{kin}} = \mathcal{H}^0_\uparrow + \mathcal{H}^0_\downarrow \tag{2.56}$$

with $\mathcal{H}^0$ the quadratic Hamiltonian (2.37).

The interactions between fermions are now given by all processes in Fig. 2.4. The g_4 processes are of the form

$$\mathcal{H}_4 = \sum_{r=R,L} \sum_{\sigma=\uparrow,\downarrow} \int dx \left[\frac{g_{4\parallel}}{2}\, \rho_{r\sigma}(x)\rho_{r\sigma}(x) + \frac{g_{4\perp}}{2}\, \rho_{r\sigma}(x)\rho_{r\bar{\sigma}}(x) \right] \tag{2.57}$$

where the $g_{4\parallel}$ process couples fermions with equal spins on each side of the Fermi surface and the $g_{4\perp}$ process couples fermions with opposite spins. Note that $\bar{\sigma} = \downarrow$ for $\sigma = \uparrow$ and vice versa. On the other hand, the g_2 processes coupling fermions on both sides of the Fermi surface are equal to

$$\mathcal{H}_2 = \sum_{\sigma=\uparrow,\downarrow} \int dx \big[g_{2\parallel} \rho_{R\sigma}(x)\rho_{L\sigma}(x) + g_{2\perp} \rho_{R\sigma}(x)\rho_{L\bar{\sigma}}(x) \big] \tag{2.58}$$

These interactions translated into the boson language introduce terms such as $(\partial_x\phi_\uparrow)^2$ and $\partial_x\phi_\uparrow\partial_x\phi_\downarrow$ and similar terms with $\theta_\uparrow$ and $\theta_\downarrow$. In the abscence of g_1 processes the Hamiltonian remains quadratic in the fields ϕ and θ but is not diagonal any more in the spin index due to the coupling of different spin species. A convenient way to diagonalize the Hamiltonian is to introduce charge and spin degrees of freedom defined by

$$\rho(x) = \frac{1}{\sqrt{2}}\big[\rho_\uparrow(x) + \rho_\downarrow(x)\big] \tag{2.59}$$

$$\sigma(x) = \frac{1}{\sqrt{2}}\big[\rho_\uparrow(x) - \rho_\downarrow(x)\big] \tag{2.60}$$

This is a unitary transformation for the bosons and allows us to define new fields

$$\phi_\rho(x) = \frac{1}{\sqrt{2}}\big[\phi_\uparrow(x) + \phi_\downarrow(x)\big] \tag{2.61}$$

$$\theta_\rho(x) = \frac{1}{\sqrt{2}}\big[\theta_\uparrow(x) + \theta_\downarrow(x)\big] \tag{2.62}$$

$$\phi_\sigma(x) = \frac{1}{\sqrt{2}}\big[\phi_\uparrow(x) - \phi_\downarrow(x)\big] \tag{2.63}$$

$$\theta_\sigma(x) = \frac{1}{\sqrt{2}}\big[\theta_\uparrow(x) - \theta_\downarrow(x)\big] \tag{2.64}$$

The charge (ρ) and spin (σ) fields commute whereas the fields (ϕ_ν, ρ_ν) with $\nu = \rho, \sigma$ obey the standard commutation rules. All operators such as the single-particle operator can be expressed in terms of these fields.

Substituting the fields (2.61)–(2.64) into the kinetic part $\mathcal{H}_{\text{kin}}$ we obtain

$$\mathcal{H}_{\text{kin}} = \mathcal{H}^0_\rho + \mathcal{H}^0_\sigma \tag{2.65}$$

with $\mathcal{H}^0$ the quadratic Hamiltonian (2.37). The Hamiltonian of the g_4 interaction processes now reads

$$\begin{aligned}
\mathcal{H}_4 &= \mathcal{H}_{4\parallel} + \mathcal{H}_{4\perp} \\
\mathcal{H}_{4\parallel} &= \frac{g_{4\parallel} + g_{4\perp}}{(2\pi)^2}\int dx\big[(\partial_x\phi_\rho)^2 + (\partial_x\theta_\rho)^2\big] \\
\mathcal{H}_{4\perp} &= \frac{g_{4\parallel} - g_{4\perp}}{(2\pi)^2}\int dx\big[(\partial_x\phi_\sigma)^2 + (\partial_x\theta_\sigma)^2\big]
\end{aligned} \tag{2.66}$$

while the g_2 interaction processes lead to

$$\begin{aligned}
\mathcal{H}_2 &= \mathcal{H}_{2\parallel} + \mathcal{H}_{2\perp} \\
\mathcal{H}_{2\parallel} &= \frac{g_{2\parallel} + g_{2\perp}}{(2\pi)^2}\int dx\big[(\partial_x\phi_\rho)^2 - (\partial_x\theta_\rho)^2\big] \\
\mathcal{H}_{2\perp} &= \frac{g_{2\parallel} - g_{2\perp}}{(2\pi)^2}\int dx\big[(\partial_x\phi_\sigma)^2 - (\partial_x\theta_\sigma)^2\big]
\end{aligned} \tag{2.67}$$

In order to bosonize the g_1 processes one has to take a little bit more care. In the fermion language using the standard anti-commutation relations for the fermions,

one recovers that the $g_{1\parallel}$ process is identical to the $g_{2\parallel}$ process but with an additional minus sign due to a permutation of operators. The $g_{1\parallel}$ process can thus be easily incorporated into the interaction Hamiltonian by setting $g_{2\parallel} \to g_{2\parallel} - g_{1\parallel}$. On the other hand, the $g_{1\perp}$ process can be bosonized as (see e.g. [17])

$$\mathcal{H}_{1\perp} = \frac{2g_{1\perp}}{(2\pi\alpha)^2} \int dx \cos(\sqrt{8}\phi_\sigma(x)) \tag{2.68}$$

where α is the cutoff introduced in Eq. (2.38) for the single-particle operator.

Putting together all the interactions we obtain an important result. The Hamiltonian of a generic interacting system in one dimension separates into two parts, a charge and a spin Hamiltonian:

$$\mathcal{H} = \mathcal{H}_\rho + \mathcal{H}_\sigma \quad \text{with} \quad [\mathcal{H}_\rho, \mathcal{H}_\sigma] = 0 \tag{2.69}$$

The charge part is quadratic of the form ($\hbar = 1$)

$$\mathcal{H}_\rho = \frac{u_\rho K_\rho}{2\pi} \int dx \left[(\partial_x \theta_\rho)^2 + \frac{(\partial_x \phi_\rho)^2}{K_\rho^2} \right] \tag{2.70}$$

with coefficients u_ρ and K_ρ defined by

$$u_\rho = v_F \left[\left(1 + \frac{g_{4\rho}}{2\pi v_F} \right)^2 - \left(\frac{g_{2\rho}}{2\pi v_F} \right)^2 \right]^{1/2} \tag{2.71}$$

$$K_\rho = \left(\frac{1 + g_{4\rho}/(2\pi v_F) - g_{2\rho}/(2\pi v_F)}{1 + g_{4\rho}/(2\pi v_F) + g_{2\rho}/(2\pi v_F)} \right)^{1/2} \tag{2.72}$$

where we have introduced effective coupling constants for the charge part:

$$g_{4\rho} = g_{4\parallel} + g_{4\perp} \quad \text{and} \quad g_{2\rho} = g_{2\parallel} + g_{2\perp} - g_{1\parallel} \tag{2.73}$$

In a similar way, the spin part is of the form ($\hbar = 1$)

$$\mathcal{H}_\sigma = \frac{u_\sigma K_\sigma}{2\pi} \int dx \left[(\partial_x \theta_\sigma(x))^2 + \frac{(\partial_x \phi_\sigma(x))^2}{K_\sigma^2} \right] + \frac{2g_{1\perp}}{(2\pi\alpha)^2} \int dx \cos(\sqrt{8}\phi_\sigma(x)) \tag{2.74}$$

but with coefficients u_σ and K_σ given by

$$u_\sigma = v_F \left[\left(1 + \frac{g_{4\sigma}}{2\pi v_F} \right)^2 - \left(\frac{g_{2\sigma}}{2\pi v_F} \right)^2 \right]^{1/2} \tag{2.75}$$

$$K_\sigma = \left(\frac{1 + g_{4\sigma}/(2\pi v_F) - g_{2\sigma}/(2\pi v_F)}{1 + g_{4\sigma}/(2\pi v_F) + g_{2\sigma}/(2\pi v_F)} \right)^{1/2} \tag{2.76}$$

Here, the effective coupling constants for the spin part are defined as

$$g_{4\sigma} = g_{4\parallel} - g_{4\perp} \quad \text{and} \quad g_{2\sigma} = g_{2\parallel} - g_{2\perp} - g_{1\parallel} \tag{2.77}$$

Note that the bare coupling constants $g_{4\perp}$ and $g_{2\perp}$ enter with different signs in Eqs. (2.73) and (2.77).

The result (2.69) for spinful interacting fermions shows that there is a complete separation of spin and charge degrees of freedom in one dimension. This is known as *spin-charge separation*. Thus, any kind of single-particle excitation which would carry both charge and spin quantum numbers is impossible. This resembles the previous statement that in one dimension a single fermionic excitation breaks up into two elementary excitations, i.e. into a collective charge excitation with velocity u_ρ and a collective spin excitation with velocity u_σ. The velocities are in general different.

2.3.5 Symmetries and Conservation Laws

Finally, let us discuss the symmetries and conservation laws of the one-dimensional Tomonaga-Luttinger model in the abscence of backscattering, $g_1 = 0$. As we have seen in the previous sections, we can rewrite the Hamiltonian of a generic interacting system in one dimension as the sum of a charge and a spin Hamiltonian,

$$\mathcal{H} = \mathcal{H}_\rho + \mathcal{H}_\sigma \tag{2.78}$$

The physical origin of the conservation laws below can be traced back to the restriction of interactions to the Fermi surface which in one dimension consists of only two disjoint points. Due to small momentum transfer interaction processes scattering electrons from one Fermi point to the other are excluded from the model.

Charge and Spin Conservation

The Hamiltonian not only conserves the total charge (ρ) and spin (σ) of the system,

$$[N_\rho, \mathcal{H}] = 0, \quad [N_\sigma, \mathcal{H}] = 0 \tag{2.79}$$

but it does so on each branch $r = R, L$,

$$[N_{r,\rho}, \mathcal{H}] = 0, \quad [N_{r,\sigma}, \mathcal{H}] = 0 \tag{2.80}$$

This clearly implies that the charge and spin currents are conserved,

$$[J_\rho, \mathcal{H}] = 0, \quad [J_\sigma, \mathcal{H}] = 0 \tag{2.81}$$

From the conservation of charge and spin on each branch it follows that the Hamiltonian is invariant under the gauge transformations

$$\psi_{r\sigma}(x) \to e^{i\alpha_r}\psi_{r\sigma}(x) \tag{2.82}$$

for each branch separately. In other words, the Hamiltonian of the Tomonaga-Luttinger model posseses in addition to the usual gauge symmetry

$$\psi_{r\sigma}(x) \to e^{i\alpha}\psi_{r\sigma}(x) \tag{2.83}$$

a chiral symmetry

$$\psi_{r\sigma}(x) \to e^{ir\alpha}\psi_{r\sigma}(x) \tag{2.84}$$

Spin Rotation

In addition, for specific values of the interaction constants, i.e.

$$g_{2\parallel} = g_{2\perp}, \quad g_{4\parallel} = g_{4\perp} \tag{2.85}$$

the Hamiltonian is invariant under a spin rotation,

$$\psi_{r\sigma}(x) \to \sum_{\sigma'} U_{\sigma\sigma'} \psi_{r\sigma'}(x) \tag{2.86}$$

where $U = \exp(i\mathbf{\Omega} \cdot \sigma)$ is a SU(2)-matrix. Note that in this case also the correlation functions are invariant under spin rotation.

Charge Conjugation

Finally, the linear dispersion of the Tomonaga-Luttinger model and the normal ordering of operators involved in the density operators make the model charge-conjugation symmetric,

$$\psi_{r\sigma}(x) \to \psi^\dagger_{r\sigma}(x) \tag{2.87}$$

2.4 The Tomonaga-Luttinger Model as Effective Model

Finally, we present a few specific systems that can be mapped onto the Tomonaga-Luttinger Hamiltonian. Starting with a brief summary of the sine-Gordon Hamiltonian, we discuss the two-dimensional Coulomb gas and the XY model as important examples of the well-known Berezinski-Kosterlitz-Thouless transition. Another class of systems covers spin 1/2 systems which turn out to be simple realizations of Luttinger liquid physics.

2.4.1 The sine-Gordon Hamiltonian

We have seen in Sec. 2.3.4 that the Hamiltonian (2.69) of interacting spinful fermions contains a cosine term, known as the *sine-Gordon Hamiltonian*

$$\mathcal{H}_{\mathrm{SG}} = \frac{2g_{1\perp}}{(2\pi\alpha)^2} \int dx \cos(\sqrt{8}\phi_\sigma(x)) \tag{2.88}$$

The fact that non-quadratic terms are generated, for example by interactions, occurs quite often in one-dimensional systems. On a physical level, the effect of the sine-Gordon Hamiltonian is obvious. The cosine term would like to lock the ϕ field into one of its minima, in contrast to the quadratic term which promotes fluctuations of the ϕ field. There will thus be a competition between the kinetic part and the cosine term. In the following, we briefly disucss the low-energy properties of the sine-Gordon Hamiltonian. In order to obtain these properties one uses a renormalization procedure (see e.g. [17]).

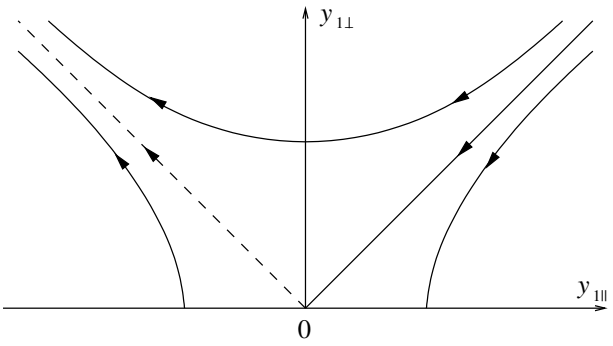

Figure 2.5: The renormalization group flow diagram of the sine-Gordon model. The trajectories shown are hyperbolas. The diagonal line in the right half is separatrix between a regime where $y_{1\perp}$ is irrelevant and a regime where $y_{1\perp}$ flows to strong coupling. (Figure taken from [17].)

Introducing the dimensionless variables $y = g/(\pi v_F)$, the relevant beta functions are given by (see e.g. [17])

$$\frac{\partial y_{1\parallel}}{\partial \ln b} = -y_{1\perp}^2 \tag{2.89}$$

$$\frac{\partial y_{1\perp}}{\partial \ln b} = -y_{1\parallel} y_{1\perp} \tag{2.90}$$

Although these beta functions are perturbative in y they are exact in the interaction K. These equations are identical to the ones derived for the XY model discussed in the next section. The corresponding flow diagram is shown in Fig. 2.5. On the $y_{1\parallel} = y_{1\perp}$ line which is a separatrix between two different regimes the cosine operator is marginally irrelevant. If one starts with a spin rotation invariant system ($y_{1\parallel} = y_{1\perp}$) then the rotation invariance is preserved. The fixed point corresponds to $y_{1\parallel}^* = y_{1\perp}^* = 0$ and thus $K^* = 1$. When $y_{1\perp} < y_{1\parallel}$ the cosine operator is irrelevant, and the fixed point corresponds to $y_{1\perp}^* = 0$ and finite $y_{1\parallel}^*$. However, close to the fixed point the trajectory is nearly vertical, thus the resulting K^* is different from unity. For $y_{1\perp} > y_{1\parallel}$ the trajectories tend to $y_{1\parallel} \to -\infty$ and $y_{1\perp} \to \infty$, that means the flow goes to strong coupling. The line $y_{1\parallel} = -y_{1\perp}$ corresponds also to a spin rotation invariant system but the flow goes to strong coupling. In the strong coupling regime the ϕ field becomes locked in one of the minima of the cosine. In other words, the excitation spectrum develops a gap.

2.4.2 The 2D Coulomb Gas and the XY model

Let us consider a two-dimensional classical XY model with a classical spin

$$\mathbf{S}_i = (\cos(\phi_i), \sin(\phi_i)) \tag{2.91}$$

on each site i. The Hamiltonian of *2D XY model* reads

$$\mathcal{H} = -\frac{J}{2}\sum_{i,a}\cos(\phi_{i+a} - \phi_i) \tag{2.92}$$

where a is a set of nearest neighbor vectors. Based on the observation that terms such as $e^{i\phi}$ are proportional to the density of the system, the density-density correlations for the Luttinger liquid correspond to the spin-spin correlations of the XY model, provided that we interpret one of the classical dimensions as imaginary time for the quantum problem. Assuming that ϕ is a smooth field we can expand the difference $\phi_{i+a} - \phi_i$ and the XY Hamiltonian becomes in the continuous limit

$$\mathcal{H}_{\mathrm{XY}} = \frac{J}{2}\int dx\, dy\big[(\partial_x\phi)^2 + (\partial_y\phi)^2\big] \tag{2.93}$$

Note that this expansion is valid only for small temperatures. At higher temperatures the XY model undergoes a phase transition towards a disordered phase, the so-called *Berezinskii-Kosterlitz-Thouless transition*. For low enough temperatures we thus have an equivalence between the XY model and the Tomonaga-Luttinger model.

At higher temperatures vortex configurations where the field ϕ is singular become important. For the quantum problem, the operator $e^{i2\theta(x)}$ is the corresponding vortex creation operator for the ϕ field. Similarly, the operator $e^{i2\phi(x)}$ creates vortices in the θ field. A reasonable Hamiltonian is thus

$$\mathcal{H} = \frac{uK}{2\pi}\int dx\left[(\partial_x\theta)^2 + \frac{(\partial_x\phi)^2}{K^2}\right] + g_\phi\int dx\cos(\sqrt{8}\phi) + g_\theta\int dx\cos(\sqrt{8}\theta) \tag{2.94}$$

The partition function of this Hamiltonian turns out to be exactly the same as the one of a gas of classical particles with fugacity g_ϕ. The classical system can be described as a gas of classical charges with unit charge at temperature $T = 1/(2K)$ and interaction $V(r_i - r_j) \sim \log(r_i - r_j)$. This problem is the well-known Coulomb gas problem in two dimensions. The sine-Gordon model thus maps exactly to the Coulomb gas in 2D which in turn is equivalent to the 2D XY model. This is but one example of the correspondence between different models.

2.4.3 The Spin 1/2 Chain

Finally, let us consider a chain of spin 1/2. On each site i there is a spin $S_i = \sigma_i/2$ where σ_i is the vector of Pauli matrices. The three components of the spin, $S_i = (S_i^x, S_i^y, S_i^z)$, obey the commutation relations

$$[S_i^\alpha, S_j^\beta] = i\delta_{ij}\epsilon_{\alpha\beta\gamma}S_i^\gamma \tag{2.95}$$

with $\epsilon_{\alpha\beta\gamma}$ the totally antisymmetric tensor. The Hamiltonian of a one-dimensional spin 1/2 chain with nearest neighbor interaction is equal to

$$\mathcal{H} = J\sum_i\big(S_i^xS_{i+1}^x + S_i^yS_{i+1}^y + \Delta S_i^zS_{i+1}^z\big) \tag{2.96}$$

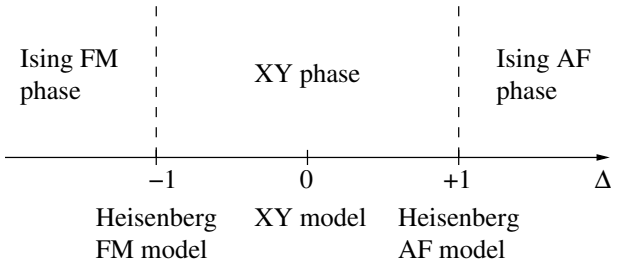

Figure 2.6: The different regimes and models for a spin 1/2 chain as a function of the anisotropy Δ. (Figure taken from [17].)

This model is known as *XXZ Hamiltonian* if the couplings in the xy plane and the z direction are different. For $\Delta = 1$ the interaction between spins is totally invariant by rotation, and this is the well-known *Heisenberg Hamiltonian*. In the case $J > 0$ antiferromagnetic order of the spins is favored, while $J < 0$ obviously favors ferromagnetic order. Note that $\Delta = -1$ is the ferromagnetic isotropic point and $\Delta = 1$ is the antiferromagnetic isotropic point. $\Delta = 0$ is the XY point.

If there are only nearest neighbor interactions present as in Eq. (2.96), some simplifications are possible. If we perform the canonical transformation

$$S_i^x \to (-1)^i S_i^x, \quad S_i^y \to (-1)^i S_i^y, \quad S_i^z \to S_i^z \tag{2.97}$$

it changes the coupling constants as $J \to -J$ and $\Delta \to -\Delta$. It is thus enough to consider the antiferromagnetic system $J > 0$.

In order to map the spin 1/2 system to a bosonic problem we first replace the spin operators by their corresponding raising and lowering operators. Using the identity $S_i^{\pm} = S_i^x \pm i S_i^y$ the XXZ Hamiltonian (2.96) becomes

$$\mathcal{H} = \frac{J}{2} \sum_i \left(S_i^+ S_{i+1}^- + S_i^- S_{i+1}^+ \right) + \Delta J \sum_i S_i^z S_{i+1}^z \tag{2.98}$$

In a second step, we apply a Jordan-Wigner transformation which maps the spin 1/2 operators onto spinless fermions:

$$S_i^+ \to c_i^\dagger \exp\left(i\pi \sum_{j<i} c_j^\dagger c_j \right), \quad S_i^- \to \exp\left(-i\pi \sum_{j<i} c_j^\dagger c_j \right) c_i, \quad S_i^z \to c_i^\dagger c_i - \frac{1}{2} \tag{2.99}$$

Note that the Jordan-Wigner string ensures proper anti-commutation relations. At first sight, the non-local character of the exponentials makes it appear infeasible to work with the string. But many operators have quite simple representations in the fermion language because the string simplifies. The XXZ Hamiltonian (2.96) thus becomes after the transformation

$$\mathcal{H} = \frac{J}{2} \sum_i \left(c_i^\dagger c_{i+1} + c_{i+1}^\dagger c_i \right) + \Delta J \sum_i \left(c_i^\dagger c_i - \frac{1}{2} \right) \left(c_{i+1}^\dagger c_{i+1} - \frac{1}{2} \right) \tag{2.100}$$

To obtain a more conventional form one makes the canonical transformation (2.97) which is equivalent to

$$c_i \to (-1)^i c_i \tag{2.101}$$

By applying this transformation we shift the momentum of the fermions by π. The transformation (2.101) leads to the Hamiltonian

$$\mathcal{H} = -t\sum_i \left(c_i^\dagger c_{i+1} + c_{i+1}^\dagger c_i\right) + V\sum_i \left(c_i^\dagger c_i - \frac{1}{2}\right)\left(c_{i+1}^\dagger c_{i+1} - \frac{1}{2}\right) \tag{2.102}$$

with $t = J/2$ and $V = \Delta J$. The spin 1/2 chain is thus equivalent to a chain of spinless fermions. The fermions can hop between neighboring sites with a hopping amplitude t and experience a nearest neighbor interaction V. A local interaction is precluded for spinless fermions by the Pauli principle. Note that an additional magnetic field along the z direction for the spin chain is simple a chemical potential for the fermions:

$$-h\sum_i S_i^z = -h\sum_i \left(c_i^\dagger c_i - \frac{1}{2}\right) \tag{2.103}$$

Since $\langle S_i^z\rangle = 0$ the fermion density is $\langle c_i^\dagger c_i\rangle = 1/2$, that means the fermionic band is half-filled. Thus, the Fermi momentum is $k_F = \pi/(2a)$.

The Hamiltonian (2.102) is written in a way to obey particle-hole symmetry which can be easily seen by making the canonical transformation $c_i \to (-1)^i c_i^\dagger$. This particle-hole symmetry reflects the spin reversal symmetry in the XXZ Hamiltonian (2.96).

Let us now use the technique of bosonization to solve the interacting spin chain problem. We take the continuum limit and define operators in real space as

$$S^\alpha(x_i) \equiv a^{-1/2} S_i^\alpha \tag{2.104}$$

where $x_i = ia$ and a is the lattice spacing. We can use the bosonization representation of the fermion operators to rewrite the Hamiltonian (2.102). The kinetic energy can be diagonalized by going to Fourier space:

$$\mathcal{H}_{\text{kin}} = \sum_k \epsilon_k c_k^\dagger c_k \tag{2.105}$$

where the dispersion is the standard tight-binding energy,

$$\epsilon_k = -J\cos(ka) \approx v_F k \quad \text{with} \quad v_F = Ja\sin(k_F a) \tag{2.106}$$

with the last line valid close to the Fermi level. One has to take more care upon bosonizing the interaction Hamiltonian since one can take the continuous limit $r_{j+1} \sim r_j \to r$ for the fields only. Using the boson mapping carefully, the interaction part becomes

$$\mathcal{H}_{\text{int}} = \frac{a\Delta J}{\pi^2}\int dx\,(1-\cos(2k_F a))(\partial_x\phi)^2 - \frac{2}{(2\pi\alpha)^2}\int dx\cos(4\phi(x)) \tag{2.107}$$

The spin chain Hamiltonian can thus be written as

$$\mathcal{H} = \frac{uK}{2\pi}\int dx\left[(\partial_x\theta)^2 + \frac{(\partial_x\phi)^2}{K^2}\right] - \frac{2g_3}{(2\pi\alpha)^2}\int dx\cos(4\phi(x)) \tag{2.108}$$

with the parameters

$$uK = v_F = Ja\sin(k_F a) \tag{2.109}$$

$$\frac{u}{K} = v_F\left[1 + \frac{2\Delta Ja}{\pi v_F}(1-\cos(2k_F a))\right] \tag{2.110}$$

$$g_3 = a\Delta J \tag{2.111}$$

Note that at half-filling $k_F = \pi/(2a)$.

Finally, one should note that these expressions are obtained in the perturbative limit around the XY point where Δ is small. The phase diagram of Hamiltonian (2.108) can be obtained from the sine-Gordon phase diagram. The cosine termin is irrelevant for $K > 1/2$ and the system flows to a regime which is Luttinger liquid like, i.e. to a quadratic Hamiltonian. Since $K = 1$ is the non-interacting point which corresponds to the XY limit, the Luttinger phase is thus an XY like phase. For $K < 1/2$ the cosine terms is relevant. The excitations of the spin chain develop a gap, and this phase is dominated by Ising-like interactions along the z direction.

2.5 Summary

Thanks to the Abelian bosonization method we have determined the low-energy properties of the Tomonaga-Luttinger model. Although this model has a strictly linear spectrum, most of its properties hold quite generally for a large spectrum of one-dimensional gapless systems with short range interactions. It has also been shown that the mapping of two-dimensional classical systems onto one-dimensional quantum systems can be very useful when one is interested in the low-energy properties of such classical systems.

Chapter 3

Two-Band Quantum Wire

In this chapter, we present a model of interacting electrons in a quantum wire. Due to the low dimensionality of the model, the conductance is expected to be quantized in units of the conductance quantum $G_0 = 2e^2/\hbar$ where e is the elementary charge and the factor of 2 accounts for spin degeneracy. This property is expected to remain when one includes interactions into the model. Upon tuning the chemical potential the second band becomes activated which results in a jump of the zero temperature conductance.

For simplicity we restrict ourselves here to spinless fermions which are usually studied as a model for the more interesting but also more difficult case of spin 1/2 electrons. Physically, spinless fermions can be considered as completely polarized spin 1/2 electrons in a (high) magnetic field.

First, in Sec. 3.1, we briefly summarize the effect of interactions in a one-dimensional systems with two subbands. An estimate of the gap between the two subbands is given. Section 3.2 introduces the Hamiltonian describing the two-band quantum wire. The first filled subband is treated as a Luttinger liquid exchanging pairs of electrons with the second subband, in addition to the usual density-density interaction. In Sec. 3.3, we discuss the relevance of the pair-transfer operator when one performs perturbation theory in the inter-band interaction. It is shown that the Hamiltonian can be simplified by applying a unitary transformation removing either the density-density coupling or the pair-transfer operator. Finally, in Sec. 3.4, the Lagrangian action of the two-band quantum wire is given.

3.1 Interactions Between Electrons

A principal question that we have to address first is under what conditions the interactions are "weak" in comparison to the kinetic energy, i.e. when a perturbative approach in the interacting electron system makes sense. If the electrons in the quantum wire are confined to one dimension, for example by a steep external poten-

tial, their physics is controlled by the one-dimensional density $n_e \sim 1/r_0$ where r_0 is the mean distance between electrons. Using the Heisenberg uncertainty principle we can estimate the minimum kinetic energy and interaction energy. In terms of the density n_e the kinetic energy per electron is of order

$$E_{\text{kin}} \sim \frac{\hbar^2}{m}\frac{1}{r_0^2} \tag{3.1}$$

On the other hand, assuming that the electrons interact predominantly with its nearest neighbors only, the Coulomb energy is of order

$$E_{\text{int}} \sim \frac{e^2}{r_0} \tag{3.2}$$

The ratio of the two energy scales defines a dimesionless density parameter

$$r = \frac{E_{\text{int}}}{E_{\text{kin}}} = \frac{e^2}{r_0}\frac{mr_0^2}{\hbar^2} = \frac{r_0}{a_B} \tag{3.3}$$

where $a_B = \hbar^2/(me^2)$ is the Bohr radius. At low densities, $n_e \to 0$, the kinetic energy scales to zero faster than the interaction energy, and thus $r \gg 1$. In this limit the repulsive Coulomb interaction dominates and the electrons behave classically. In order to minimize their mutual interaction they are expected to form a periodic one-dimensional structure, the so-called *Wigner crystal*. At small but finite density this quasi-long-range order is smeared out by quantum fluctuations [20], but the short-range order remains as long as $r > 1$, i.e. as long as the distance between electrons r_0 is larger than the Bohr radius a_B. In the opposite limit of high density, $r \ll 1$, or weak interactions, the electrons occupy subbands of transverse quantization. In this regime, weak interactions lead to a coupling between the subbands, and electron wavefunctions can thus be represented in terms of products of eigenstates of the subbands.

Another question related to interactions is whether or not an electron system can be viewed as one-dimensional. In quantum wires a change in the effective dimensionality can be observed when the chemical potential, μ, is tuned by applying a gate voltage. At low densities or strong interactions, the electrons form a Wigner crystal and the system remains one-dimensional until the interaction energy overcomes the confining potential. The Wigner crystal eventually splits into two chains forming a zigzag structure [21]. Due to interactions the two chains are locked and only one gapless mode, the plasmon mode, remains which corresponds to the transition of the Wigner crystal along the quantum wire. Near the quantum phase transition when the second subband becomes activated, Meyer *et al.* [6] estimate a linear behavior for the gap in excitation spectrum,

$$\Delta \sim |\mu - \mu_c| \tag{3.4}$$

where μ_c is the critical chemical potential at which the quantum phase transition takes place. On the other hand, at weak interactions electrons occupy subbands of transverse quantization, and the system is one-dimensional until the chemical potential reaches the bottom of the second subband. Although the density-density coupling between the two subband renormalizes the velocities of the low-energy excitations, a spectral gap does not emerge. However, the transfer of pairs of electrons between both subbands can, in principle, lead to a BCS-like gap in the spectrum of transverse quantization. In the vicinity of the quantum phase transition, Meyer *et al.* [6] estimate the gap as

$$\Delta \sim |\mu - \mu_c|^{\alpha} \tag{3.5}$$

with a non-universal exponent $\alpha \gg 1$. Thus the spectral gap does not only exist for strong interactions, but also when interaction are weak.

3.2 Hamiltonian

In order to understand the evolution of the transition between the two limiting cases of strong and weak interactions, Meyer *et al.* propose an effective Hamiltonian for a system of interacting electrons in a one-dimensional quantum wire at intermediate interactions [6]. In a grand canonical setup, the Hamiltonian consists of three parts,

$$\mathcal{H} = \mathcal{H}_{\mathrm{pl}} + \mathcal{H}_{\mathrm{el}} + \mathcal{H}_{\mathrm{el-pl}} \tag{3.6}$$

3.2.1 First Subband: Luttinger Liquid

The low-energy properties of the first (lower) subband are described in terms of a Luttinger liquid since only the low-energy properties near the Fermi level are important, as shown in Fig. 3.1. The density-density interactions within the first

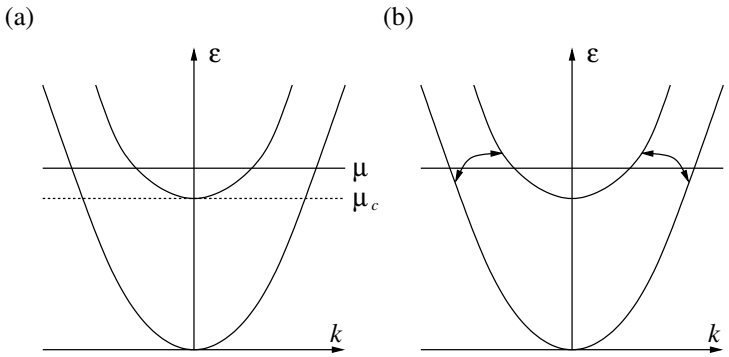

Figure 3.1: (a) Spectrum of a one-dimensional quantum wire with two subbands. (b) Scattering processes transferring pairs of electrons between the subbands.

subband are described by the g_4 and g_2 interaction processes. Note that for spinless fermions the g_2 and g_1 processes are indistinguishable (cf. Sec. 2.3.3). For simplicity let us consider the case of identical interaction constants, $g_2 = g_4 = \gamma_1$. Chapter 2 the low-energy charge excitations of the first subband, i.e. the density fluctuations, can be described in terms of phonons, Using the bosonization approach presented in Chapter 2, the low-energy charge excitations of the first subband, i.e. the density fluctuations, can be described in terms of plasmons with acoustic spectrum,

$$\mathcal{H}_{\rm pl} = \frac{v_{F1}}{2\pi} \int dx \left[(\partial_x \theta)^2 + \frac{(\partial_x \phi)^2}{K^2} \right] \tag{3.7}$$

Here, v_{F1} is the Fermi velocity in the first subband, and the bosonic fields ϕ and θ describe the density fluctuations in the first subband. Using Eq. (2.54) the Luttinger liquid parameter K is equal to

$$K = \left(\frac{1}{1 + \gamma_1/(\pi v_{F1})} \right)^{1/2} \tag{3.8}$$

3.2.2 Second Subband: Fermions at the Bottom of a Band

Near the quantum phase transition the density of electrons in the second subband is low and thus the average distance between electrons large. When the distance between electrons is large, the interactions between them become effectively local. As a consequence of the Pauli principle, spinless fermions never occupy the same place, and thus the electrons effectively do not interact with each other. Under these conditions the second subband can be described in terms of one-dimensional spinless fermions at the bottom of the upper band,

$$\mathcal{H}_{\rm el} = \int dx\, \psi^\dagger \left(-\frac{1}{2m} \partial_x^2 - \mu \right) \psi \tag{3.9}$$

Here, ψ and $\psi^\dagger$ are the electron annihilation and creation operators, respectively, and the chemical potential μ tunes the distance to quantum criticality at μ_c. Note that the curvature of the electron spectrum is important in the regime of intermediate interactions since kinetic energy and interactions between electrons are of the same order.

3.2.3 Inter-Subband Interactions

Finally, the interactions between the two subbands consists of two parts,

$$\mathcal{H}_{\rm el-pl} = \gamma_x \int dx\, (\partial_x \phi) \psi^\dagger \psi + \gamma_t \int dx\, \left\{ [(\partial_x \psi)\psi - \psi \partial_x \psi] e^{i2\theta} + \text{h.c.} \right\} \tag{3.10}$$

The first term describes the density-density interactions between the two subbands, while the second term accounts for the possibility of transferring pairs of electrons from one subband to the other, as shown in Fig. 3.1 (b). Note that all Klein factors have been omitted in Eq. (3.10) to yield the simplest form of the interaction.

3.3 Pair Transfer Operator

It is now tempting to proceed by perturbation theory in the inter-band interactions $\mathcal{H}_{\mathrm{el-pl}}$. However, a perturbative approach is not feasible since the inter-band interaction consists of two parts, the density-density interactions and the pair transfer of electrons between the two subbands, the latter one favoring superconducting fluctuations between the subbands.

Rather than treating either the density-density interaction or the pair transfer of electrons as a perturbation we can apply to the Hamiltonian a unitary transformation, $\mathcal{H} \to U^\dagger \mathcal{H} U$, and eliminate the density-density coupling between the two subbands. Since the θ field is the conjugate momentum of $\partial_x \phi$ (cf. Eq. (2.32)) a reasonable choice to remove the density-density coupling is the non-local unitary operator

$$U(x) = \exp\left(ia \int_{-\infty}^{x} dx'\, \theta(x') \psi^\dagger(x') \psi(x') \right) \tag{3.11}$$

Using the Baker-Hausdorff theorem,

$$e^{-B} A e^{B} = \sum_{n=0}^{\infty} \frac{1}{n!} [A, B]_n = A + [A, B] + \frac{1}{2} [[A, B], B] + \ldots \tag{3.12}$$

where $[A, B]_n = [[A, B]_{n-1}, B]$ and $[A, B]_0 = A$, we immediately see that the application of the unitary operator $U(x)$ shifts the ϕ field,

$$\partial_x(x)\phi \to U^\dagger(x) \partial_x \phi(x) U(x) = \partial_x \phi(x) + a\pi \psi^\dagger(x) \psi(x) \tag{3.13}$$

while the fermion fields ψ and $\psi^\dagger$ acquire a phase:

$$\psi(x) \to U^\dagger(x) \psi(x) U(x) = \psi(x) e^{ia\theta(x)} \tag{3.14}$$

$$\psi^\dagger(x) \to U^\dagger(x) \psi^\dagger(x) U(x) = \psi^\dagger(x) e^{-ia\theta(x)} \tag{3.15}$$

We can thus remove the density-density coupling between the two subbands by applying to $\mathcal{H}$ a unitary transformation with $a = -K^2 \gamma_x / v_{F1}$. The remaining interaction between the subbands reads

$$\mathcal{H}_{\mathrm{el-pl}} = \gamma_t \int dx \left\{ [(\partial_x \psi)\psi - \psi \partial_x \psi] e^{i2\kappa\theta} + \mathrm{h.c.} \right\} + \mathcal{H}_{\mathrm{irr}} \tag{3.16}$$

with a phase factor

$$\kappa = 1 - \frac{K^2 \gamma_x}{v_{F1}} \tag{3.17}$$

The residual interaction term

$$\mathcal{H}_{\mathrm{irr}} = \int dx\, \frac{1}{2m} \left[ia \partial_x^2 \theta - a^2 (\partial_x \theta)^2 \right] \psi^\dagger \psi \tag{3.18}$$

which stems from the spatial gradients acting on the unitary operator U turns out to be irrelevant in the renormalization group sense. This is due to the fact that its

scaling dimension is smaller than the scaling dimension of the original interaction term which is a marginal term with respect to free fermionic Hamiltonian.

The irrelevance of the couplings (3.18) suggests that at long time and distances the transformed fermion and plasmon correlation functions asymptotically factorize, and eventually the electron-plasmon interaction itself will be irrelevant. The possible irrelevance of the interaction can be understood in the following picture. For large κ, i.e. in the weak coupling limit, the phase factor $e^{i2\kappa\theta}$ oscillates rapidly which suppresses the transfer of pairs of electrons between the two subbands. Thus, the electron pair transfer is but a perturbation to the fermions. On the other hand, for small κ, i.e. in the strong coupling limit, one can carry out a Taylor expansion of the exponential, and using simple scaling arguments one can easily show that the remainder of the inter-band interaction is indeed a relevant perturbation. However, this naive picture is oversimplified in that one has to seriously take care of the exponential of the field θ.

Let us be more formal. In order to calculate the scaling dimension of the interaction we consider the operator which transfers pairs of electrons from one subband to the other,

$$\mathcal{O}(x,\tau) = \left\{[(\partial_x\psi)\psi - \psi\partial_x\psi]e^{i2\kappa\theta} + \text{h.c.}\right\} \tag{3.19}$$

and compute the correlation function

$$G_{\mathcal{O}\mathcal{O}}(x,\tau;x',\tau') = \langle\mathcal{O}(x,\tau)\mathcal{O}(x',\tau')\rangle \tag{3.20}$$

Note that this correlation function would naturally appear when calculating the self-energy corrections in a perturbation theory in γ_t. Without loss of generality we can set $x' = 0$ and $\tau' = 0$ since the model is translational invariant in space and imaginary time. The correlaction function can thus be rewritten as

$$G_{\mathcal{O}\mathcal{O}}(x,\tau) \sim \left\{\left[\partial_x G_{\psi\psi^\dagger}(x,\tau)\right]^2 - G_{\psi\psi^\dagger}(x,\tau)\partial_x^2 G_{\psi\psi^\dagger}(x,\tau)\right\}\langle e^{i2\kappa[\theta(x,\tau)-\theta(0,0)]}\rangle \tag{3.21}$$

where $G_{\psi\psi^\dagger}(x,\tau) = \langle\psi(x,\tau)\psi^\dagger(0,0)\rangle$ is the usual fermion propagator for free fermions, and prefactors have been omitted for simplicity. One thus has to compute correlation functions of exponentials of the field θ. However, such correlations are easy to compute. Using the functional field integral one can prove the quite general Debye-Waller relation (see e.g. [17])

$$\left\langle T_\tau \exp\left\{\sum_j i[A_j\phi(r_j) + B_j\theta(r_j)]\right\}\right\rangle = \exp\left\{-\frac{1}{2}\left\langle T_\tau\left(\sum_j [A_j\phi(r_j) + B_j\theta(r_j)]\right)^2\right\rangle\right\} \tag{3.22}$$

where the imaginary time ordering operator T_τ emphasizes that this relation is indeed valid for operators. This leads to

$$\langle e^{i2\kappa[\theta(x,\tau)-\theta(0,0)]}\rangle = e^{-2\kappa^2\langle[\theta(x,\tau)-\theta(0,0)]^2\rangle} \tag{3.23}$$

where the correlation function of θ is given by (see e.g. [17])

$$G_{\theta\theta}(x,\tau) = \langle[\theta(x,\tau) - \theta(0,0)]^2\rangle = \frac{1}{2K}\log\left[\frac{x^2 + (v_{F1}\tau + \alpha)^2}{\alpha^2}\right] \tag{3.24}$$

Here, α is a cutoff which mimics a finite bandwidth since the integrals over momentum would diverge at large k. Thus, the correlation function of $\mathcal{O}$ is given by

$$G_{\mathcal{O}\mathcal{O}}(x,\tau) \sim \frac{1}{\tau^2}\exp\left\{\frac{ix^2}{\tau}\right\}\frac{1}{[x^2 + (v_{F1}\tau + \alpha)^2]^{\kappa^2/K}} \tag{3.25}$$

The exponential factor suggests the scaling $x^2 \sim \tau$ which corresponds to a quadratic dispersion for the fermions. Upon performing a renormalization group transformation the unit length is rescaled by a factor of b^{-1}, i.e. an interval in space Δx is scaled down to $\Delta x' = b^{-1}\Delta x$. Denoting the scaling dimension of spatial coordinates by $\dim[x] = -1$, imaginary time has the scaling dimension $\dim[\tau] = -2$. This leads to the result that

$$\dim[G_{\mathcal{O}\mathcal{O}}] = 4\left(1 + \frac{\kappa^2}{K}\right) \tag{3.26}$$

and thus the scaling dimension of the pair transfer operator $\mathcal{O}$ is given by

$$\dim[\mathcal{O}] = 2\left(1 + \frac{\kappa^2}{K}\right) \tag{3.27}$$

On the other hand, the kinetic energy of the fermions is given by the usual quadratic dispersion. Using the scaling dimension of the fermion fields, $\dim[\psi] = 1/2$, we get

$$\dim[\psi^\dagger\partial_x^2\psi] = 3 \tag{3.28}$$

Comparing the scaling dimensions of the pair transfer operator $\mathcal{O}$, cf. Eq. (3.27), and the kinetic energy $\psi^\dagger\partial_x^2\psi$, cf. Eq. (3.28), we can now give an estimate for the relevance or irrelevance of the pair transfer term with respect to the kinetic term in the Hamiltonian:

$$\begin{aligned} \kappa^2 < \frac{K}{2}: &\quad \mathcal{O} \text{ relevant} \\ \kappa^2 > \frac{K}{2}: &\quad \mathcal{O} \text{ irrelevant} \end{aligned} \tag{3.29}$$

In the strong coupling limit, $\kappa \to 0$, the transfer of pairs of electrons is a relevant interaction process and has to be taken into account. On the other hand, in the weak coupling limit, $\kappa \to 1$, the pair transfer operator becomes less relevant and we are left with the usual density-density interaction between the two subbands, see Fig. 3.2.

In order to better understand the quantum phase transition at $\mu = \mu_c$ and the emerging gap between the two bands, we follow a perturbative approach starting from the strong coupling limit $\kappa \to 0$. As we have seen in the previous section, the pair transfer of electrons is a relevant interaction process in the strong coupling limit which we thus have to take into account in the following analysis. In order to

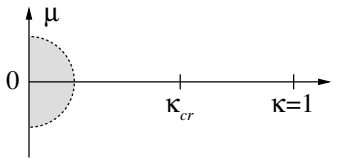

Figure 3.2: Parameters of our model. The points $\kappa = 0$ and $\kappa = 1$ correspond to the strong and weak coupling limits, respectively. For $\kappa < \kappa_{\rm cr}$ the pair transfer of electrons between the subbands is a more relevant term in the Hamiltonian than the kinetic energy. The chemical potential μ tunes the distance to quantum criticality at $\mu = 0$. The shaded area depicts the strong coupling regime we are interested in.

make calculations as simple as possible we perform a unitary transformation which removes the phase factor $e^{i2\theta}$. This leads to the effective interaction

$$\mathcal{H}_{\rm el-pl} = \lambda \int dx\, (\partial_x \phi)\psi^\dagger \psi \tag{3.30}$$

where the renormalized coupling constant is given by

$$\lambda = \gamma_x - \frac{v_{F1}}{K^2} = -\frac{v_{F1}\kappa}{K^2} \tag{3.31}$$

Note that the strong coupling limit corresponds to small values of λ. Thus, the Hamiltonian describing the fermions at the bottom of the upper band reads

$$\mathcal{H}_{\rm el} = \int dx\, \psi^\dagger \left(-\frac{1}{2m}\partial_x^2 - \mu\right)\psi + \gamma_t \int dx \left\{[(\partial_x\psi)\psi - \psi\partial_x\psi] + \text{h.c.}\right\} \tag{3.32}$$

Note that in the vicinity of the quantum critical point μ_c, i.e. for small μ, we can neglect the quadratic dispersion of the upper subband because it is less relevant than the pair transfer term. In other words, the kinetic energy scales like $k_{F2}^2 \sim \mu$ and thus faster to zero than the pair transfer term which scales like $k_{F2} \sim \sqrt{\mu}$. Hence, we are left with a Hamiltonian of critical Ising fermions,

$$\mathcal{H}_{\rm el} = -\mu \int dx\, \psi^\dagger \psi + \gamma_t \int dx \left\{[(\partial_x\psi)\psi - \psi\partial_x\psi] + \text{h.c.}\right\} \tag{3.33}$$

3.4 Action of the Two-Band Quantum Wire

To sum up, let us consider the action of a model of interacting spin-polarized fermions. The action of a quantum wire is given by $\mathcal{S} = \int_0^\beta d\tau \mathcal{L}$ where the Lagrangian consists of three parts, $\mathcal{L} = \mathcal{L}_{\rm pl} + \mathcal{L}_{\rm el} + \mathcal{L}_{\rm el-pl}$. The first part describes the low-energy excitations of the lower subband in terms of plasmons,

$$\mathcal{L}_{\rm pl} = \frac{1}{2}\int dx\, \frac{1}{\pi K v}\left[(\partial_\tau\phi)^2 + v^2(\partial_x\phi)^2\right] \tag{3.34}$$

where $v = v_{F1}/K$ is the plasmon velocity, v_{F1} is the Fermi velocity in the first subband, and K is the Luttinger liquid parameter. The Lagrangian $\mathcal{S}_{\rm el}$ describes

the excitations of the second subband in terms of Ising fermions,

$$\mathcal{L}_{\text{el}} = \int dx\, \psi^\dagger(\partial_\tau - \mu)\psi + \gamma_t \int dx\, \left\{[(\partial_x\psi)\psi - \psi\partial_x\psi] + \text{h.c.}\right\} \tag{3.35}$$

where the chemical potential μ tunes the distance to quantum criticality at μ_c. Finally, the interaction between electrons and plasmons is given by

$$\mathcal{L}_{\text{el}-\text{pl}} = \lambda \int dx\, (\partial_x\phi)\psi^\dagger\psi \tag{3.36}$$

For the following calculations we will need the action in Fourier space. Using the Fourier transformation identity

$$\begin{aligned} f(x,\tau) &= \frac{1}{\beta L}\sum_{k,\omega_n} e^{i(kx-\omega_n\tau)} f_{k,\omega_n} \\ f_{k,\omega_n} &= \int_0^\beta d\tau \int dx\, e^{-i(kx-\omega_n\tau)} f(x,\tau) \end{aligned} \tag{3.37}$$

where L is the one-dimensional volumen of our model and $\beta = 1/(k_B T)$ is the inverse of temperature, our model $\mathcal{S} = \mathcal{S}_{\text{pl}} + \mathcal{S}_{\text{el}} + \mathcal{S}_{\text{el}-\text{pl}}$ is given by

$$\mathcal{S}_{\text{pl}} = \frac{1}{2}\frac{1}{\beta L}\sum_{q,\Omega_n} \phi^*_{q,\Omega_n}\mathcal{D}_0^{-1}(q,\Omega_n)\phi_{q,\Omega_n} \tag{3.38}$$

$$\mathcal{S}_{\text{el}} = \frac{1}{2}\frac{1}{\beta L}\sum_{k,\omega_n} \Psi^\dagger_{k,\omega_n}\mathcal{G}_0^{-1}(k,\omega_n)\Psi_{k,\omega_n} \tag{3.39}$$

$$\mathcal{S}_{\text{el}-\text{pl}} = \frac{1}{2}\frac{1}{(\beta L)^2}\sum_{q,\Omega_n}\sum_{k,\omega_n} \Gamma_0(q,\Omega_n;k,\omega_n) iq\phi_{q,\Omega_n}\Psi^\dagger_{k+q,\omega_n+\Omega_n}\sigma^3\Psi_{k,\omega_n} \tag{3.40}$$

where we introduced a Nambu spinor notation for the Ising fermions:

$$\Psi^\dagger_{k,\omega_n} = (\psi^\dagger_{k,\omega_n}, \psi_{-k,-\omega_n}), \quad \Psi_{k,\omega_n} = \begin{pmatrix} \psi_{k,\omega_n} \\ \psi^\dagger_{-k,-\omega_n} \end{pmatrix} \tag{3.41}$$

The plasmon and fermion propagators and the interaction vertex are defined by

$$\mathcal{D}_0(q,\Omega_n) = \frac{-\pi K v}{(i\Omega_n)^2 - (vq)^2} \tag{3.42}$$

$$\mathcal{G}_0(k,\omega_n) = \frac{1}{(i\omega_n)^2 - \omega_k^2}\left[-i\omega_n \mathbb{1} + \mu\sigma^3 - uk\sigma^2\right] \tag{3.43}$$

$$\Gamma_0(q,\Omega_n;k,\omega_n) = \lambda \tag{3.44}$$

where $u \equiv 4\gamma_t$ is the fermion velocity, and the eigenenergies of the Ising fermions are given by $\omega_k = \sqrt{\mu^2 + (uk)^2}$. Finally, σ^i are the usual Pauli matrices defined by

$$\sigma^1 = \begin{pmatrix} 0 & 1 \\ 1 & 0 \end{pmatrix}, \quad \sigma^2 = \begin{pmatrix} 0 & -i \\ i & 0 \end{pmatrix}, \quad \sigma^3 = \begin{pmatrix} 1 & 0 \\ 0 & -1 \end{pmatrix} \tag{3.45}$$

Chapter 4

Perturbative Renormalization Group Analysis

In this chapter, we use renormalization group methods to study our model of a two-band quantum wire. In order to become acquainted with the renormalization group, we start with a brief description of the general idea of renormalization group methods in Sec. 4.1. In Sec. 4.2, we perform a perturbative approach to the strong coupling limit of the model and calculate the leading-order self-energy corrections for the plasmons and fermions as well as the vertex correction. In Sec. 4.3, we then renormalize our theoretical model. With different conditions we obtain complementary but equivalent sets of β functions which describe the flow of coupling constants under subsequent renormalization group transformation. Finally, in Sec. 4.4, we discuss the solutions of these sets of β functions. It turns out that our model is described most easily when we allow for a generic dynamical exponent z.

4.1 Renormalization Group: General Idea

Let us consider a cubic lattice in d dimensions with a real scalar field $\phi(r_n)$ at each site labeled by the vector r_n. The classical statistical mechanics of this system is described by the partition function $\mathcal{Z} = \int \mathcal{D}(\phi(r_n))\, e^{-\mathcal{S}(\phi(r_n))}$ where $\mathcal{D}(\phi(r_n)) \equiv \prod_{r_n} d\phi(r_n)$ is the integration measure, and $\mathcal{S}$ is the action of the system. For a finite number of sites $\mathcal{S}$ is a regular function and $\mathcal{Z}$ a multiple integral. However, in the limit of infinite sites, the action becomes a functional and the partition function a functional integral. Note that one can also describe quantum-mechanical problems in d spatial dimensions as a functional integral of classical configurations in $d+1$ dimensions where dimension $d+1$ is then imaginary time.

In condensed matter physics we are often interested only in the physics at long distances compared to the lattice spacing. A typical quantity one is interested in is the two-point correlation function or *propagator* $G(r) = G(r_1 - r_2) = \langle \phi(r_1)\phi(r_2) \rangle$.

For large spatial separations the two-point correlation function typically falls off exponentially as

$$G(r_1 - r_2) \sim e^{-|r_1 - r_2|/\xi} \tag{4.1}$$

where ξ is the so-called *correlation length*. However, the leading behavior of the correlation function changes drastically in the vicinity of a critical point. Here, it falls off as a power law,

$$G(r_1 - r_2) \sim \frac{1}{|r_1 - r_2|^x} \tag{4.2}$$

where x is a *critical exponent*. Likewise, other critical exponents may characterize other power laws of different correlation functions at the critical point.

Since we are interested in the large-distance behavior of such correlation functions let us define two sets of variables for modes with small and large momentum, respectively:

$$\begin{aligned} \phi_<(k) &= \phi(k) \quad \text{for } k \in [0, \Lambda/b] \text{ (slow modes)} \\ \phi_>(k) &= \phi(k) \quad \text{for } k \in [\Lambda/b, \Lambda] \text{ (fast modes)} \end{aligned} \tag{4.3}$$

Here, Λ is a momentum cutoff and $0 < \ln b \ll 1$ is the control parameter of the renormalization group. The first step in the renormalization group scheme is to integrate out the fast modes and obtain an effective action for the slow modes. In a formal way, let us consider the action as follows:

$$\mathcal{S}(\phi) = \mathcal{S}(\phi_<, \phi_>) = \mathcal{S}_0(\phi_<) + \mathcal{S}_0(\phi_>) + \mathcal{S}_{\text{int}}(\phi_<, \phi_>) \tag{4.4}$$

with $\mathcal{S}_0$ being a quadratic function of its arguments that separates into a slow and a fast piece, and $\mathcal{S}_{\text{int}}$ contains the interaction which mixes both slow and fast modes. The partition function can thus be rewritten as

$$\mathcal{Z} = \int \mathcal{D}(\phi_<)\mathcal{D}(\phi_>)\, e^{-[\mathcal{S}_0(\phi_<) + \mathcal{S}_0(\phi_>) + \mathcal{S}_{\text{int}}(\phi_<, \phi_>)]} = \mathcal{Z}_{0>} \int \mathcal{D}(\phi_<)\, e^{-\mathcal{S}_{\text{eff}}(\phi_<)} \tag{4.5}$$

where $\mathcal{Z}_{0>}$ is the partition function of the fast modes. The effective action $\mathcal{S}_{\text{eff}}(\phi_<)$ is thus given by

$$e^{\mathcal{S}_{\text{eff}}(\phi_<)} = e^{\mathcal{S}_0(\phi_<)} \left\langle e^{\mathcal{S}_{\text{int}}(\phi_<, \phi_>)} \right\rangle_{0>} \tag{4.6}$$

Here, $\langle \cdots \rangle_{0>}$ denotes the functional average with respect to the fast modes. Let us assume in the following discussion that the theory is *renormalizable*, i.e. that the physical quantities are independent of the cutoff upon taking the limit $\Lambda \to \infty$ [23]. This implies that the effective action S_{eff} is of the same form as the initial action up to irrelevant terms generated by integrating out the fast modes.

After performing this mode elimination, the effective action $S_{\text{eff}}(\phi_<)$ provides a good description of the low-energy physics. However, if we compare the old and new theory we see immediately that they are defined on two different kinematical

regions, and thus we cannot compare the various parameters in the interactions. In order to solve this problem we rescale momenta after the mode elimination,

$$k' = bk \tag{4.7}$$

such that k' runs over the same momentum range $[0, \Lambda]$ as the initial momentum k did before mode elimination. Having restored the initial momentum cutoff Λ there remains just one more problem. Certain changes in the parameters are not of physical importance because they can be absorbed by field rescaling. To eliminate this problem let us define new fields,

$$\phi'(k') = \mathcal{N}^{-1}\phi_<(k'/b) \tag{4.8}$$

and choose $\mathcal{N}$ such that a certain coupling, e.g. the kinetic term in the quadratic part of the action has a fixed coefficient. The final effective action $\mathcal{S}$ will then be expressed in terms of these new fields.

In the final analysis of the renormalization group the so-called β *function* plays a central role. For a generic coupling constant g it is defined as

$$\beta(g) = \frac{dg}{dl} \tag{4.9}$$

where $l = \ln b$ is the logarithmic control parameter of the renormalization group transformation. Note that throughout this chapter we use the convention that upon increasing l the momentum cutoff Λ decreases.

To sum up, the renormalization group program is a three stage process: In the first step one eliminiates the fast modes, i.e. reduces the momentum cutoff from Λ to Λ/b. Then one rescales momenta, $k' = bk$, which restores the initial cutoff. Afterwards, one introduces rescaled fields $\phi'(k')$ and rewrites the effective action in terms of them which then has the same coefficient for a certain quadratic term. Finally, one can infer from the renormalized effective action the β functions for the coupling constants of the system.

With this definition of the renormalization group scheme we have a mapping of the initial action defined in a certain phase space to actions in the same phase space but with renormalized couplings. Thus, representing the initial action as a point in a coupling constant space, this point will flow to another point in the same space under renormalization group transformation. The flow of coupling constants as described by the β functions opens up the possibility of *fixed points*. These are points at which the action remains unchanged under a renormalization group transformation. Physically, if the system had a correlation length ξ it must be either zero or infinite at the fixed point since it must remain the same under a renormalization group transformation. Due to this divergence fixed points play a special role in the renormalization group flow.

First, there are *stable* fixed points, i.e. attractive points in the coupling constant space. Starting with an action in the coupling space somewhere near to the fixed point, the action will flow towards and, at least asymptotically, reach the fixed point. Couplings which are renormalized to zero are called *irrelevant* since they make no difference in the long-range properties. Physically, looking on larger and larger length scales the system resembles more and more the infinitely large correlations. Complementary to the stable fixed points are the *unstable* fixed points. Any deviation in coupling constant space from the fixed point values will force the action to flow away from it. A coupling that gets amplified under renormalization group transformation is called *relevant*. The long-distance behavior of correlation functions typically corresponds to exponential decay. Finally, there exists a class of generic fixed points with both relevant and irrelevant couplings. These points are of particular interest since they can be associated with phase transitions. In the general problem, there can also be *marginal* perturbations which neither grow nor decay under the renormalization group transformation.

This concludes our brief summary of the concept renormalization group methods. However, there are a lot of interesting points such as critical phenomena and phase transitions which can be studied in the framework of renormalization group. A variety of applications of renormalization group methods has been the focus of many textbooks and reviews, see e.g. [11, 22].

4.2 Perturbative Approach

We consider the model of a spinless electrons in a two-band quantum wire. The action of the system consists of three parts, $\mathcal{S} = \mathcal{S}_{\text{pl}} + \mathcal{S}_{\text{el}} + \mathcal{S}_{\text{el-pl}}$. The first part describes the density excitations of the lower subband as plasmons with acoustic spectrum,

$$\mathcal{S}_{\text{pl}} = \frac{1}{2}\frac{1}{\beta L}\sum_{q,\Omega_n} \phi^*_{q,\Omega_n} \mathcal{D}_0^{-1}(q,\Omega_n)\phi_{q,\Omega_n} \tag{4.10}$$

where $\mathcal{D}_0$ is the plasmon propagator defined as

$$\mathcal{D}_0(q,\Omega_n) = \frac{-\pi K v}{(i\Omega_n)^2 - (vq)^2} \tag{4.11}$$

Here, L is the one-dimensional volume or length of our model, $\beta = 1/(k_B T)$ is the inverse of temperature, $v = v_{F1}/K$ is the plasmon velocity, v_{F1} is the Fermi velocity in the first (lower) subband, and K is the Luttinger liquid parameter. The second part, $\mathcal{S}_{\text{el}}$, represents the excitations of the second subband in terms of Ising fermions,

$$\mathcal{S}_{\text{el}} = \frac{1}{2}\frac{1}{\beta L}\sum_{k,\omega_n} \Psi^\dagger_{k,\omega_n} \mathcal{G}_0^{-1}(k,\omega_n)\Psi_{k,\omega_n} \tag{4.12}$$

where the fermion propagator $\mathcal{G}_0$ is defined as

$$\mathcal{G}_0(k,\omega_n) = \frac{1}{(i\omega_n)^2 - \omega_k^2}\left[-i\omega_n \mathbb{1} + \mu\sigma^3 - uk\sigma^2\right] \tag{4.13}$$

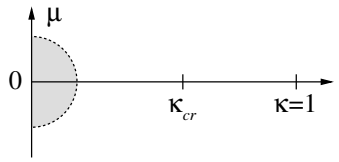

Figure 4.1: Parameters for our model of interacting electrons in a two-band quantum wire. The points $\kappa = 0$ and $\kappa = 1$ correspond to the strong and weak coupling limits, respectively. There exists a multicritical point at $(\kappa, \mu) = (\kappa_{\rm cr}, 0)$ where for $\kappa > \kappa_{\rm cr}$ the electron pair transfer operator becomes less relevant than the quadratic dispersion of the fermions. The chemical potential μ tunes the distance to quantum criticality at $\mu = \mu_c = 0$. The inter-band density-density coupling $\lambda \sim \kappa$ is treated perturbatively in a renormalization group approach (shaded area).

with u the fermion velocity and $\omega_k = \sqrt{\mu^2 + (uk)^2}$ the eigenenergies. The chemical potential μ tunes the distance to quantum criticality. Note that we introduced here a Nambu spinor notation for the Ising fermions:

$$\Psi^\dagger_{k,\omega_n} = (\psi^\dagger_{k,\omega_n}, \psi_{-k,-\omega_n}), \quad \Psi_{k,\omega_n} = \begin{pmatrix} \psi_{k,\omega_n} \\ \psi^\dagger_{-k,-\omega_n} \end{pmatrix} \tag{4.14}$$

Finally, the interaction between the plasmons and Ising fermions is given by

$$\mathcal{S}_{\rm el-pl} = \frac{1}{2}\frac{1}{(\beta L)^2}\sum_{q,\Omega_n}\sum_{k,\omega_n}\Gamma_0(q,\Omega_n;k,\omega_n) iq\phi_{q,\Omega_n}\Psi^\dagger_{k+q,\omega_n+\Omega_n}\sigma^3\Psi_{k,\omega_n} \tag{4.15}$$

with the bare coupling constant

$$\Gamma_0(q,\Omega_n;k,\omega_n) = \lambda \tag{4.16}$$

We now turn to the calculation of the one-loop order self-energies and vertex corrections in a perturbative approach. In the strong coupling limit, i.e. $\kappa \to 0$, we perform perturbation theory in the small inter-band density-density coupling $\lambda \sim \kappa$ (cf. Eq. (3.31)), and we obtain perturbative corrections for the fermion and plasmon propagators as well as the interaction vertex. In general, the self-energy is defined as the difference between the bare propagator in the non-interacting system and the propagator in the interacting system, and thus it describes the renormalization effects of the bare propagator due to interactions. In Sec. 4.2.1 and 4.2.2, we calculate these self-energy corrections for the plasmons, Π, and for the fermions, Σ, to leading order in λ. In Sec. 4.2.3, we calculate the leading-order vertex correction, $\delta\Gamma$. Both leading-order self-energies and the vertex correction contain logarithmic divergencies which are evaluated with a hard momentum cutoff. For detailed calculations on the leading order corrections see App. A. Finally, we obtain the modified plasmon and fermion propagators and interaction vertex.

4.2.1 Plasmon Self-Energy

The self-energy for the plasmons, Π, is given by the Dyson equation,

$$\mathcal{D}^{-1}(q,\Omega_n) = \mathcal{D}_0^{-1}(q,\Omega_n) - \Pi(q,\Omega_n) \tag{4.17}$$

Here, $\mathcal{D}$ is the full propagator and $\mathcal{D}_0$ is the bare plasmon propagator as defined by the corresponding plasmon action. Performing perturbation theory in λ, the plasmon self-energy in a one-loop order expansion reads (cf. Fig. 4.2)

$$\Pi(q,\Omega_n) = -\frac{1}{2!}\lambda^2 q^2 \frac{1}{\beta L}\sum_{k,\omega_n} \mathrm{Tr}\{\sigma^3 \mathcal{G}_0(k,\omega_n)\sigma^3 \mathcal{G}_0(k+q,\omega_n+\Omega_n)\} \tag{4.18}$$

$$= -\lambda^2 q^2 \frac{1}{\beta L}\sum_{k,\omega_n} \frac{i\omega_n(i\omega_n+i\Omega_n) - u^2 k(k+q) + \mu^2}{[(i\omega_n)^2-\omega_k^2][(i\omega_n+i\Omega_n)^2-\omega_{k+q}^2]} \tag{4.19}$$

Since we are interested in the large distance and large time behavior of the system, we consider the external momentum q and frequence $i\Omega_n$ to be small compared to a momentum cutoff Λ. Thus, let us carry out a Taylor expansion for small momentum q and frequency Ω_n. In the vicinity of the quantum critical point, $\mu = 0$, the leading-order term of the plasmon self-energy reads

$$\Pi(q,\Omega_n) = -\lambda^2 q^2 \frac{1}{\beta L}\sum_{k,\omega_n} \frac{(i\omega_n)^2 - u^2 k(k+q) + \mu^2}{[(i\omega_n)^2-\omega_k^2][(i\omega_n)^2-\omega_{k+q}^2]}$$

The summation over fermionic Matsubara frequencies, $\omega_n = (2n+1)\pi/\beta$, is performed in a standard way [11]. Rewriting the sum over ω_n as a contour integral in complex frequency space we obtain

$$\frac{1}{\beta}\sum_{\omega_n} \frac{(i\omega_n)^2 - u^2 k(k+q) + \mu^2}{[(i\omega_n)^2-\omega_k^2][(i\omega_n)^2-\omega_{k+q}^2]} = -\int \frac{dz}{2\pi i}\, n_F(z) \frac{z^2 - u^2 k(k+q) + \mu^2}{[z^2-\omega_k^2][z^2-\omega_{k+q}^2]}$$

$$= \sum_{\alpha=\pm 1}\left[n_F(\alpha\omega_k)\frac{\omega_k^2 - u^2 k(k+q) + \mu^2}{2\alpha\omega_k(\omega_k^2-\omega_{k+q}^2)} + n_F(\alpha\omega_{k+q})\frac{\omega_{k+q}^2 - u^2 k(k+q) + \mu^2}{2\alpha\omega_{k+q}(\omega_{k+q}^2-\omega_k^2)}\right]$$

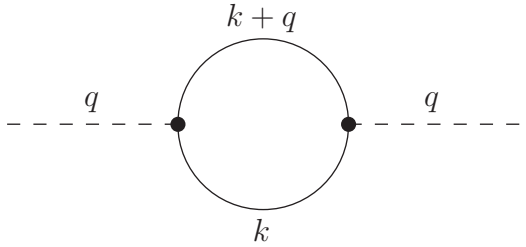

Figure 4.2: Leading-order self-energy diagram for the plasmons, Π. (Fermion fields are depicted by solid lines, plasmon fields by dashed lines, and the interaction vertex is depicted by a dot.)

where $n_{F/B}(\epsilon) = \left(1 \pm e^{\beta\epsilon}\right)^{-1}$ are the Fermi and Bose occupation factors, respectively. At zero temperature both occupation factors take a simple form,

$$n_{F/B}(\epsilon) \to \pm\Theta(-\epsilon) \quad \text{for} \quad \beta \to \infty \tag{4.20}$$

where $\Theta(x)$ is the Heaviside step function. Therefore, the plasmon self-energy (4.19) at zero temperature is equal to

$$\Pi(q, \Omega_n) = \lambda^2 q^2 \frac{1}{L} \sum_k \left[\frac{\omega_k^2 - u^2 k(k+q) + \mu^2}{2\omega_k(\omega_k^2 - \omega_{k+q}^2)} + \frac{\omega_{k+q}^2 - u^2 k(k+q) + \mu^2}{2\omega_{k+q}(\omega_{k+q}^2 - \omega_k^2)} \right]$$

The remaining momentum integral contains a logarithmic divergence for large k. This ultraviolet divergence can be evaluated with a hard spatial momentum cutoff Λ. Assuming that the external momentum q is small compared to the cutoff Λ the logarithmic divergence of the plasmon self-energy is given by

$$\Pi(q, \Omega_n) \approx \lambda^2 q^2 \int_{-\Lambda}^{\Lambda} \frac{dk}{2\pi} \frac{1}{2|u||k|} = \frac{\lambda^2 q^2}{2\pi|u|} \ln \Lambda \tag{4.21}$$

Thus, the Green function of the interacting system reads (cf. Eq. (4.17))

$$\mathcal{D}^{-1}(q, \Omega_n) = \frac{-1}{\pi K v} \left[(i\Omega_n)^2 - \left(1 - \frac{\lambda^2 K}{2|u|v} \ln \Lambda \right) (vq)^2 \right] \tag{4.22}$$

For a detailed calculation of the plasmon self-energy see Appendix A.1.

4.2.2 Fermion Self-Energy

Similar to the plasmon self-energy, the self-energy for the fermions, Σ, is given by

$$\mathcal{G}^{-1}(k, \omega_n) = \mathcal{G}_0^{-1}(k, \omega_n) - \Sigma(k, \omega_n) \tag{4.23}$$

where $\mathcal{G}$ is the full propagator and $\mathcal{G}_0$ is the bare fermion propagator as defined by the fermion action. In a one-loop order expansion, the fermion self-energy Σ reads (cf. Fig. 4.3)

$$\Sigma(k, \omega_n) = \lambda^2 \frac{1}{\beta L} \sum_{q, \Omega_n} q^2 \mathcal{D}_0(q, \Omega_n) \sigma^3 \mathcal{G}_0(k+q, \omega_n + \Omega_n) \sigma^3 \tag{4.24}$$

$$= \lambda^2 \frac{1}{\beta L} \sum_{q, \Omega_n} q^2 \frac{-\pi K v}{(i\Omega_n)^2 - (vq)^2} \frac{-(i\omega_n + i\Omega_n)\mathbb{1} + \mu\sigma^3 + u(k+q)\sigma^2}{(i\omega_n + i\Omega_n)^2 - \omega_{k+q}^2} \tag{4.25}$$

The summation of bosonic Matsubara frequencies, $\Omega_n = 2n\pi/\beta$, is again performed by means of a contour integral. However, one has to take care since the Bose occupation factor changes into a Fermi factor upon adding a fermionic Matsubara frequencu in its argument:

$$n_B(z + i\omega_n) = -n_F(z) \tag{4.26}$$

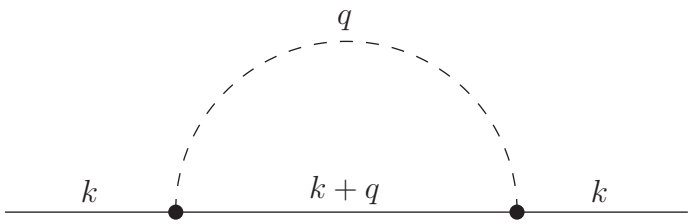

Figure 4.3: Leading-order self-energy diagram for the Ising fermions, Σ. (Fermion fields are depicted by solid lines, plasmon fields by dashed lines, and the interaction vertex is depicted by a dot.)

After performing the Matsubara summation one can then carry out a Taylor expansion for small external momentum k and frequency ω_n and evaluate the remaining momentum integral. As for the plasmon self-energy, the remaining momentum integral over q contains a logarithmic ultraviolet divergence which can be extracted by using the same momentum cutoff Λ. The leading-order term in the self-energy at zero temperature for fermions is given by

$$\Sigma(k,\omega_n) \approx -\frac{\lambda^2 K}{2(v+|u|)^2}\left[-i\omega_n \mathbb{1} + \frac{v+|u|}{|u|}\,\mu\sigma^3 - uk\sigma^2\right]\ln\Lambda \tag{4.27}$$

Thus, to leading order in λ the modified Green function at zero temperature reads

$$\begin{aligned}\mathcal{G}^{-1}(k,\omega_n) = &\left(1+\frac{\lambda^2 K}{2(v+|u|)^2}\ln\Lambda\right)(-i\omega_n)\mathbb{1} \\ &-\left(1-\frac{\lambda^2 K}{2|u|(v+|u|)}\ln\Lambda\right)\mu\sigma^3 + \left(1-\frac{\lambda^2 K}{2(v+|u|)^2}\ln\Lambda\right)uk\sigma^2\end{aligned} \tag{4.28}$$

For a detailed calculation of the fermion self-energy see Appendix A.2.

4.2.3 Vertex Correction

Finally, the vertex correction $\delta\Gamma$ to the interaction is defined by

$$\Gamma(q,\Omega_n;k,\omega_n) = \Gamma_0(q,\Omega_n;k,\omega_n) + \delta\Gamma(q,\Omega_n;k,\omega_n) \tag{4.29}$$

where Γ denotes the full interaction and Γ_0 is the bare interaction vertex. The vertex correction in a one-loop order expansion is given by (cf. Fig. 4.4)

$$\begin{aligned}\delta\Gamma(q,\Omega_n;k,\omega_n) = &\frac{1}{2!}\lambda^3\frac{1}{\beta L}\sum_{q',\Omega_n'} q'^2\mathcal{D}_0(q',\Omega_n') \\ &\times \mathrm{Tr}\big\{\sigma^3\mathcal{G}_0(k+q',\omega_n+\Omega_n')\sigma^3\mathcal{G}_0(k+q+q',\omega_n+\Omega_n+\Omega_n')\big\}\end{aligned} \tag{4.30}$$

The Matsubara summation is performed in the same way as in the previous sections. Since the interaction is a marginal term in the Hamiltonian, it suffices to

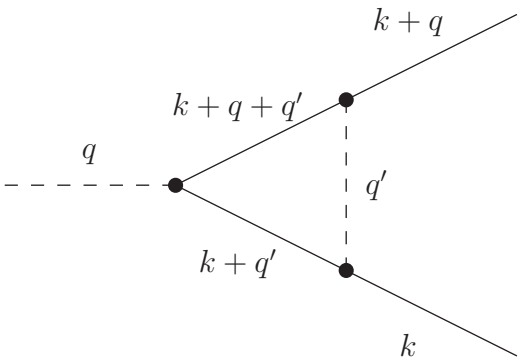

Figure 4.4: Leading-order self-energy diagram for the vertex correction, $\delta\Gamma$.

set the external momenta and frequencies to zero in order to obtain the leading-order behavior of $\delta\Gamma$. After evaluating the remaining ultraviolet divergence of the momentum integral with a hard momentum cutoff Λ the vertex correction at zero temperature reads

$$\delta\Gamma(q,\Omega_n;k,\omega_n) \approx -\frac{\lambda^3 K}{2|u|(v+|u|)}\ln\Lambda \tag{4.31}$$

To leading order in λ, the modified interaction vertex at zero temperature is

$$\Gamma(q,\Omega_n;k,\omega_n) = \lambda\left(1-\frac{\lambda^2 K}{2|u|(v+|u|)}\ln\Lambda\right) \tag{4.32}$$

For a detailed calculation of the vertex correction see Appendix A.3.

4.3 Renormalization of the Theory

Let us now turn to a renormalization group analysis of our model. According to the general renormalization group scheme, we integrate out in a first step the fast modes which lie in the momentum shell $[\Lambda/b,\Lambda]$ with $0<\ln b\ll 1$. This mode elimination leads to perturbative corrections to the Green functions and to the interaction vertex in the form given by Eqs. (4.22), (4.28) and (4.32), but with the cutoff Λ replaced by b. In a second step, we rescale momentum

$$k' = bk, \quad q' = bq \tag{4.33}$$

and frequency

$$\omega_n' = b^{\tilde{z}}\omega_n, \quad \Omega_n' = b^{\tilde{z}}\Omega_n \tag{4.34}$$

in order to restore the momentum cutoff Λ for the slow modes. Note that we rescale frequencies with a generic scale $b^{\tilde{z}}$. Later it will turn out that the particular choice of a non-universal exponent $\tilde{z}$ allows for an easier interpretation of the β functions. Finally, we rescale the slow bosonic field by

$$\phi'(q',\Omega_n') = Z_B^{-1/2} b^{-(3+\tilde{z})/2}\phi(q'/b,\Omega_n'/b^{\tilde{z}}) \tag{4.35}$$

and the slow fermionic fields by

$$\Psi'(k',\omega_n') = Z_F^{-1/2} b^{-(2+\tilde{z})/2} \Psi(k'/b, \omega_n'/b^{\tilde{z}}) \tag{4.36}$$

$$\Psi'^{\dagger}(k',\omega_n') = Z_F^{-1/2} b^{-(2+\tilde{z})/2} \Psi^{\dagger}(k'/b, \omega_n'/b^{\tilde{z}}) \tag{4.37}$$

Here, the renormalization parameters Z_B and Z_F are left unspecified for the moment. This rescaling of momenta, frequencies and fields leads to an effective theory for the slow modes but with renormalized Green function and interaction vertex given by

$$\mathcal{D}'^{-1}(q',\Omega_n') = \frac{-Z_B}{\pi K v}\left[b^{2(1-\tilde{z})}(i\Omega_n')^2 - \left(1 - \frac{\lambda^2 K}{2|u|v}\ln b\right)(vq')^2\right] \tag{4.38}$$

$$\begin{aligned}\mathcal{G}'^{-1}(k',\omega_n') = Z_F\Bigg[&\left(1 + \frac{\lambda^2 K}{2(v+|u|)^2}\ln b\right) b^{1-\tilde{z}}(-i\omega_n')\mathbb{1} \\ &- \left(1 - \frac{\lambda^2 K}{2|u|(v+|u|)}\ln b\right) b\mu\sigma^3 + \left(1 - \frac{\lambda^2 K}{2(v+|u|)^2}\ln b\right) uk'\sigma^2\Bigg]\end{aligned} \tag{4.39}$$

$$\Gamma'(q',\Omega_n';k',\omega_n') = Z_B^{1/2} Z_F b^{(1-\tilde{z})/2}\lambda\left(1 - \frac{\lambda^2 K}{2|u|(v+|u|)}\ln b\right) \tag{4.40}$$

Note that the factor of b accompanying the chemical potential μ reflects its engineering scaling dimension. In order to continue our analysis we have to specify renormalization conditions on the Green functions and the interaction vertex. In the following we will discuss three different choices for $\tilde{z}$, Z_B and Z_F. Note that the physics in our model remains unaffected by the choice of a particular set of renormalization conditions. However, as we see below the renormalization group flow is easier to interpret under certain conditions.

4.3.1 Renormalization Conditions: Set I

Our first ansatz towards a renormalization of the theory is the choice to set the exponent to unity, $\tilde{z} = 1$, and to fix the prefactors in front of the frequency dependence of both Green funtions in the following way:

$$\mathcal{D}'^{-1}(q',\Omega_n')\Big|_{q'=0} = \frac{-1}{\pi K' v'}(i\Omega_n')^2 = \frac{-1}{\pi K v}(i\Omega_n')^2 \tag{4.41a}$$

$$\mathcal{G}'^{-1}(k',\omega_n')\Big|_{k'=0} = -i\omega_n'\mathbb{1} \tag{4.41b}$$

In the last equation we considered the quantum critical point where $\mu = 0$. These conditions can be satisfied by setting

$$Z_F^{-1} = 1 + \frac{\lambda^2 K}{2(v+|u|)^2}\ln b \tag{4.42a}$$

$$Z_B^{-1} = 1 \tag{4.42b}$$

Note that this renormalization conditions imply in particular that the combination

$$K'v' = Kv = v_{F1} \tag{4.43}$$

is an invariant of the renormalization group flow. The effective theory for the slow modes now takes the same form as the original one but with the following renormalized parameters:

$$v'^2 = v^2\left(1 - \frac{\lambda^2 v_{F1}}{2|u|v^2}\ln b\right) \tag{4.44a}$$

$$u' = u\left(1 - \frac{\lambda^2 v_{F1}}{v(v+|u|)^2}\ln b + \mathcal{O}\big((\ln b)^2\big)\right) \tag{4.44b}$$

$$\mu' = \mu\left[1 + \left(1 - \frac{\lambda^2 v_{F1}}{2|u|v(v+|u|)} - \frac{\lambda^2 v_{F1}}{2v(v+|u|)^2}\right)\ln b + \mathcal{O}\big((\ln b)^2\big)\right] \tag{4.44c}$$

$$\lambda' = \lambda\left[1 - \left(\frac{\lambda^2 v_{F1}}{2|u|v(v+|u|)} + \frac{\lambda^2 v_{F1}}{2v(v+|u|)^2}\right)\ln b + \mathcal{O}\big((\ln b)^2\big)\right] \tag{4.44d}$$

Here we substituted the Luttinger liquid parameter K by the invariant v_{F1}. We can infer from the renormalized parameters the β functions as follows:

$$\beta(v) = -\frac{\lambda^2 v_{F1}}{4|u|v} \tag{4.45a}$$

$$\beta(u) = -\frac{\lambda^2 v_{F1} u}{v(v+|u|)^2} \tag{4.45b}$$

$$\beta(\mu) = \mu\left[1 - \frac{\lambda^2 v_{F1}}{2}\left(\frac{1}{v|u|(v+|u|)} + \frac{1}{v(v+|u|)^2}\right)\right] \tag{4.45c}$$

$$\beta(\lambda) = -\frac{\lambda^3 v_{F1}}{2}\left(\frac{1}{v|u|(v+|u|)} + \frac{1}{v(v+|u|)^2}\right) \tag{4.45d}$$

Note that $\beta(g) = \partial g/\partial \ln b$ as defined in Sec. 4.1.

4.3.2 Renormalization Conditions: Set II

Instead of fixing the Fermi velocity v_{F1} we can demand that the Luttinger liquid parameter K does not flow under renormalization group transformation. With $\tilde{z} = 1$ this implies the following conditions:

$$\mathcal{D}'^{-1}(q', \Omega'_n)\Big|_{q'=0} = \frac{-1}{\pi K v'}(i\Omega'_n)^2 \tag{4.46a}$$

$$\mathcal{G}'^{-1}(k', \omega'_n)\Big|_{k'=0} = -i\omega'_n \mathbb{1} \tag{4.46b}$$

In the last equation we again considered the quantum critical point, $\mu = 0$. These conditions can be satisfied by setting

$$Z_F^{-1} = 1 + \frac{\lambda^2 K}{2(v+|u|)^2}\ln b \tag{4.47a}$$

$$Z_B^{-1} = \frac{v'}{v} \tag{4.47b}$$

leading to renormalized parameters as follows:

$$v'^2 = v^2\left(1 - \frac{\lambda^2 K}{2v|u|}\ln b\right) \tag{4.48a}$$

$$u' = u\left(1 - \frac{\lambda^2 K}{(v+|u|)^2}\ln b\right) \tag{4.48b}$$

$$\mu' = \mu\left[1 + \left(1 - \frac{\lambda^2 K}{2|u|(v+|u|)} - \frac{\lambda^2 K}{2(v+|u|)^2}\right)\ln b + \mathcal{O}\big((\ln b)^2\big)\right] \tag{4.48c}$$

$$\lambda' = \lambda\left[1 - \left(\frac{\lambda^2 K}{2|u|(v+|u|)} + \frac{\lambda^2 K}{2(v+|u|)^2} - \frac{\lambda^2 K}{8v|u|}\right)\ln b + \mathcal{O}\big((\ln b)^2\big)\right] \tag{4.48d}$$

Note that in the derivation of λ' we used

$$Z_B^{1/2} = \left(1 - \frac{\lambda^2 v_{F1}}{2|u|v^2}\ln b\right)^{-1/4} \approx 1 + \frac{1}{4}\frac{\lambda^2 v_{F1}}{2|u|v}\ln b + \mathcal{O}\big((\ln b)^2\big)$$

The resulting β functions for this set of renormalization conditions thus read

$$\beta(v) = -\frac{\lambda^2 K}{4|u|} \tag{4.49a}$$

$$\beta(u) = -\frac{\lambda^2 K u}{(v+|u|)^2} \tag{4.49b}$$

$$\beta(\mu) = \mu\left[1 - \frac{\lambda^2 K}{2}\left(\frac{1}{|u|(v+|u|)} + \frac{1}{(v+|u|)^2}\right)\right] \tag{4.49c}$$

$$\beta(\lambda) = -\frac{\lambda^3 K}{2}\left(\frac{1}{|u|(v+|u|)} + \frac{1}{(v+|u|)^2} - \frac{1}{4|u|v}\right) \tag{4.49d}$$

Note that the β functions for the fermion and plasmon velocities v and u and for the chemical potential μ are equal to the β functions obtained in set I upon substituting $K = v_{F1}/v$. On the other hand, the β function for the coupling λ differs slightly in its form by an additional term. This is due to the fact that we used different conditions to fix the Luttinger liquid parameter K instead of the Fermi velocity $v_{F1} = Kv$.

4.3.3 Renormalization Conditions: Set III

Finally, we consider a third set where neither the plasmon velocity v nor the Luttinger liquid parameter K are allowed to flow under renormalization group transformations. Additionally, we fix the prefactor of the frequency dependence of the fermion Green function. This implies the conditions

$$\mathcal{D}'^{-1}(q', \Omega'_n)\Big|_{q'=0} = \frac{-1}{\pi K v}(i\Omega'_n)^2 \tag{4.50a}$$

$$\mathcal{D}'^{-1}(q', \Omega'_n)\Big|_{\Omega'_n=0} = \frac{1}{\pi K v}(vq')^2 \tag{4.50b}$$

$$\mathcal{G}'^{-1}(k', \omega'_n)\Big|_{k'=0} = -i\omega'_n \mathbb{1} \tag{4.50c}$$

and in the last equation we again considered the quantum critical point, $\mu = 0$. Note that in contrast to the sets I and II we allow here for a generic exponent $\tilde{z}$. By setting

$$b^{2(1-\tilde{z})} = Z_B^{-1} \tag{4.51a}$$

$$Z_F^{-1} = 1 + \frac{\lambda^2 K}{2(v+|u|)^2} \ln b \tag{4.51b}$$

$$Z_B^{-1} = 1 - \frac{\lambda^2 K}{2|u|v} \ln b \tag{4.51c}$$

these conditions are satisfied. Solving the first condition one obtains the exponent

$$\tilde{z}(b) = 1 + \frac{\lambda^2(b) K}{4v|u(b)|} + \mathcal{O}(\ln b) \tag{4.52}$$

Note that this exponent now is explicitly interaction-dependent. In set III, the renormalized parameters of the system are given by

$$v' = v \tag{4.53a}$$

$$u' = u\left[1 + \left((z-1) - \frac{\lambda^2 K}{(v+|u|)^2}\right) \ln b + \mathcal{O}\big((\ln b)^2\big)\right] \tag{4.53b}$$

$$\mu' = \mu\left[1 + \left(z - \frac{\lambda^2 K}{2}\left(\frac{1}{|u|(v+|u|)} + \frac{1}{(v+|u|)^2}\right)\right) \ln b + \mathcal{O}\big((\ln b)^2\big)\right] \tag{4.53c}$$

$$\lambda' = \lambda\left[1 + \left(\frac{z-1}{2} - \frac{\lambda^2 K}{2}\left(\frac{1}{|u|(v+|u|)} + \frac{1}{(v+|u|)^2} - \frac{1}{2|u|v}\right)\right) \ln b + \mathcal{O}\big((\ln b)^2\big)\right] \tag{4.53d}$$

and the resulting β functions read

$$\beta(v) = 0 \tag{4.54a}$$

$$\beta(u) = -\lambda^2 K u\left(\frac{1}{(v+|u|)^2} - \frac{1}{4|u|v}\right) \tag{4.54b}$$

$$\beta(\mu) = \mu\left[1 - \frac{\lambda^2 K}{2}\left(\frac{1}{|u|(v+|u|)} + \frac{1}{(v+|u|)^2} - \frac{1}{2|u|v}\right)\right] \tag{4.54c}$$

$$\beta(\lambda) = -\frac{\lambda^3 K}{2}\left(\frac{1}{|u|(v+|u|)} + \frac{1}{(v+|u|)^2} - \frac{3}{4|u|v}\right) \tag{4.54d}$$

The β functions for the plasmon velocity v vanishes identically due to our renormalization condition that v and K do not flow. Moreover, the remaining β functions for the fermion velocity u, the chemical potential μ, and the coupling λ are quite different from the β functions obtained in sets I and II. This is due to the fact that in the derivation of set III we do not fix the exponent to $\tilde{z} = 1$. Thus, the resulting β functions of sets I (II) may be directly compared with the β functions of set III.

4.4 Solving the β Functions

In the previous section, we have derived complementary sets of β functions describing the flow of the fermion and plasmon velocities u and v, the coupling constant λ,

and the chemical potential μ in different pictures. Although the partial differential equations for u, v and λ are coupled and non-linear in their structure, an analytical solution is actually feasible. Without loss of generalization, let us assume u to be positive. In a first step, we solve the differential equation

$$\frac{dv}{du} = \frac{\beta(v)}{\beta(u)} \tag{4.55}$$

for v as a function of u. With this solution in mind we can solve a similar differential equation for λ in a second step:

$$\frac{d\lambda}{du} = \frac{\beta(\lambda)}{\beta(u)}\bigg|_{v=v(u)} \tag{4.56}$$

This enables us to solve in a third step the remaining differential equation for u,

$$\frac{du}{d\ln b} = \beta(u)\bigg|_{v=v(u),\lambda=\lambda(u)} \tag{4.57}$$

which yields a solution for $\ln b$ as a function of u. Upon inverting this relation we finally obtain the flow of the couplings as function of the control parameter b, i.e. $u(b)$, $v(b)$ and $\lambda(b)$, respectively. Finally, it is convenient to absorb the engineering scaling dimension of the chemical potential into the gap function $\Delta(b)$ which is defined by $\Delta(b) = b^{-1}\mu(b)$. In the following sections we apply the above procedure to solve the sets I–III of β functions.

4.4.1 Solution of Set I

Following the procedure as described above we obtain the following exact solutions for our model:

$$v(u) = u\left[1 - 4\left(\frac{4u_0}{u_0 - v_0} + \ln\frac{u}{u_0}\right)^{-1}\right] \tag{4.58}$$

$$\lambda(u) = \lambda_0 \frac{16\sqrt{u_0}}{(u_0 - v_0)^2}\, u^{3/2}\left(\frac{4u_0}{u_0 - v_0} + \ln\frac{u}{u_0}\right)^{-2} \tag{4.59}$$

$$\begin{aligned}\ln b(u) = -\frac{(u_0 - v_0)^4}{960 u_0 v_{F1} \lambda_0^2}\Bigg[3\left(2\frac{u_0 + v_0}{u_0 - v_0} + \ln\frac{u}{u_0}\right)^5 - 96\left(\frac{u_0 + v_0}{u_0 - v_0}\right)^5 \\ - 20\left(2\frac{u_0 + v_0}{u_0 - v_0} + \ln\frac{u}{u_0}\right)^3 + 160\left(\frac{u_0 + v_0}{u_0 - v_0}\right)^3\Bigg]\end{aligned} \tag{4.60}$$

Finally, the gap function of the fermions is given by

$$\Delta(u) = \Delta_0 \frac{16\sqrt{u_0}}{(u_0 - v_0)^2}\, u^{3/2}\left(\frac{4u_0}{u_0 - v_0} + \ln\frac{u}{u_0}\right)^{-2} \tag{4.61}$$

which is identical in its structure to the interaction, $\lambda(u)$, due to similar β functions. Here, u_0, v_0, λ_0 and $\Delta_0 = \mu_0$ are the initial (bare) coupling constants of the model.

4.4.2 Solution of Set II

Solving the β functions of set II according to the previous section yields the same results for the physical quantities such as the velocities u, v and the excitation gap Δ. For example, the plasmon velocity v and the gap Δ are given by

$$v(u) = u\left[1 - 4\left(\frac{4u_0}{u_0 - v_0} + \ln\frac{u}{u_0}\right)^{-1}\right] \tag{4.62}$$

$$\Delta(u) = \Delta_0 \frac{16\sqrt{u_0}}{(u_0 - v_0)^2}\, u^{3/2}\left(\frac{4u_0}{u_0 - v_0} + \ln\frac{u}{u_0}\right)^{-2} \tag{4.63}$$

On the other hand, since the β function of λ contains an additional term, we may not expect that $\lambda(u)$ is of the same form as before. Indeed, the solution for λ is equal to

$$\lambda(u) = \lambda_0 \frac{16\sqrt{u_0 v_0}}{(u_0 - v_0)^2}\, u\left(\frac{4v_0}{u_0 - v_0} + \ln\frac{u}{u_0}\right)^{-1/2}\left(\frac{4u_0}{u_0 - v_0} + \ln\frac{u}{u_0}\right)^{-3/2} \tag{4.64}$$

Finally, the fermion velocity u as a function of $\ln b$ is implicitly given by

$$\begin{aligned}\ln b(u) = -\frac{(u_0 - v_0)^4}{960 u_0 v_0 K \lambda_0^2}\Bigg[3\left(2\frac{u_0 + v_0}{u_0 - v_0} + \ln\frac{u}{u_0}\right)^5 - 96\left(\frac{u_0 + v_0}{u_0 - v_0}\right)^5 \\ - 20\left(2\frac{u_0 + v_0}{u_0 - v_0} + \ln\frac{u}{u_0}\right)^3 + 160\left(\frac{u_0 + v_0}{u_0 - v_0}\right)^3\Bigg]\end{aligned} \tag{4.65}$$

Note that this solution is of the same form as in set I.

4.4.3 Solution of Set III

Let us now consider the complementary set III which differs considerably in its derivation from the first two sets. First of all, the β function of the plasmon velocity v vanishes due to our renormalization condition that v does not flow under renormalization group transformations. Thus,

$$v(u) = v_0 = const \tag{4.66}$$

The solution for the inter-band density-density coupling constant λ is given by

$$\lambda(u) = \lambda_0\left(\frac{u - v_0}{u_0 - v_0}\right)^2\left(\frac{u}{u_0}\right)^{-1/2} \tag{4.67}$$

Solving the β function of u to obtain $\ln b$ (cf. Eq. (4.57)) yields a much simpler relation than in sets I and II above:

$$\begin{aligned}\ln b(u) = -\frac{2v_0}{15u_0(u_0 - v_0)K\lambda_0^2}\Bigg[\left(\frac{u_0 - v_0}{u - v_0}\right)^5\left(15u^3 + 5u^2 v_0 + 5uv_0^2 - v_0^3\right) \\ - \left(15u_0^3 + 5u_0^2 v_0 + 5u_0 v_0^2 - v_0^3\right)\Bigg]\end{aligned} \tag{4.68}$$

Finally, upon integrating the β function of the chemical potential we obtain the following solution for the gap function Δ,

$$\Delta(u) = \Delta_0 \left(\frac{u - v_0}{u_0 - v_0} \right)^2 \left(\frac{u}{u_0} \right)^{-1} \exp\left\{ 2 \left(\frac{v_0}{u - v_0} - \frac{v_0}{u_0 - v_0} \right) \right\} \tag{4.69}$$

Note that the solutions for u, v, λ and Δ cannot be compared with the solutions of sets I and II due to the fact that we have choosen a completely different set of renormalization conditions and that we allow for a generic dynamical exponent z.

4.5 Discussion

Let us now discuss the solutions of the β functions. First, we consider set II where the Luttinger liquid parameter K does not flow, cf. Eqs. (4.49), in different regimes of the initial fermion and plasmon velocities u_0 and v_0. The resulting renormalization group diagram summarizes the non-analytic behavior of the solutions within these renormalization conditions. Afterwards, we discuss set III where we allow for a generic dynamical exponent, cf. Eqs. (4.54). The non-analyticity observed in set II can be easily understood here due to the interaction dependent dynamical exponent. Finally, we compare the results of the two sets.

4.5.1 Discussion of Set II

First of all, let us consider the case where the initial velocity of the Ising fermions is smaller than the plasmon velocity, $u_0 < v_0$. In this case, both velocities $u(b)$ and $v(b)$ decrease upon increasing the renormalization group control parameter b, as shown in Fig. 4.5 (a)–(c). Moreover, the flow of the inter-band density-density coupling strength λ is towards weak coupling, i.e. $\lambda(b) \to 0$ for $b \to \infty$. From Eq. (4.65) we can infer the asymptotic behavior of the fermion velocity v for large b,

$$u(b) = u_0 e^{-(\mathcal{C} \ln b)^{1/5}} \quad \text{with} \quad \mathcal{C} = 320 \frac{u_0 v_0 K \lambda_0^2}{(u_0 - v_0)^4} \tag{4.70}$$

A similar relation holds for the plasmon velocity v,

$$v(b) \sim u_0 e^{-(\mathcal{C} \ln b)^{1/5}} \left[1 + \frac{4}{(\mathcal{C} \ln b)^{1/5}} \right] \tag{4.71}$$

In order to better understand the decrease of u and v let us consider the mean velocity, $V = (v + u)/2$, and the (dimensionless) velocity difference, $\epsilon = (v - u)/v$. For large b the two velocities u and v approach each other as

$$\epsilon(b) = \frac{v(b) - u(b)}{v(b)} \sim \frac{4}{(\mathcal{C} \ln b)^{1/5}} \tag{4.72}$$

while the mean velocity decreases non-algebraically as

$$V(b) = \frac{v(b) + u(b)}{2} \sim u_0 e^{-(\mathcal{C} \ln b)^{1/5}} \sim u_0 e^{-4/\epsilon(b)} \tag{4.73}$$

It is this non-analyticity of the mean velocity V on the parameter ϵ that prevents us from analyzing the asymptotic behavior of u and v directly on the level of their β functions. However, the non-analyticity of the solutions can be easily captured when allowing for a generic dynamical exponent z as in set III (see Sec. 4.5.2).

Now let us turn to the case where the initial fermion velocity is larger than the plasmon velocity, $u_0 > v_0$. In this case we find that the fermion and plasmon velocities $u(b)$ and $v(b)$ decrease as b increased, as well as the interaction strength $\lambda(b)$ decreases. However, there exists a scale b^* at which $\lambda(b)$ diverges towards strong coupling as shown in Fig. 4.5 (d)–(f). From Eqs. (4.64) and (4.65) we infer that this strong coupling scale is given by

$$\ln b^* = \frac{2v_0}{15u_0(u_0 - v_0)K\lambda_0^2}\left(15u_0^3 + 5u_0^2 v_0 + 5u_0 v_0^2 - v_0^3\right) \tag{4.74}$$

At the strong coupling scale, b^*, the plasmon velocity vanishes while the fermion velocity remains finite,

$$v(b^*) = 0, \tag{4.75}$$

$$u(b^*) = u_0 e^{-4v_0/(u_0 - v_0)} \tag{4.76}$$

and the inter-band density-density coupling strength diverges,

$$\lambda(b) \to \infty \quad \text{for} \quad b \to b^* \tag{4.77}$$

It is noteworthy that the plasmon velocity vanishes at the strong coupling scale. In order to understand this peculiarity, let us consider the compressibility κ which measures the relative change in the systems volume when a pressure is applied. The compressibility of a Luttinger liquid is given by the inverse of its plasmon velocity, $\kappa^{-1} \sim v$ (see e.g. [17]). Thus, at the strong coupling scale the compressibility diverges as v vanishes. This might indicate a first order transition in the Luttinger liquid part of our model.

Finally, let us consider the case where the initial fermion and plasmon velocities are equal, $u_0 = v_0$. In this case, the β functions (4.54) simplify and read

$$\beta(v) = -\frac{\lambda^2 K}{4v} \tag{4.78a}$$

$$\beta(u) = -\frac{\lambda^2 K}{4v} \tag{4.78b}$$

$$\beta(\mu) = \mu\left(1 - \frac{3}{2}\frac{\lambda^2 K}{4v}\right) \tag{4.78c}$$

$$\beta(\lambda) = -\frac{\lambda^3 K}{4v^2} \tag{4.78d}$$

These β functions allow for a simple solution,

$$\frac{v(b)}{v_0} = \frac{u(b)}{u_0} = \frac{\lambda(b)}{\lambda_0} = b^{-K\lambda_0^2/(4v_0^2)} \tag{4.79}$$

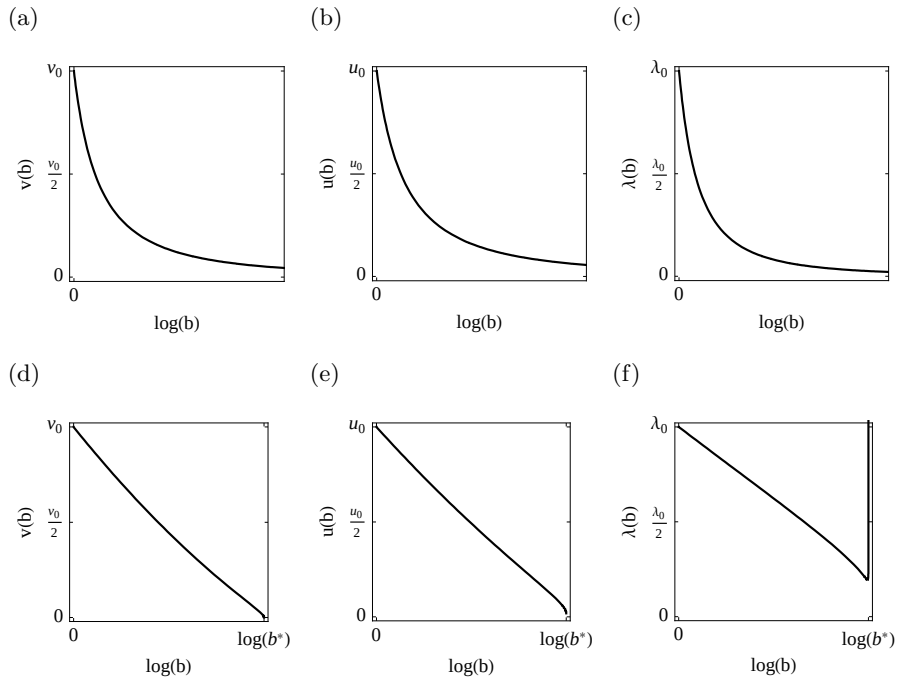

Figure 4.5: Renormalization group flow of the plasmon velocity v, the fermion velocity u, and the inter-band density-density coupling strength λ. Fig. (a)–(c) show the case $u_0 < v_0$ where the flow is towards weak coupling, $\lambda \to 0$. Fig. (d)–(f) show the case $u_0 > v_0$ where the flow is towards strong coupling, $\lambda \to \infty$. At the strong coupling scale b^* the plasmon velocity vanishes while the fermion velocity remains finite, and λ diverges.

while the gap function is given by

$$\frac{\Delta(b)}{\Delta_0} = \left(b^{-K\lambda_0^2/(4v_0^2)}\right)^{3/2} \tag{4.80}$$

Obviously, the renormalization group flow is still towards weak coupling as $\lambda \to 0$ for $b \to \infty$. Likewise, the fermion and plasmon velocities $u(b)$ and $v(b)$ still decrease as b is increased. However, the ratio of velocities $v(b)/u(b) = v_0/u_0 = 1$ remains constant for all b. This indicates that the dispersion relation is modified by an effective dynamical exponent z,

$$\omega \sim vk^z \quad \text{with} \quad z = 1 + \frac{K\lambda_0^2}{4v_0^2} = const \tag{4.81}$$

Note that this dynamical exponent is *not* the exponent of frequency rescaling $\tilde{z} = 1$ (cf. Eq. (4.34)). In the case of a non-interacting Luttinger liquid, $\tilde{z} = z = 1$ [17]. Finally, let us note that the role of the line $u_0 = v_0$ can be interpreted as a separatrix in the renormalization group diagram below.

The above results for set II are depicted in Fig. 4.6. In the case where the initial fermion velocity is smaller than the plasmon velocity, $\epsilon_0 = v_0 - u_0 > 0$, the renormalization group flow is towards weak coupling, $\lambda \to 0$ and $\epsilon \to 0$. On

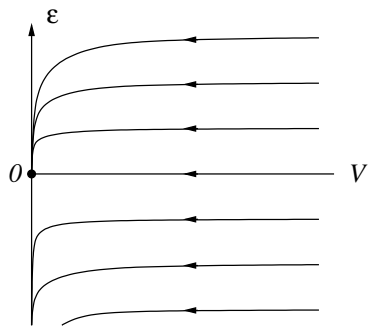

Figure 4.6: Renormalization group diagram in the (V, ϵ)-plane. The velocity difference $\epsilon = (v - u)/v$ is shown as function of the mean velocity $V = (v + u)/2$. For a discussion see the main text.

the other hand, in the case where the fermion velocity is larger than the plasmon veocity, $\epsilon_0 < 0$, the flow is towards strong coupling, $\lambda \to \infty$. Finally, the line $\epsilon_0 = 0$ corresponds to a separatrix where the flow is still towards weak coupling but the ratio $u/v = 1$ is constant. The non-analyticity of the asymptotic solutions manifests itself in the nearly horizontal flow along the V axis for small ϵ.

4.5.2 Discussion of Set III

Let us now consider set III, cf. Eqs. (4.54). We have seen in above discussion of set II that both velocities u and v decrease upon increasing b. Moreover, the mean velocity obtains a non-analytic dependence on the velocity difference ϵ between u and v. The flow along the trajectories, as depicted in the renormalization group diagram 4.6, is determined by the dependence of the β functions on ϵ. Thus, an expansion of set III in small ϵ is sufficient to determine its asymptotical behavior. Since the plasmon velocity v is kept constant in set III we substitute $u = v(1 - \epsilon)$ and carry out a Taylor expansion in small ϵ:

$$\beta(\epsilon) = -\frac{\lambda^2 K}{v^2}\frac{\epsilon^2}{16} \tag{4.82a}$$

$$\beta(\lambda) = -\frac{\lambda^3 K}{v^2}\frac{\epsilon}{8} \tag{4.82b}$$

$$\beta(\mu) = \mu\left(1 - \frac{\lambda^2 K}{8v^2}\right) \tag{4.82c}$$

Note that the asymptotic behavior of the model is completely described by the β functions of ϵ and λ. Their solution can be obtained in a way similar to the one described above. As a result the velocity difference is equal to

$$\epsilon(b) = \frac{4}{\left[\mathcal{C}\ln(b/b^*)\right]^{1/5}} \quad \text{with} \quad \mathcal{C} = 320\frac{K\lambda_0^2}{v_0^2\epsilon_0^4} \tag{4.83}$$

where $\mathcal{C}$ is an invariant of the renormalization group flow. Moreover, this invariant can be identified with the same invariant in Eq. (4.72) upon expanding the latter

one in ϵ and keeping only leading order terms. Similarly, b^* is defined as

$$\ln b^* = -\frac{1024}{\mathcal{C}\epsilon_0^5} \tag{4.84}$$

which for $\epsilon_0 < 0$ coincides with the strong coupling scale b^* defined by Eq. (4.74) upon expanding the latter one to leading order in ϵ. Likewise, the solution of the interaction strength λ reads

$$\lambda(b) = \lambda_0 \left[\frac{\ln(1/b^*)}{\ln(b/b^*)}\right]^{2/5} \tag{4.85}$$

Note that these solutions are in agreement with the asymptotic behavior obtained from the exact solutions of set II.

Let us now discuss the behavior of $\epsilon(b)$ for different regimes of the initial value of ϵ_0. In the case where the fermion velocities is smaller than the plasmon velocity, $\epsilon_0 > 0$, we get $b^* < 1$, and thus the renormalization group flow is towards weak coupling, $\lambda \to 0$ for $b \to \infty$. In the opposite case where the fermion velocity is larger than the plasmon velocity, $\epsilon_0 < 0$, the flow is towards strong coupling as λ diverges for $b \to b^*$. Finally, in the case when both velocities are equal, $\epsilon_0 = 0$, the β functions of ϵ and λ vanish, indicating that the line $\epsilon = 0$ is actually a line of fixed points. Along this line, the interaction λ is constant, and thus

$$\tilde{z} = z = 1 + \frac{K\lambda_0^2}{4v_0^2} = const \tag{4.86}$$

This suggests that the interactions between electrons effectively modifies the dispersion relation of the Luttinger liquid and the Ising fermions, $\omega \sim vk^z$. This agrees with our findings in set II. Moreover, from the β function of the chemical potential, cf. Eq. (4.82) we can infer that the correlation length exponent ν is also modified,

$$\nu = 1 - \frac{K\lambda_0^2}{8v_0^2} = const \tag{4.87}$$

Note that in our one-loop approach $\nu = 2/(3 - z)$. Note also that in the non-interacting case $z = \nu = 1$.

Moreover, it is possible to discuss these results directly on the level of the β functions. At the quantum critical point, $\mu = 0$, the β function for the chemical potential vanishes, and the renormalization group diagram is completely determined by the β functions for the velocity distance, ϵ, and the inter-band interaction strength, λ. Using the invariant $\mathcal{C}$ (cf. Eq. (4.83)) it is easy to see that the trajectories in the renormalization group diagram are given by $\epsilon \sim \sqrt{\lambda}$, as shown in Fig. 4.7. For $\epsilon_0 > 0$, i.e. in the case where the plasmons are faster than the fermions, the flow is towards the non-interacting symmetric case as λ and ϵ decrease. In the opposite case, $\epsilon_0 < 0$, we see that the flow is away from the non-interacting system as λ increases. Finally, note that the line $\epsilon = 0$ is a line of fixed points as $\beta(\epsilon) = \beta(\lambda) = 0$ on this line.

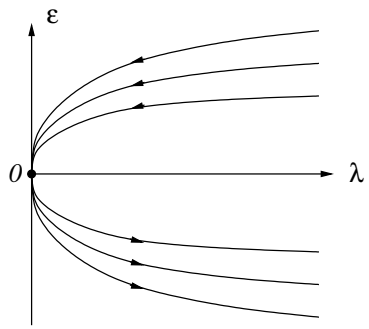

Figure 4.7: Renormalization group diagram in the (λ, ϵ)-plane. The velocity difference ϵ is shown as function of the inter-band interaction strength λ. The line $\epsilon = 0$ is a line of fixed points as $\beta(\epsilon) = \beta(\lambda) = 0$. For a detailed discussion see the main text.

In order to be able to compare the results of set III with those of set II we have to take into account the scale-dependent dynamical exponent,

$$z(b) = 1 + \frac{\lambda(b)^2 K}{4v^2(1-\epsilon(b))} \approx \frac{1+\lambda^2(b)}{4v^2} = 1 + \frac{\mathcal{C}}{1280}\,\epsilon(b)^4 \tag{4.88}$$

Here, we used the invariant $\mathcal{C}$ in the last equation, cf. Eq. (4.83). At each step during the renormalization group transformations we have rescaled the dynamical exponent z in order to independently fix the plasmon velocity v and the Luttinger liquid parameter K. To obtain the plasmon velocity $v(b)$ at scale b we have to reverse this rescaling. Thus,

$$\begin{aligned} v(b) &= v_0 \exp\left\{ -\int_0^{\ln b} d(\ln b')\,[z(b')-1] \right\} \\ &= v_0 \exp\left\{ -\left(\mathcal{C} \ln \frac{b}{b^*} \right)^{1/5} + \left(\mathcal{C} \ln \frac{1}{b^*} \right)^{1/5} \right\} \end{aligned} \tag{4.89}$$

The fermion velocity $u(b)$ at scale b is obtained in a similar way, which in combination with $v(b)$ reproduces the asymptotic behavior of the mean velocity $V = (v+u)/2$.

It is noteworthy that we have been able to derive this asymptotic behavior of ϵ and V directly from set III upon expanding it in ϵ. This contrasts set II where the non-analyticity of V prevented us from deriving such an asymptotic behavior directly on the level of β functions. However, the asymptotic results of both sets comply with each other, provided we take into account the interaction-dependend dynamical exponent z.

4.6 Summary of Results

Our model of interacting spinless electrons in a two-band quantum wire can be easily investigated with renormalization group methods. Here, the density-density

interaction between the two bands is treated as a weak perturbation. Integrating out the fast modes, we obtain the self-energies and the vertex correction to leading order in λ. The renormalization of the theory itself is done by imposing different conditions resulting in complementary sets of β functions. Each set amounts for an analytical solution although the sets consist of coupled non-linear differential equations and are thus rather complex. The physical interpretation is of course the same, regardless of which set we consider in particular.

In both set II and III we see that our peturbative renormalization group approach is well-behaved for the initial flow parameters $|u_0| < v_0$, i.e. when the fermions are slower than the plasmons. The renormalization group flow is towards a non-interacting fixed point with equal velocities, or in other words, the velocity difference scales to zero as b is increased, $\epsilon = (v-u)/v \to 0$. The dynamical exponent obtains logarithmic corrections, $z = 1 + (\text{log. corrections})$. However, for large b these corrections are negligible. To sum up:

$$|u_0| < v_0 : \quad \begin{cases} \lambda \to 0 \\ |u| \to v \quad \text{for} \quad b \to \infty \\ z \to 1 \end{cases} \tag{4.90}$$

Thus, for each b the critical theory looks like a conformal invariant theory of three Majorana fields, provided we rewrite the Luttinger liquid in terms of two Majorana fields. However, a careful analysis of the β functions reveals that not only the velocity difference ϵ decreases but so does the mean velocity V due to residual logarithmically strong interactions. Although the decrease of V is logarithmically slow, it clearly shows that the critical theory is *not* a conformal field theory of three Majorana fermions as one might have guessed in the first place. Instead, we see that the renormalization group flow is towards a non-interacting theory while both plasmon and fermion velocities decrease logarithmically.

In the case when both plasmons and fermions are equally fast, i.e. for $|u_0| = v_0$, or in other words $\epsilon_0 = 0$, much of what has been said above prevails. The renormalization group flow is still benign and is towards a weak coupling fixed point with equal velocities. However, the dispersion relation $\omega \sim k^z$ of both bands is modified by the interaction between electrons, resulting in an effective dynamical exponent equal to

$$\omega \sim v k^z \quad \text{with} \quad z = 1 + \frac{K\lambda_0^2}{4v_0^2} = const \tag{4.91}$$

Note that this dynamical exponent is far from being universal due to its dependence

on the parameters of our model. Summarizing:

$$|u_0| = v_0 : \quad \begin{cases} \lambda \to 0 \\ |u| = v \\ z > 1 \end{cases} \quad \text{for} \quad b \to \infty \tag{4.92}$$

Finally, let us consider the case when the plasmons are slower than the fermions, i.e. $|u_0| > v_0$. Here, our perturbation theory breaks down at some strong coupling scale b^* where the interaction λ diverges. However, following the renormalization group flow we see that the plasmon velocity v vanishes at this scale, $v(b^*) = 0$. On the other hand, the fermion velocity remains finite, $u(b^*) > 0$. The fact that the plasmon velocity vanishes implies a diverging compressibility $\kappa^{-1} \sim v$ which, in general, indicates a first order phase transition in the Luttinger liquid part of our model. However, we are not able to further investigate this possibility on the level of β functions. In summary:

$$|u_0| > v_0 : \quad \begin{cases} \lambda \to \infty \\ v \to 0 \\ |u| > 0 \\ z \to 1 \end{cases} \quad \text{for} \quad b \to b^* \tag{4.93}$$

This concludes the analysis of our model on the level of renormalization group methods. To gain more insight into the physics of our model, we should have a closer look at the thermodynamic properties, for example the specific heat and the compressiblity.

Chapter 5

Thermodynamics

In this chapter, we focus on thermodynamical properties of the two-band quantum wire. First, a brief review about the general concepts of a quantum phase transition and of a quantum critical point are given. In Sec. 5.2, we introduce the specific heat coefficient which is expected to show some characteristic features near the quantum phase transition. These are investigated in the framework of a scaling analysis in Sec. 5.3. In our model, we expect the specific heat coefficient to diverge close the quantum critical point. In Sec. 5.4, we calculate explicitly the leading behavior of the specific heat. Finally, in Sec. 5.5, we discuss the results focusing on the non-universal power-law behavior in the vicinity of the quantum critical point.

5.1 Quantum Phase Transitions

Most phase transitions in condensed matter physics are governed by the appearance of a spontaneously broken symmetry below a certain critical tuning parameter, for example below a critical temperature T_c. The low-temperature phase of a continuous phase transition can usually be characterized by an order parameter which, in the simplest case, is of density type like the total magnetization in a ferromagnetic transition. In general, an order parameter is a thermodynamic quantity that vanishes in one (the disordered) phase and is non-zero in the other (the ordered) phase. While the thermodynamic average of the order parameter itself is zero in the disordered phase, its fluctuations are non-zero. Approaching the phase transition from the disordered phase, the spatial correlations of the order parameter fluctuations become larger and larger. Close to the critical point their typical length scale, the *correlation length* ξ, diverges as

$$\xi \sim |r|^{-\nu} \tag{5.1}$$

where ν is the *correlation length exponent* and r is the dimensionless distance of some control parameter from the critical point. For instance, it can be defined as $r = (T - T_c)/T_c$ if the transition occurs at a finite temperature T_c.

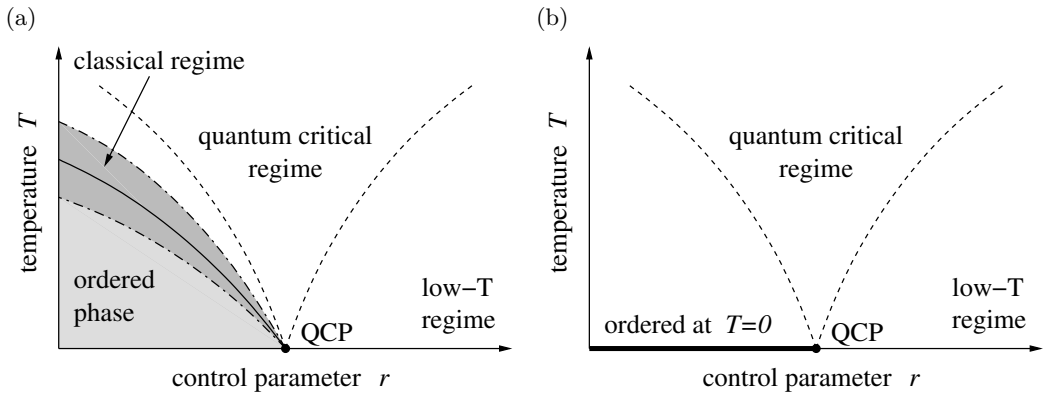

Figure 5.1: Generic phase diagram (a) with and (b) without order at finite temperatures. The dashed lines identify the crossover from the low-temperature regime to the quantum critical regime. (Figure taken from [24].)

In addition to the spatial long-range correlations there are long-range correlations in time. The typical scale for the decay of fluctuations is the so-called *correlation time* τ_c. As the critical point is approached the correlation time diverges as

$$\tau_c \sim \xi^z \sim |r|^{-\nu z} \tag{5.2}$$

where z is the *dynamical exponent*. Close to the critical point there exists no other characteristic length scale than the correlation length ξ and no other characteristic time scale than the correlation time τ_c, despite of a microscopic cutoff scale such as the lattice spacing.

However, in a quantum mechanical system a phase transition may not only be reached by lowering the temperature. Instead, at zero temperature the tuning of an external control parameter r, e.g. by varying pressure p, doping x, magnetic field h or some other physical quantity, may also drive the system from the disordered phase into the ordered phase. The so-called *quantum phase transition* occurs when the control parameter r vanishes, and the point $r = 0$ in parameter space is called the *quantum critical point*. In many cases the quantum critical point is the zero temperature endpoint of a line of second order phase transitions at finite temperatures. A generic phase diagram in the (r, T)-plane is shown in Fig. 5.1 (a). Note that the quantum critical point at zero temperature is qualitatively different from the rest of the phase boundary at finite temperatures. The critical fluctuations at zero temperature are exclusively of quantum mechanical nature.

Quite naturally, one may ask to what extent quantum mechanics is important for understanding a continuous phase transition, or in other words, how the competition between thermal and quantum fluctuations affects critical properties of the system. It turns out that quantum mechanics does not play any role for the critical behavior if the transition occurs at a finite temperature. There are, of course, exceptions

to this statement such as the phase transition to a superconducting state where the underlying order parameter is inherently quantum mechanical. In general, the phase transition at finite temperature is driven by thermal fluctuations, thus the system behaves classically in the classical regime. However, the portion of the phase diagram that can be described in terms of classical degrees of freedom is quite small near the quantum critical point, and the classical regime quickly shrinks to zero as the temperature is lowered. In fact, the critical behavior associated with classical phase transitions is practically unobservable at low enough temperatures.

On the other hand, for low temperatures away from the quantum critical point the quantum fluctuations around the quantum mechanical ground state still prevail. Their dominance is however challenged when the temperature is comparable to their typical energy scale,

$$k_B T \sim \hbar\omega_c \sim \hbar/\tau_c \sim \xi^{-z} \sim |r|^{\nu z} \tag{5.3}$$

which defines a crossover to the quantum critical regime, see Fig 5.1. In the quantum critical regime, the competition between thermal and quantum fluctuations is very strong, and this opens up the possibility that thermodynamic quantities show an interesting behavior. Although the quantum phase transition occurs only at zero temperature, it strongly influences the physics at finite temperatures.

Finally, let us consider low-dimensional systems. Upon decreasing the dimensionality the fluctuations become more and more relevant, and when the spatial dimension d is sufficiently low, i.e. below the lower critical dimension, the thermal fluctuations will totally supress the ordered phase according to the Mermin-Wagner theorem. Thus, no phase transition at finite temperatures exists. However, there may still exist a quantum phase transition due to its enhanced dimensionality $d+z$. A phase diagram of such a system is shown in Fig. 5.1 (b).

For a more extensive introduction into quantum phase transitions and applications see, for example, [25, 26, 27, 28, 29].

5.2 Specific Heat Coefficient

As mentioned above, the phase boundary in the phase diagram Fig. 5.1 is a line of classical finite-temperature transitions ending in a quantum critical point. In the (r, T)-plane there exists only one direction to approach the phase boundary, i.e. the direction perpendicular to it. On the other hand, there exist two distinct directions to approach the quantum critical point. Therefore we can expect that we get additional information about the quantum critical point along these two directions.

For the sake of concreteness, let us consider the entropy S. Its total differential

in the (r, T)-plane,

$$dS = \left.\frac{\partial S}{\partial T}\right|_r dT + \left.\frac{\partial S}{\partial r}\right|_T dr \tag{5.4}$$

is characterized by two derivatives specifying the change in entropy upon tuning either temperature T or the control parameter T. The first derivative, i.e. the variation of entropy S with respect to temperature T, is measured by the *specific heat coefficient* γ,

$$\gamma = \frac{c_r}{T} = \frac{1}{V}\left.\frac{\partial S}{\partial T}\right|_r = -\frac{1}{V}\frac{\partial^2 F}{\partial T^2} \tag{5.5}$$

where c_r is the specific heat coefficient at constant control parameter r, and V is the volume of the system. $F = F(r, T)$ is the Gibbs free energy which depends on some generalized pressure r and on temperature T. The second derivate, i.e. the variation of entropy S with respect to the control parameter r, is the quantity complementary to the specific heat. Depending on the experimental realization this derivative can be identified with some well-known thermodynamic quantities. In the case where the quantum phase transition is approached by pressure tuning, $r \approx (p - p_c)/p_c$, it is proportional to the *thermal expansion* α,

$$\alpha_p = \frac{1}{V}\left.\frac{\partial V}{\partial T}\right|_p = \frac{1}{V}\frac{\partial^2 F}{\partial T \partial p} = -\frac{1}{V}\left.\frac{\partial S}{\partial p}\right|_T = -\frac{1}{V p_c}\left.\frac{\partial S}{\partial r}\right|_T \tag{5.6}$$

In the case where the quantum phase transition is controlled by tuning the chemical potential, $r \approx (\mu - \mu_c)/\mu_c$, the second term is proportional to the *compressibility* κ,

$$\kappa = \left.\frac{\partial N}{\partial \mu}\right|_T = \frac{\partial^2 F}{\partial \mu^2} \tag{5.7}$$

In the following, we focus on the specific heat coefficient, γ, and determine its behavior close to the quantum critical point. However, we will restrict ourselves to the cases $|u| \leq v$ since our perturbative renormalization group approach breaks down in the opposite case.

5.3 Scaling Theory

In this section, we analyze the thermodynamic quantities introduced in the previous section in the framework of scaling theory. This is subject of several textbooks and reviews, for example, see e.g. [25, 30, 31].

5.3.1 Scaling Ansatz

First of all, let us define the scaling dimensions of the system parameters involved. Traditionally, the scaling dimension of the control parameter r is given by $1/\nu$ (cf. Eq. (5.1)), and the temperature scales with the dynamical exponent z (cf. Eq. (5.3)). Additionally, we define the scaling dimension y_f for the singular part of the free

energy per volume, f_{cr}. In the case where hyperscaling applies [30], this scaling dimension is equal to the effective dimensionality, $y_f = d + z$. Upon rescaling the unit length by a factor of b an interval in space, Δx, is scaled down to $\Delta x' = b^{-1}\Delta x$ and thus has the scaling dimension $\dim[x] = -1$.

The scaling behavior of the control parameter r, the temperature T, and the singular part of the free energy f_{cr} can be summarized as follows:

$$\begin{aligned} \Delta x &\to \Delta x' = b^{-1}\Delta x \\ r &\to r' = b^{1/\nu} r \\ t &\to t' = b^{z} t \\ f_{\mathrm{cr}} &\to f'_{\mathrm{cr}} = b^{y_f} f_{\mathrm{cr}} \end{aligned} \tag{5.8}$$

Note that $t = T/T_0$ is a dimensionless temperature, and T_0 is some temperature scale which is left unspecified at the moment.

The scaling hypothesis we use here is based on the assumption that close to the critical point there is only one characteristic length scale, namely the correlation length ξ, that determines the singular properties near quantum criticality. In a formal way, scale invariance at criticality is defined by the relation

$$f_{\mathrm{cr}}(r,t) \stackrel{!}{=} b^{-y_f} f_{\mathrm{cr}}(b^{1/\nu} r, b^z t), \tag{5.9}$$

i.e. the scale transformation of the control parameter r and the dimensionless temperature t in the arguments of the free energy per volume can be absorbed into the scale factor of the free energy itself. From Eq. (5.9) we can derive the scaling properties of the specific heat coefficient, γ. Using the scaling ansatz (5.9) and the definition of γ, cf. Eq. (5.5), we obtain

$$\begin{aligned} \gamma(r,t) = -\frac{\partial^2 f_{\mathrm{cr}}(r,t)}{\partial t^2} &\stackrel{!}{=} -\frac{\partial^2 \left[b^{-y_f} f_{\mathrm{cr}}(b^{1/\nu} r, b^z t) \right]}{\partial t^2} \\ &= -b^{-y_f+2z} \frac{\partial^2 f_{\mathrm{cr}}(b^{1/\nu} r, b^z t)}{\partial (b^z t)^2} = b^{-y_f+2z} \gamma(b^{1/\nu} r, b^z t) \end{aligned} \tag{5.10}$$

Therefore, the specific heat coefficient γ has the scaling dimension

$$\dim[\gamma] = \dim[f_{\mathrm{cr}}] - 2z = y_f - 2z = d - z \tag{5.11}$$

where the last relation holds when hyperscaling applies. Note that the specific heat coefficient diverges within this scaling approach when $z > d$. In particular, for our two-band quantum model Eq. (5.11) implies that γ diverges when $|u| = v$ as $z > 1$ in this case.

5.3.2 Behavior of the Specific Heat Coefficient

The engineering scaling dimension of the specific heat coefficient, $\dim[\gamma] = d - z$, shows that γ diverges at the quantum critical point if $z > d$. However, we have

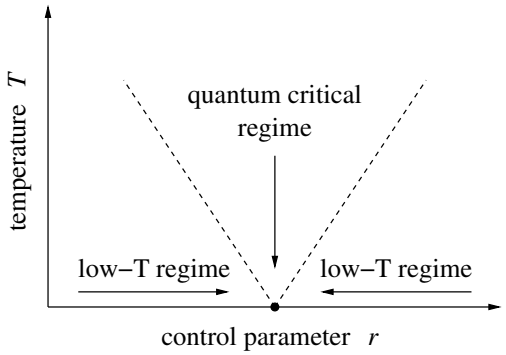

Figure 5.2: Different regimes in the (r, T)-plane. The crossover lines (dashed lines) are defined by the condition $|r| \sim T^{1/(\nu z)}$. (Figure taken from [24].)

to distinguish how exactly the quantum critical point is approached. Depending on the relative values of the control parameter r and the temperature T there exist two different directions, as shown in Fig. 5.2. The two regimes are separated by crossover lines at which

$$|r|t^{-1/(\nu z)} \sim \mathcal{O}(1) \tag{5.12}$$

In the *quantum critical regime* this particular combination is small, $|r|t^{-1/(\nu z)} \ll 1$. In order to determine the behavior of γ in this regime let us choose a definite value for the scale factor b in Eq. (5.10), i.e. $b^z t = 1$. The leading behavior of the specific heat coefficient is thus given by

$$\gamma(r,t) = t^{-\frac{2z-y_f}{z}} \gamma\big(rt^{-\frac{1}{\nu z}}, 1\big) \quad \text{for} \quad |r|t^{-\frac{1}{\nu z}} \ll 1 \tag{5.13}$$

Obviously, the specific heat coefficient diverges upon decreasing the temperature with an exponent $-(2z - y_f)/z$. In the other regime, the *low-temperature regime* where $|r|t^{-1/(\nu z)} \gg 1$, we choose instead the scale b such that $|r|b^{1/\nu} = 1$. In this case,

$$\gamma(r,t) = |r|^{-\nu(2z-y_f)} \gamma\big(1, t|r|^{-\nu z}\big) \quad \text{for} \quad |r|t^{-1/(\nu z)} \gg 1 \tag{5.14}$$

Thus, in the low-temperature regime the specific heat coefficient diverges upon decreasing the control parameter r with an exponent $-\nu(2z - y_f)$.

5.3.3 Universality of the Scaling Ansatz

Although Eqs. (5.13) and (5.13) provide some insight into the divergence of γ upon approaching the quantum critical point, we can bring these scaling relations into a more formal representation. To this end, let us go back to the scaling relation (5.9) for singular part of free energy per volume, $f_{\rm cr}$. Differentiating with respect to temperature we obtain the scaling relation for the entropy per volume,

$$s_{\rm cr}(r,t) = b^{-y_f+z} s_{\rm cr}(b^{1/\nu} r, b^z t) \tag{5.15}$$

It is now convenient to rewrite the entropy by introducing scaling functions for the quantum critical regime and the low-temperature regime. Repeating the above procedure by choosing certain scales in both regimes, the entropy can be written as

$$s_{\mathrm{cr}} = \begin{cases} t^{\frac{y_f - z}{z}} s_{\mathrm{cr}}(t^{-1/(\nu z)} r, 1) & \text{for } |r| t^{-1/(\nu z)} \ll 1 \\ |r|^{\nu(y_f - z)} s_{\mathrm{cr}}(\mathrm{sign}(r)|r|^{-\nu z} t) & \text{for } |r| t^{-1/(\nu z)} \gg 1 \end{cases} \tag{5.16}$$

$$= \begin{cases} \left(\frac{T}{T_0}\right)^{\frac{y_f - z}{z}} \Psi_{\mathrm{QC}}\left(r \left(\frac{T}{T_0}\right)^{-\frac{1}{\nu z}}\right) & \text{for } |r| (T/T_0)^{-1/(\nu z)} \ll 1 \\ |r|^{\nu(y_f - z)} \Psi_{\mathrm{LT}}^{\mathrm{sign}(r)}\left(\frac{T}{T_0} |r|^{-\nu z}\right) & \text{for } |r| (T/T_0)^{-1/(\nu z)} \gg 1 \end{cases} \tag{5.17}$$

Here, we have introduced some *a priori* unknown but universal scaling functions Ψ_{QC} and $\Psi_{\mathrm{LT}}^{\pm}$. Note that in the low-temperature regime there are two scaling functions for positive and negative values of the control parameter r, respectively. Moreover, we have replaced the dimensionless temperature t by T/T_0 in order to show that the arguments of the scaling functions have the engineering dimension zero.

In order to obtain the leading behavior of the entropy per volume and the specific heat coefficient we have to expand the scaling functions for small arguments. First, the scaling function Ψ_{QC} is expected to be regular for small arguments since there no phase transition takes place at $r = 0$ for finite temperature. Thus,

$$\Psi_{\mathrm{QC}}(x) \approx \Psi_{\mathrm{QC}}(0) + \Psi'_{\mathrm{QC}}(0)\, x + \ldots \quad \text{for} \quad x \to 0 \tag{5.18}$$

On the other hand, the scaling functions $\Psi_{\mathrm{LT}}^{\pm}$ describes the low-temperature behavior of the phases to left and to the right hand side of the quantum critical point, see Fig. 5.2. According to the third law of thermodynamics, the entropy has to vanish upon approaching zero temperature. This condition restricts the form of $\Psi_{\mathrm{LT}}^{\pm}$ for small arguments. Assuming that the entropy vanishes algebraically, a low-temperature expansion of $\Psi_{\mathrm{LT}}^{\pm}$ takes the form

$$\Psi_{\mathrm{LT}}^{\pm}(x) \approx a^{\pm} x^{b^{\pm}} + \ldots \quad \text{for} \quad x \to 0 \tag{5.19}$$

where $a^{\pm}$ are constants, and the positive exponents $b^{\pm} > 0$ characterize the power-law behavior of the specific heat in the low-temperature phase, i.e. $c \sim T^{b^{\pm}}$. Gapped systems in which the entropy vanishes exponentially in the low-temperature regime are described by the scaling function

$$\Psi_{\mathrm{LT}}^{\pm}(x) \approx a^{\pm} x^{b^{\pm}} e^{-c^{\pm}/x} + \ldots \quad \text{for} \quad x \to 0 \tag{5.20}$$

where $a^{\pm}$ and $c^{\pm}$ are some positive constants, and $b^{\pm}$ is a positive or negative exponent.

The limiting behavior the specific heat coefficient γ is then easily obtained. Differentiating the entropy per volume s_{cr} (cf. Eq. (5.17) with respect to temperature

yields

$$\gamma(r,T) = \begin{cases} \frac{1}{T_0}\frac{y_f - z}{z}\,\Psi_{\mathrm{QC}}(0)\left(\frac{T}{T_0}\right)^{\frac{y_f-2z}{z}} & \text{for } |r|(T/T_0)^{-1/(\nu z)} \ll 1 \\ \frac{1}{T_0}a^{\pm}b^{\pm}|r|^{\nu(y_f-z-zb^{\pm})}\left(\frac{T}{T_0}\right)^{b^{\pm}-1} & \text{for } |r|(T/T_0)^{-1/(\nu z)} \gg 1 \end{cases} \tag{5.21}$$

Note that in Eq. 5.21 we consider only the case where the entropy vanishes algebraically as zero temperature is approached. The constants $a^{\pm}$ and the exponents $b^{\pm}$ are to be understood for either positive or negative values of the control parameter r, respectively.

5.4 Analytical Results for the Specific Heat Coefficient

In this section, we present an explicit calculation of the free energy and the specific heat coefficient for our model of a two-band quantum wire. Due to the two-band structure there exist two contributions to the specific heat coefficient, one from the plasmon excitations of the Luttinger liquid in the first subband, and one from the Ising fermions in the second subband. We compare the results with the prediction of our scaling ansatz. Finally, note that for the following calculations we only consider the case where the fermions velocity is less than or equal to the plasmon velocity, $|u| \leq v$. In the opposite case, we might encounter a first order transition in the Luttinger liquid. This scenario requires more elaborate work and has not yet been subject of our analysis. For details on the calculations of the specific heat coefficient see App. B.

5.4.1 Non-Interacting System

First of all, we consider the non-interacting system, $\lambda = 0$. From Eqs. (4.52) and (4.87) we infer that the dynamical exponent z and the correlation length exponent ν are equal to

$$z = \nu = 1 \tag{5.22}$$

In the non-interacting case, the two bands are completely decoupled and we expect the specific heat coefficient to consist of two independent contributions, one from each subband. The Luttinger liquid in the first band has the specific heat coefficient (see e.g. [17])

$$\gamma_{\mathrm{pl}} = \frac{\pi}{3v} \tag{5.23}$$

where $v = v_{F1}/K$ is the plasmon velocity. On the other hand, critical Ising fermions have the specific heat coefficient

$$\gamma_{\mathrm{el}} = \frac{\pi}{6|u|} \quad \text{for} \quad \mu = 0 \tag{5.24}$$

where u is the velocity of the Ising fermions. We expect the following calculations to reproduce the above results upon taking the limits $z \to 1$ and $\nu \to 1$.

Free Energy

Let us consider the free energy per volume of the plasmon excitations in the Luttinger liquid. In general, the free energy is given by

$$f_{\mathrm{pl}} = \frac{1}{L} F_{\mathrm{pl}} = -\frac{T}{L} \ln Z_{\mathrm{pl}} = \frac{T}{2L} \operatorname{Tr}\{\det \mathcal{D}_0^{-1}\} \tag{5.25}$$

where L is the one-dimensional volume or length of the model, Z_{pl} is the plasmon partition function, $\mathcal{D}_0$ is the plasmon propagator, and the trace runs over momentum and frequency space. The summation over bosonic Matsubara frequencies, $\Omega_n = 2n\pi/\beta$, is performed by means of the residue theorem. Converting the remaining sum over momenta into a momentum integral we obtain the plasmon contribution to the free energy per volume,

$$f_{\mathrm{pl}} = 2T \int_0^\Lambda \frac{dk}{2\pi} \ln\left[2 \sinh\left(\frac{vk}{2T}\right)\right] \tag{5.26}$$

where Λ is the ultraviolet momentum cutoff introduced in Chapter 4 to regularize the integral. For a detailed calculation of f_{pl} see Appendix B.1.1.

In a similar way, the contribution of the Ising fermions to the free energy per volume is given by

$$f_{\mathrm{el}} = \frac{1}{L} F_{\mathrm{el}} = -\frac{T}{L} \ln Z_{\mathrm{el}} = -\frac{T}{2L} \operatorname{Tr}\{\det \mathcal{G}_0^{-1}\} \tag{5.27}$$

where $\mathcal{G}_0$ is the electron propagator. Note that $\mathcal{G}_0$ actually has a matrix structure, thus the trace contains a summation over momentum and frequency space as well as a summation of the eigenvalues of $\mathcal{G}_0$. Performing the Matsubara summation by means of the residue theorem the electron free energy per volume is equal to

$$f_{\mathrm{el}} = -2T \int_0^\Lambda \frac{dk}{2\pi} \ln\left[2 \cosh\left(\frac{\sqrt{\mu^2 + (uk)^2}}{2T}\right)\right] \tag{5.28}$$

For a detailed calculation of f_{el} see Appendix B.1.2.

Now let us calculate the specific heat coefficient γ which is given by the second derivative of the free energy per volume with respect to temperature (cf. Eq. (5.5)),

$$\gamma = \left.\frac{\partial^2 f}{\partial T^2}\right|_\mu \tag{5.29}$$

Note that in our model the control parameter of the quantum phase transition is the chemical potential, $r = \mu$.

Quantum Critical Regime: $|\mu| T^{-1/(\nu z)} \ll 1$

Differentiating the plasmon free energy (5.26) twice with respect to temperature yields the plasmon contribution to the specific heat coefficient,

$$\gamma_{\mathrm{pl}} = \frac{1}{2T^3} \int_0^\Lambda \frac{dk}{2\pi} \frac{(vk)^2}{\sinh^2\left[\frac{vk}{2T}\right]} \tag{5.30}$$

In the limit $\Lambda \to \infty$ we obtain

$$\gamma_{\mathrm{pl}} = \frac{\pi}{3v} \quad \text{for} \quad \lambda = 0, |\mu| T^{-1/(\nu z)} \ll 1 \tag{5.31}$$

which is in agreement with our expectations. Note that this results holds also in the low-temperature regime. For details on the calculation of Eq. (5.30) see Sec. B.2.1.

Likewise, the electron contribution to the specific heat coefficient is obtained by differentiating the fermion free energy (5.28) twice with respect to temperature,

$$\gamma_{\mathrm{el}} = \frac{1}{2T^3} \int_0^\Lambda \frac{dk}{2\pi} \frac{\mu^2 + (uk)^2}{\cosh^2\left[\frac{1}{2T}\sqrt{\mu^2 + (uk)^2}\right]} \tag{5.32}$$

In the quantum critical regime, $\mu T^{-1/(\nu z)} \ll 1$, we can neglect the explicit dependence of γ on the chemical potential since it yields only subleading corrections. In the limit $\Lambda \to \infty$ we get (for details see Sec. B.2.2)

$$\gamma_{\mathrm{el}} = \frac{\pi}{6|u|} \quad \text{for} \quad \lambda = 0, |\mu| T^{-1/(\nu z)} \ll 1 \tag{5.33}$$

Note that at the symmetric point of our model, $|u| = v$, the specific heat coefficient of the plasmons, γ_{pl}, is twice as large as the electron one, γ_{el}. This is due to the fact that for $|u| = v$ our model can be rewritten in terms of three Majorana fields. We note here that the Luttinger liquid is described in terms of two Majorana fields while the fermions are described by only one Majorana field. Hence, we observe above an integer relation between the specific heat coefficients γ_{pl} and γ_{el} as described.

Low-Temperature Regime: $|\mu| T^{-1/(\nu z)} \gg 1$

In the low-temperature regime, we can carry out a Taylor expansion of Eq. (5.32) in its small argument $T/|\mu| \ll 1$:

$$\begin{aligned}
\gamma_{\mathrm{el}} &= \frac{1}{2T^3} \int_0^\infty \frac{dk}{2\pi} \frac{\mu^2 + (uk)^2}{\cosh^2\left[\frac{1}{2T}\sqrt{\mu^2 + (uk)^2}\right]} \\
&\approx \frac{1}{\pi|u|} \left(\frac{|\mu|}{T}\right)^3 \int_0^\infty dx\, (1 + x^2) \exp\left(-\frac{|\mu|}{T}\sqrt{1 + x^2}\right)
\end{aligned}$$

where the limit $\Lambda \to \infty$ is taken. Thus, the electron contribution to the specific heat coefficient in the low-temperature regime is exponentially suppressed (for details see Sec. B.2.2),

$$\gamma_{\mathrm{el}} \approx \frac{1}{\sqrt{2\pi}|u|} \left(\frac{|\mu|}{T}\right)^{5/2} e^{-|\mu|/T} \quad \text{for} \quad \lambda = 0, |\mu| T^{-1/(\nu z)} \gg 1 \tag{5.34}$$

This results is once again in agreement with the prediction from our previous scaling analysis of the specific heat coefficient.

5.4.2 Interacting System

Now let us consider the interacting system, $\lambda \neq 0$. In this case, the interactions between electrons in the two bands lead to a renormalization of the model parameters u, v, μ and λ, as shown in Chapter 4. Additionally, the dynamical exponent z and the correlation length exponent ν are different from unity, cf. Eqs. (4.52) and (4.87). Note that we consider $|u| \leq v$ only, as mentioned above.

Free Energy

In the interacting case, the free energy per volume is also modified due to electron interactions. In the spirit of the momentum-shell renormalization group methods, the mode elimination renormalizes the bare velocities u, v, the chemical potential μ, and the interaction λ. Afterwards, the integrand is rescaled which restores the ultraviolet momentum cutoff. In a final step, the plasmon and electron fields are renormalized to keep certain quadratic parts in the action invariant. In addition to the β functions that have been derived in Chapter 4, this scheme yields the following β function for the free energy per volume,

$$\beta(f) = y_f f(b) + \delta f(b) \tag{5.35}$$

Here, $y_f = d + z$ is the engineering scaling dimension of f, and $\delta f(b)$ are the momentum-shell corrections due to interactions between electrons. Note that the engineering scaling dimension of f can be absorbed by defining $\tilde{f} = b^{-y_f} f(b)$ which leads to

$$\beta(\tilde{f}) = b^{-y_f} \delta f(b) \tag{5.36}$$

The leading-order corrections consists of two contributions, $\delta f(b) = \delta f_{\mathrm{pl}}(b) + \delta f_{\mathrm{el}}(b)$, which resemble the renormalization effects of u, v and μ. There exist logarithmic corrections $\delta f_{\mathrm{el-pl}}(b)$ to the free energy per volume which stem from the interaction between the electrons in the two subbands. However, since the interaction term in the Hamiltonian is marginal we expect these additional term to be small and thus neglect it in the following discussion.

Integrating the β function for the free energy per volume we can rewrite it as an integral along the trajectory in parameter space. In the limit $b \to \infty$,

$$f = \int_0^\infty d(\ln b)\, b^{-y_f} \delta f\big(b^z T, b^{1/\nu}\mu, v(b), u(b)\big) \tag{5.37}$$

where we have rewritten the integrand $\delta f(b)$ in terms of the parameters flowing under renormalization group transformations. Note that we also have to take into account that the temperature is rescaled under renormalization group transformation. Substituting $b = \Lambda/k$ we can rewrite the plasmon and the fermion contribution as

$$f_{\mathrm{pl}} = 2T \int_0^\Lambda \frac{dk}{2\pi} \ln\left[2\sinh\left(\frac{v\left(\frac{\Lambda}{k}\right)k}{2T}\right)\right] \tag{5.38}$$

and

$$f_{\mathrm{el}} = -2T \int_0^\Lambda \frac{dk}{2\pi} \ln\left[2\cosh\left(\frac{1}{2T}\sqrt{\Delta^2\left(\frac{\Lambda}{k}\right) + u^2\left(\frac{\Lambda}{k}\right)k^2}\right)\right] \tag{5.39}$$

where the limit $\Lambda \to \infty$ is implicit. Note that we have replaced the chemical potential by the corresponding gap function, $\Delta(b) = b^{-1}\mu(b)$, to account for the engineering scaling dimension of the chemical potential. For details on the derivation of f_{pl} and f_{el} see Sec. B.3.

Obviously, the net effect of the renormalization group analysis is but to introduce a momentum-dependence for the parameter u, v and μ in our model. We can thus easily calculate the specific heat coefficient γ by using the above formulas upon substituting the renormalized parameters. However, we have to keep in mind that the renormalization group flow of the parameters stops at a certain cut-off scale b^* which is defined by the relations

$$T(b^*) \sim u(b^*)\Lambda \tag{5.40a}$$

$$\mu(b^*) \sim u(b^*)\Lambda \tag{5.40b}$$

The latter condition comes from the calculation of the fermionic self-energy Σ where we perform a Taylor expansion in $\mu \ll uk$ and consider leading-order terms only. Note that in the symmetric case, $|u| = v$, the renormalization group flow follows a power-law. Thus, the cut-off scale b^* can be rewritten as

$$b^* = \min\left\{\left(\frac{E_0}{|\mu|}\right)^{\nu}, \left(\frac{E_0}{T}\right)^{1/z}\right\} \tag{5.41}$$

where ν is the correlation length exponent, z the effective dynamical exponent, and $E_0 = E_0(\Lambda) \sim \mathcal{V}\Lambda$ is an energy scale that depends on the momentum cutoff used in our perturbative renormalization group approach. Finally, note that $\mathcal{V}$ is some velocity to get the correct physical dimensions for the energy scale E_0.

Quantum Critical Regime: $|\mu|T^{-1/(\nu z)} \ll 1$

In the interacting case we have to distinguish between the symmetric model, $|u| = v$, and the generic, asymmetric model, $|u| < v$.

Symmetric Case ($|u| = v$): The renormalization group flow of the plasmon velocity is simply given by its solution from set II,

$$v(b) = \begin{cases} vb^{1-z} & \text{for } b < b^* \\ v^* & \text{for } b \geq b^* \end{cases} \quad \text{with} \quad z = 1 + \frac{\lambda^2 K}{4v^2} = const \tag{5.42}$$

Here, the velocity at the cutoff scale is equal to $v^* = v(b^*)^{1-z}$ with $b^* = (E_0/T)^{1/z} = (\mathcal{V}\Lambda/T)^{1/z}$, cf. Eq. (5.41). Note that in the symmetric model the interaction between electrons generates an effective dynamical exponent $z \neq 1$, see Sec. 4.5.1.

Differentiating the free energy per volume twice with respect to the temperature we obtain the specific heat coefficient,

$$\gamma_{\mathrm{pl}} = \frac{1}{2T^3}\int_0^\Lambda \frac{dk}{2\pi}\frac{v^2\big(\frac{\Lambda}{k}\big)^2 k^2}{\sinh^2\big[\frac{k}{2T}\,v\big(\frac{\Lambda}{k}\big)\big]} \tag{5.43}$$

which corresponds to the non-interacting relation for γ_{pl}, cf. Eq. (5.30), but with a momentum-dependent plasmon velocity $v(\Lambda/k)$. The integral can be calculated in a straightforward way yielding (see Sec. B.4.1 for details)

$$\gamma_{\mathrm{pl}} \approx C_1(z)\frac{2}{\pi v}\left(\frac{\mathcal{V}\Lambda}{T}\right)^{\frac{z-1}{z}} \quad \text{for} \quad \lambda \neq 0, |u| = v, |\mu| T^{-1/(\nu z)} \ll 1 \tag{5.44}$$

with $C_1(z) = \frac{z+1}{z^2}\,\Gamma\big(\frac{z+1}{z}\big)\,\zeta\big(\frac{z+1}{z}\big)$ being an interaction-dependent prefactor. From Eq. (5.44) we immediately see that the specific heat coefficient γ_{pl} diverges as zero temperature is approached with an exponent $-(z-1)/z$. Moreover, γ_{pl} obtains an explicit dependence on the momentum cutoff Λ. It is also noteworthy that Eq. (5.44) is consistent with our scaling prediction for the quantum critical regime, cf. Eq. (5.21). Finally, in the limit $\lambda \to 0$, we re-obtain the result from the non-interacting case as $C_1(0) = \pi^2/6$, and the exponent is equal to zero.

In a similar way we can calculate the specific heat coefficient for the electrons which in general is given by

$$\gamma_{\mathrm{el}} = \frac{1}{2T^3}\int_0^\Lambda \frac{dk}{2\pi}\frac{\Delta^2\big(\frac{\Lambda}{k}\big) + u^2\big(\frac{\Lambda}{k}\big)k^2}{\cosh^2\Big[\frac{1}{2T}\sqrt{\Delta^2\big(\frac{\Lambda}{k}\big) + u^2\big(\frac{\Lambda}{k}\big)k^2}\Big]} \tag{5.45}$$

The fermion velocity is given by

$$u(b) = \begin{cases} u b^{1-z} & \text{for } b < b^* \\ u^* & \text{for } b \geq b^* \end{cases} \quad \text{with} \quad z = 1 + \frac{\lambda^2 K}{4v^2} = const \tag{5.46}$$

where the velocity at the cutoff scale is given by $u^* = u(b^*)^{1-z}$ with $b^* = (E_0/T)^{1/z} = (\mathcal{V}\Lambda/T)^{1/z}$. We thus easily obtain the relation (see Sec. B.4.2 for details)

$$\gamma_{\mathrm{el}} \approx C_2(z)\frac{1}{\pi|u|}\left(\frac{\mathcal{V}\Lambda}{T}\right)^{\frac{z-1}{z}} \quad \text{for} \quad \lambda \neq 0, |u| = v, |\mu| T^{-1/(\nu z)} \ll 1 \tag{5.47}$$

where $C_2(z) = 2(1 - 2^{-1/z})C_1(z)$ differs by a factor from $C_1(z)$. Note that the fermion specific heat coefficient diverges in the same way as γ_{pl} diverges as zero temperature is approached. Likewise, in limit $\lambda \to 0$, we obtain the previous result from the non-interacting case since $C_2(0) = C_1(0) = \pi^2/6$.

Asymmetric Case ($|u| < v$): In this case, the renormalization group flow of the plasmon velocity is asymptotically given by

$$v(b) \approx \begin{cases} v e^{-(\mathcal{C}\ln b)^{1/5}} & \text{for } b < b^* \\ v^* & \text{for } b \geq b^* \end{cases} \quad \text{with} \quad \mathcal{C} = 320\frac{uvK\lambda^2}{(u-v)^4} \tag{5.48}$$

Here, the plasmon velocity at the cutoff scale is equal to $v^* = ve^{-(\mathcal{C}\ln b^*)^{1/5}}$ with $b^* = (E_0/T)^{1/z} = (\mathcal{V}\Lambda/T)^{1/z}$. The explicit calculation shows that the specific heat coefficient $\gamma_{\rm pl}$ is proportional to the plasmon velocity at the cut-off scale, i.e.

$$\gamma_{\rm pl} \approx \frac{\pi}{3v^*} = \frac{\pi}{3v}\, e^{\left(\mathcal{C}z^{-1}\ln\frac{\mathcal{V}\Lambda}{T}\right)^{1/5}} \quad \text{for} \quad \lambda \neq 0, |u| < v, |\mu| T^{-1/(\nu z)} \ll 1 \tag{5.49}$$

For details on the calculation see Sec. B.4.1.

Similarly, the electron contribution to the specific heat coefficient is proportional to the fermion velocity at the cut-off scale (see Sec. B.4.2 for details),

$$\gamma_{\rm el} \approx \frac{\pi}{6|u^*|} = \frac{\pi}{6|u|}\, e^{\left(\mathcal{C}z^{-1}\ln\frac{\mathcal{V}\Lambda}{T}\right)^{1/5}} \quad \text{for} \quad \lambda \neq 0, |u| < v, |\mu| T^{-1/(\nu z)} \ll 1 \tag{5.50}$$

Obviously, both specific heat coefficients $\gamma_{\rm pl}$ (cf. Eq. (5.49)) and $\gamma_{\rm el}$ (cf. Eq. (5.50)) diverge logarithmically as zero temperature is approached. In the limit $\lambda \to 0$, i.e. for $\mathcal{C} \to 0$ and $z \to 1$, we re-obtain the results for the non-interacting system.

Low-Temperature Regime: $|\mu| T^{-1/(\nu z)} \gg 1$

The low-temperature regime is characterized by the fact that the cutoff of the renormalization group flow is now given by $b^* = (E_0/|\mu|)^\nu$. We again have to distinguish between the cases of the symmetric model with $|u| = v$ and the asymmetric case, $|u| < v$.

Symmetric Case ($|u| = v$): In the symmetric case, the overall form of the specific heat coefficient of the plasmons prevails, but the cutoff dependence is changed (see Sec. B.4.1 for details):

$$\gamma_{\rm pl} \approx C_1(z)\frac{2}{\pi v}\left(\frac{\mathcal{V}\Lambda}{|\mu|}\right)^{\nu(z-1)} \quad \text{for} \quad \lambda \neq 0, |u| = v, |\mu| T^{-1/(\nu z)} \gg 1 \tag{5.51}$$

However, $\gamma_{\rm pl}$ diverges as the quantum critical point is approached upon decreasing the chemical potential $|\mu|$ with a power of $-\nu(z-1)$. This results for $\gamma_{\rm pl}$ agrees with our scaling prediction (5.21) for $b^\pm = 1$ and $y_f = d + z = 1 + z$.

On the other hand, the specific heat coefficient for the electrons is obtained by carrying out a Taylor expansion of Eq. (5.45) in the small argument $T/|\mu| \ll 1$, and we get (see Sec. B.4.2 for details)

$$\gamma_{\rm el} \approx C_2\left(\frac{\nu z - 1}{\nu}\right)\frac{1}{\pi|u|}\left(\frac{\mathcal{V}\Lambda}{|\mu|}\right)^{\frac{\nu}{\nu z-1}}\left(\frac{\mathcal{V}\Lambda}{T}\right)^{\frac{\nu}{\nu z-1}-1} \quad \text{for} \quad \lambda \neq 0, |u| \neq v, |\mu| T^{-1/(\nu z)} \gg 1 \tag{5.52}$$

Here, z is the dynamical exponent and $\nu = \frac{3-z}{2}$ is the correlation length exponent as introduced in Sec. 4.5.2. The specific heat coefficient $\gamma_{\rm el}$ diverges as the quantum critical point is approached with a power $-\nu/(\nu z - 1)$. Note that Eq. (5.52) agrees

with our scaling prediction for the low-temperature regime, cf. Eq. (5.21), with $b^{\pm} = \nu/(\nu z - 1)$ and $y_f = d + z = 1 + z$. Finally, note also that this relation for γ_{el} does not allow for taking the weak coupling limit, $z \to 1$ and $\nu \to 1$. This resembles the fact that the specific heat coefficient γ_{el} in the non-interacting system is exponentially supressed, and in this sense the limit $\lambda \to 0$ is non-analytic.

Asymmetric Case ($|u| < v$): Finally, let us consider the asymmetric case, $|u| < v$. In the same way as above, the result for γ_{pl} prevails in the low-temperature regime, i.e.

$$\gamma_{\mathrm{pl}} \approx \frac{\pi}{3v^*} = \frac{\pi}{3v}\, e^{\left(\mathcal{C}\nu \ln \frac{\mathcal{V}\Lambda}{|\mu|}\right)^{1/5}} \quad \text{for} \quad \lambda \neq 0, |u| < v, |\mu| T^{-1/(\nu z)} \gg 1 \tag{5.53}$$

where v^* is the plasmon velocity at the cut-off scale, $b^* = E_0/|\mu|$ (see Sec. B.4.1 for details)

The calculation of the specific heat coefficient for the fermions is tedious, but can be performed similarly to the previous calculations (see Sec. B.4.2 for details). Finally, γ_{el} is given by

$$\gamma_{\mathrm{el}} \approx \frac{1}{\sqrt{2\pi}|u^*|}\left(\frac{|\Delta^*|}{T}\right)^{5/2} e^{-|\Delta^*|/T} \quad \text{for} \quad \lambda \neq 0, |u| < v, |\mu| T^{-1/(\nu z)} \gg 1 \tag{5.54}$$

which corresponds to the non-interacting result but with the chemical potential μ and the fermion velocity u replaced by their values Δ^* and u^* at the cut-off scale, respectively:

$$u^* = u \exp\left[-\left(\mathcal{C}\nu \ln \frac{\mathcal{V}\Lambda}{|\mu|}\right)^{1/5}\right] \quad \text{and} \quad \Delta^* = \mu \exp\left[-\frac{3}{2}\left(\mathcal{C}\nu \ln \frac{\mathcal{V}\Lambda}{|\mu|}\right)^{1/5}\right]$$

5.4.3 Summary

Let us summarize the results from above calculations in Table 5.1. Note that we explicitly list the results for the non-interacting case, $\lambda = 0$, to show the effect of interactions between electrons in the quantum wire. A discussion of the results is given in the next section.

In Table 5.1, T denotes the temperature, and the chemical potential μ tunes the distance to the quantum phase transition. $\mathcal{V}$ is an arbitrary constant with the dimension of a velocity to ensure proper physical dimensions, and Λ is the momentum cutoff introduced in the renormalization group. The functions $C_1(z) = \frac{z+1}{z^2}\,\Gamma\left(\frac{z+1}{z}\right)\zeta\left(\frac{z+1}{z}\right)$ and $C_2(z) = 2(1 - 2^{-1/z})C_1(z)$ are prefactors that depend only on the dynamical exponent z. Finally, in the last line we used that $u^* = u \exp\left[-\left(\mathcal{C}\nu \ln \frac{\mathcal{V}\Lambda}{|\mu|}\right)^{1/5}\right]$ and $\Delta^* = \mu \exp\left[-\frac{3}{2}\left(\mathcal{C}\nu \ln \frac{\mathcal{V}\Lambda}{|\mu|}\right)^{1/5}\right]$.

		plasmons	fermions
$\lambda = 0$	QC regime	$\frac{\pi}{3v}$	$\frac{\pi}{6\|u\|}$
	low-T regime	$\frac{\pi}{3v}$	$\frac{1}{\sqrt{2\pi\|u\|}}\left(\frac{\|\mu\|}{T}\right)e^{-\|\mu\|/T}$
$\lambda \neq 0$ $\|u\| = v$	QC regime	$C_1(z)\frac{2}{\pi v}\left(\frac{\mathcal{V}\Lambda}{T}\right)^{\frac{z-1}{z}}$	$C_2(z)\frac{1}{\pi\|u\|}\left(\frac{\mathcal{V}\Lambda}{T}\right)^{\frac{z-1}{z}}$
	low-T regime	$C_1(z)\frac{2}{\pi v}\left(\frac{\mathcal{V}\Lambda}{\|\mu\|}\right)^{\nu(z-1)}$	$C_2\left(\frac{\nu z-1}{\nu}\right)\frac{1}{\pi\|u\|}\left(\frac{\mathcal{V}\Lambda}{\|\mu\|}\right)^{\frac{\nu}{\nu z-1}}\left(\frac{\mathcal{V}\Lambda}{T}\right)^{\frac{\nu}{\nu z-1}-1}$
$\lambda \neq 0$ $\|u\| < v$	QC regime	$\frac{\pi}{3v}\,e^{\left(\mathcal{C}z^{-1}\ln\frac{\mathcal{V}\Lambda}{T}\right)^{1/5}}$	$\frac{\pi}{6\|u\|}\,e^{\left(\mathcal{C}z^{-1}\ln\frac{\mathcal{V}\Lambda}{T}\right)^{1/5}}$
	low-T regime	$\frac{\pi}{3v}\,e^{\left(\mathcal{C}\nu\ln\frac{\mathcal{V}\Lambda}{\|\mu\|}\right)^{1/5}}$	$\frac{1}{\sqrt{2\pi\|u^*\|}}\left(\frac{\|\Delta^*\|}{T}\right)e^{-\|\Delta^*\|/T}$

Table 5.1: Summary of the results for the specific heat coefficient, γ.

5.5 Discussion of the Results

With general arguments it is shown scale invariant combination $|r|t^{-1/(\nu z)}$ of the control parameter $r = \mu$ and the (dimensionless) temperature $t = T/T_0$ defines a crossover line which separates the phase diagram into a quantum critical regime and a low-temperature regime. The quantum critical regime is governed by a power-law behavior of the specific heat coefficient γ, while in the low-temperature regime the fermion contribution, γ_{el}, is exponentially suppressed for $|u| < v$. As expected, this is a result of of strong interaction effects close to the quantum critical point.

In the non-interacting case, the specific heat coefficient for the plasmon excitations in the Luttinger liquid is equal to $\gamma_{\mathrm{pl}} = \pi/(3v)$ which is a well-known result [17]. On the other hand, the Ising fermions have the specific heat coefficient $\gamma_{\mathrm{el}} = \pi/(6|u|)$. If the plasmons and fermions are equally fast, i.e. $|u| = v$, the specific heat coefficient of the Ising fermions is just half as much as the plasmon one. This peculiar property can be easily understood upon rewriting our model in terms of Majorana fermions: Each Majorana field has a specific heat coefficient of $\pi/(6v)$. Since the Luttinger liquid consists of two Majorana fields, its specific heat coefficient is simply given by twice this value. On the other hand, the Ising fermions can be rewritten in terms of a single Majorana field. This integer relation between γ_{el} and γ_{pl} thus indicates that our model has a higher symmetry for $|u| = v$.

When the interaction between electrons is switched on, we see that the renormalization of both plasmon and fermion velocity introduces an explicit momentum-dependence of the parameters. The calcuation of the free energy and subsequently the specific heat coefficient γ has to take into account for the renormalized parameters. It turns out that the results in the quantum critical regime are quite different from those in the low-temperature regime, at least for the fermion part of our model.

First, let us focus on the case where plasmons and fermions are equally fast,

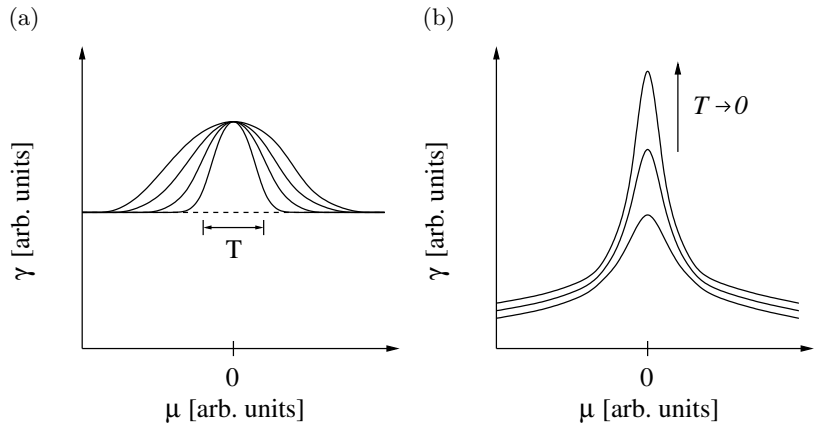

Figure 5.3: Schematic picture of the specific heat coefficient, γ. Fig. (a) shows γ in the non-interacting system where the constant contribution (dashed line) comes from the plasmons. The specific heat coefficient of the Ising fermions, γ_{el}, shows an exponential suppression in the low-temperature phase, and the width of the peak in the quantum critical regime is proportional to temperature. Fig. (b) shows γ in the interacting system. As a result, the central peak at $\mu = 0$ diverges as the quantum critical point is approached upon lowering the temperature.

$|u| = v$. Here, our renormalization group analysis shows that the interactions modify the dispersion relation $\omega \sim k^z$ by introducing an effective dynamical exponent z. Note that this dynamical exponent actually is interaction-dependent and constant, $z = z(\lambda) = const.$ Under renormalization group transformations both the plasmon and fermion velocities decrease with a power law of z. Subsequently, the specific heat coefficients of both subsystems, γ_{pl} and γ_{el}, show a power-law behavior as well. Approaching the quantum critical point by either decreasing the temperature T or the chemical potential μ, we see that the specific heat coefficients diverge at quantum criticality. The exponents obtained from explicit calculations agree with the predictions from our scaling analysis. Finally, one should also note that in the low-temperature regime the specific heat coefficient of the fermions, γ_{el}, also obeys a power-law behavior. This is in contrast to the exponential suppression of γ_{el} in the asymmetric case $|u| < v$. A schematic picture of the results is depicted in Fig. 5.3.

Now let us consider the case where the plasmons are faster than the fermions, $|u| < v$. Here we obtain results which look similar to those obtained for the non-interacting model. However, since both velocities $|u|$ and v decrease under renormalization group transformations, the corresponding specific heat coefficients diverge as the quantum critical point is approached, similarly to the case $|u| = v$. However, in contrast to the symmetric case with a power-law divergence of the specific heat coefficient γ, for the asymmetric case $|u| < v$ we observe a non-analytic divergence of γ.

Finally, the divergence of the specific heat coefficient γ shows that the critical

theory is not a conformal field theory. This can be understood in terms of the so-called central charge of a conformal field theory, c, which is defined by

$$\gamma = c\,\frac{\pi}{3\mathcal{V}} \tag{5.55}$$

Here, $\mathcal{V}$ is a typical velocity of the underlying model. In the non-interacting system, the central charge of our model at $|u| = v$ is $c = 1 + \frac{1}{2} = \frac{3}{2}$. However, once we take into account for the interaction between electrons, the velocity entering Eq. (5.55) decreases under renormalization group transformations. Although we can formulate our renormalization group approach in such a way that the plasmon velocity v remains constant, the effective dynamical exponent z already indicates that the critical theory is strongly changed. Indeed, upon rewriting the theory in the original variables we see that due to the decrease of v the central charge diverges as the quantum critical point is approached. Thus, in this picture the critical theory is *not* a conformal field theory of three Majorana fields.

Chapter 6

Summary and Outlook

In this thesis, we study a one-dimensional system of interacting spinless electrons at quantum criticality. We consider a two-band model, where the second band becomes activated as a function of the chemical potential. In our theoretical analysis we describe the lower band as a Luttinger liquid while the upper one is described in terms of Ising fermions. In addition to the usual density-density interaction between the two bands, we consider the term in the Hamiltonian which transfers pairs of electrons from one band to the other.

It is shown in Chapter 3 that the relevance of the pair-transfer operator depends crucially on the inter-band interaction strength. In the weak coupling limit it turned out that this operator is relevant and has to be taken into account. Subsequently, we rewrite the Hamiltonian performing a unitary transformation. It is shown that the net effect of the pair-transfer can be re-absorbed in a modified inter-band density-density interaction.

The unitary transformation allows us to study the model with renormalization group methods in Chapter 4. Using a momentum-shell renormalization scheme, we calculate perturbatively the self-energy and vertex corrections to leading order in the interaction. However, these corrections turn out to have a logarithmic UV divergence, as one expects for gapless one-dimensional systems. The actual renormalization of the model is performed by imposing different renormalization conditions. The resulting non-linear differential equations allow for an analytical solution. Upon integrating the equations we show that both the plasmons and fermions velocity decrease under subsequent renormalization transformations.

There is however an important difference in how the two velocities decrease. In the case where the plasmons are faster than the fermions the velocities decrease exponentially and eventually vanish, but the convergence of the flow is very slow. When the fermions are faster than the plasmons instead, there exists a scale at which the plasmon velocity is zero while the fermionic one is still finite. The vanishing plasmon velocity indicates a diverging compressibility in the Luttinger liquid sector

of our model. This would open up the possibility of a first order transition.

Finally, the case of plasmons and fermions being equally fast resulted to be special. In fact, the interaction between electrons modifies effectively the dispersion relation for the plasmons, introducing a dynamical exponent z. This dynamical exponent is interaction-dependent and non-universal.

Therefore, we started to investigate thermodynamical quantities. As a concrete example we considered the specific heat coefficient γ. In Chapter 5 we use scaling theory to guess the leading behavior of the specific heat coefficient in the quantum critical and the low-temperature regime. These predictions are confirmed by explicit analytical calculations.

As expected, the interaction between electrons modifies the thermodynamical properties. However, in the case where plasmons and fermions are equally fast, we find a non-universal power-law behavior of the specific heat coefficient in both the quantum critical regime and the low-temperature regime. In the zero temperature limit, the specific heat coefficient diverges as a function of temperature with some power law depending on the dynamical exponent z.

A natural next step is to consider additional quantities. For example, the compressibility of the Luttinger liquid would give us insights about the possibility of a first order transition preempting Ising criticality. Moreover, from an experimental point of view it is also important to look at transport properties.

Appendix A

Calculation of the Leading-Order Corrections

A.1 Plasmon Self-Energy

In general, the self-energy is defined as the difference between the bare propagator in the non-interacting system and the propagator in the interacting system. It thus describes the renormalization of the bare propagator due to interactions between the particles. According to the Dyson equation, the self-energy for the plasmons, Π, is given by the relation

$$\mathcal{D}^{-1}(q,\Omega_n) = \mathcal{D}_0^{-1}(q,\Omega_n) - \Pi(q,\Omega_n) \tag{A.1}$$

where $\mathcal{D}_0$ and $\mathcal{D}$ are the bare and full plasmon propagators, respectively.

In order to calculate the plasmon self-energy, Π, to leading order we perform perturbation theory in the strong coupling limit, i.e. for small inter-band coupling λ between the plasmons in the lower subband and the Ising fermions in the upper subband. In a one-loop order expansion, the plasmon self-energy Π reads

$$\Pi(q,\Omega_n) = -\frac{1}{2!}\,\lambda^2 q^2 \frac{1}{\beta L}\sum_{k,\omega_n} \mathrm{Tr}\big\{\sigma^3 \mathcal{G}_0(k,\omega_n)\sigma^3 \mathcal{G}_0(k+q,\omega_n+\Omega_n)\big\} \tag{A.2}$$

$$= -\lambda^2 q^2 \frac{1}{\beta L}\sum_{k,\omega_n} \frac{i\omega_n(i\omega_n+i\Omega_n) - u^2 k(k+q) + \mu^2}{[(i\omega_n)^2-\omega_k^2][(i\omega_n+i\Omega_n)^2-\omega_{k+q}^2]} \tag{A.3}$$

Here, q and Ω_n are the external momentum and frequency of the self-energy bubble, as shown in Fig. A.1. Furthermore, k and ω_n are the internal momentum and frequency degrees of freedom which are to be integrated out. $\beta = 1/(k_B T)$ is the inverse of temperature, and L is the one-dimensional volume of the model. The chemical potential μ tunes the distance to quantum criticality at $\mu_c = 0$, and the eigenenergies of the Ising fermions are given by $\omega_k = \sqrt{\mu^2 + (uk)^2}$ with u being the fermion velocity.

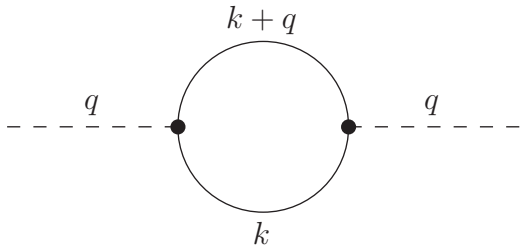

Figure A.1: Leading-order self-energy diagram for the plasmons, Π. Fermion fields are shown as solid lines, plasmon ones as dashed lines.

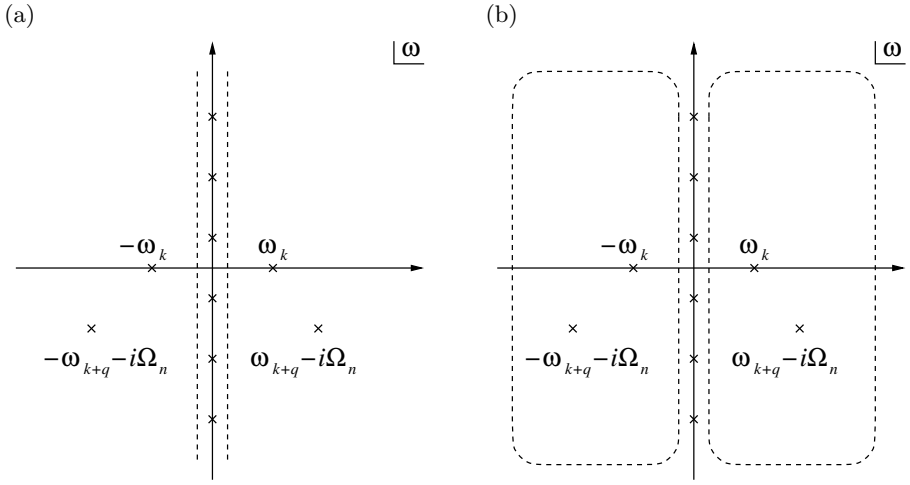

Figure A.2: A reasonable deformation of the integration contour $\mathcal{C}$ (dashed line) for the summation over fermionic Matsubara frequencies ω_n (crosses).

The summation over fermionic Matsubara frequencies, $\omega_n = (2n+1)\pi/\beta$, is performed in a standard way [12]. In a first step, we apply the residue theorem and rewrite the sum as a contour integral in the complex frequency plane (see Fig. A.2 (a)),

$$\begin{aligned}\Pi(q,\Omega_n) &= -\lambda^2 q^2 \frac{1}{\beta L} \sum_{k,\omega_n} \frac{i\omega_n(i\omega_n + i\Omega_n) - u^2 k(k+q) + \mu^2}{[(i\omega_n)^2 - \omega_k^2][(i\omega_n + i\Omega_n)^2 - \omega_{k+q}^2]} \\ &= +\lambda^2 q^2 \frac{1}{L} \sum_{k} \oint_{\mathcal{C}} \frac{dz}{2\pi i}\, n_F(z)\, \frac{z(z+i\Omega_n) - u^2 k(k+q) + \mu^2}{[z^2 - \omega_k^2][(z+i\Omega_n)^2 - \omega_{k+q}^2]}\end{aligned}$$

Here, $n_{F/B}(z) = \left(1 \pm e^{\beta\epsilon}\right)^{-1}$ are the Fermi and Bose occupation factors, respectively. The additional prefactor -1 stems from the Fermi factor and compensates the corresponding residue at $z = i\omega_n$. In a second step, we deform the integraction contour $\mathcal{C}$ in such a way that upon performing the contour integral only a finite number of poles have to be evaluated. One particular way to deform the integration contour for above integral is shown in Fig. A.2 (b).

Following the above procedure, the plasmon self-energy Π takes the form

$$\begin{aligned}\Pi(q,\Omega_n) &= -\lambda^2 q^2 \frac{1}{\beta L}\sum_{k,\omega_n} \frac{i\omega_n(i\omega_n+i\Omega_n)-u^2k(k+q)+\mu^2}{[(i\omega_n)^2-\omega_k^2][(i\omega_n+i\Omega_n)^2-\omega_{k+q}^2]} \\ &= +\lambda^2 q^2 \frac{1}{L}\sum_k \oint_{\mathcal{C}} \frac{dz}{2\pi i}\, n_F(z)\, \frac{z(z+i\Omega_n)-u^2k(k+q)+\mu^2}{[z^2-\omega_k^2][(z+i\Omega_n)^2-\omega_{k+q}^2]} \\ &= -\lambda^2 q^2 \frac{1}{L}\sum_k \sum_{\alpha=\pm 1}\Bigg[n_F(\alpha\omega_k)\, \frac{\omega_k(\omega_k+i\Omega_n)-u^2k(k+q)+\mu^2}{2\alpha\omega_k[(\omega_k+i\Omega_n)^2-\omega_{k+q}^2]} \\ &\qquad + n_F(\alpha\omega_{k+q}-i\Omega_n)\, \frac{(\omega_{k+q}-i\Omega_n)\omega_{k+q}-u^2k(k+q)+\mu^2}{2\alpha\omega_{k+q}[(\omega_{k+q}-i\Omega_n)^2-\omega_k^2]}\Bigg]\end{aligned}$$

Note that the Fermi occupation factor remains unchanged when adding a bosonic Matsubara frequency Ω_n to its argument:

$$n_F(\epsilon - i\Omega_n) = n_F(\epsilon) \quad \text{for all} \quad \Omega_n = 2n\pi/\beta \tag{A.4}$$

Moreover, in the limit of zero temperature, the structure of the Fermi and Bose occupation factors gets much simpler as

$$n_{F/B}(\epsilon) \to \pm\Theta(-\epsilon) \quad \text{for} \quad \beta\to\infty \tag{A.5}$$

where $\Theta(x)$ is the Heaviside step function. Thus,

$$\begin{aligned}\Pi(q,\Omega_n) = +\lambda^2 q^2 \frac{1}{L}\sum_k \Bigg[&\frac{\omega_k(\omega_k+i\Omega_n)-u^2k(k+q)+\mu^2}{2\omega_k[(\omega_k+i\Omega_n)^2-\omega_{k+q}^2]} \\ &+ \frac{(\omega_{k+q}-i\Omega_n)\omega_{k+q}-u^2k(k+q)+\mu^2}{2\omega_{k+q}[(\omega_{k+q}-i\Omega_n)^2-\omega_k^2]}\Bigg]\end{aligned}$$

The remaining momentum integral contains a logarithmic ultraviolet divergence which can be extracted by using a hard momentum cutoff Λ. At zero temperature the external momentum, q, and frequency, Ω_n, are small compared to the momentum cutoff Λ. In the vicinity of the quantum critical point, $\mu = 0$, a Taylor expansion of the self-energy Π to leading order in the small parameters q, Ω_n and μ gives rise to a logarithmic correction of the bare plasmon propagator,

$$\Pi(q,\Omega_n) \approx \lambda^2 q^2 \int_{-\Lambda}^{\Lambda} \frac{dk}{2\pi}\left[\frac{1}{4|u||k|}+\frac{1}{4|u||k|}\right] \approx \frac{\lambda^2 q^2}{2\pi|u|}\ln\Lambda \tag{A.6}$$

Here, Λ is the ultraviolet momentum cutoff to regularize the logarithmic divergence of the plasmon self-energy as described above.

A.2 Fermion Self-Energy

The fermion self-energy, Σ, describes the renormalization of the Ising fermions due to the inter-band density-density interaction between the two subbands. It follows from a Dyson equation similar to Eq. (A.1),

$$\mathcal{G}^{-1}(k,\omega_n) = \mathcal{G}_0^{-1}(k,\omega_n) - \Sigma(k,\omega_n) \tag{A.7}$$

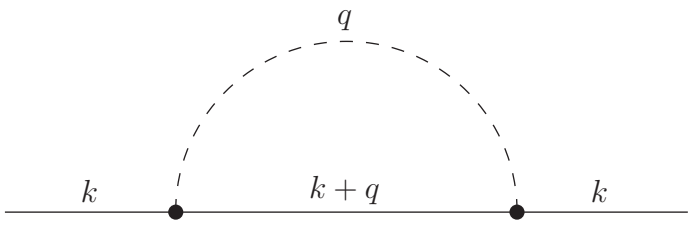

Figure A.3: Leading-order self-energy diagram for the Ising fermions, Σ. Fermion fields are shown as solid lines, plasmon ones as dashed lines.

where $\mathcal{G}_0$ and $\mathcal{G}$ are the bare and full fermion propagators, respectively. In the strong coupling limit, i.e. for small inter-band coupling λ, the fermion self-energy takes the form

$$\Sigma(k,\omega_n) = \lambda^2 \frac{1}{\beta L} \sum_{q,\Omega_n} q^2 \mathcal{D}_0(q,\Omega_n) \sigma^3 \mathcal{G}_0(k+q,\omega_n+\Omega_n)\sigma^3 \tag{A.8}$$

$$= \lambda^2 \frac{1}{\beta L} \sum_{q,\Omega_n} q^2 \frac{-\pi K v}{(i\Omega_n)^2-(vq)^2} \frac{-(i\omega_n+i\Omega_n)\mathbb{1}+\mu\sigma^3+u(k+q)\sigma^2}{(i\omega_n+i\Omega_n)^2-\omega_{k+q}^2} \tag{A.9}$$

Here, k and ω_n are the external momentum and frequency of the fermionic self-energy, as shown in Fig. A.3. The internal degrees of freedom, i.e. momentum q and frequency Ω_n, are integrated out in the following. The chemical potential μ tunes the distance to quantum criticality, $\omega_k = \sqrt{\mu^2+(uk)^2}$ are the fermionic eigenenergies with u being the fermion velocity. Finally, v is the plasmon velocity, and K the Luttinger liquid parameter of the first subband.

The summation over bosonic Matsubara frequencies, $\omega_n = 2n\pi/\beta$, is performed in a similar way as described in the previous section. In a first step, we apply the residue theorem to rewrite the sum as a contour integral in the complex frequency plane,

$$\begin{aligned}
\Sigma(k,\omega_n) &= -\lambda^2\pi K v \frac{1}{\beta L}\sum_{q,\Omega_n} q^2 \frac{-(i\omega_n+i\Omega_n)\mathbb{1}+\mu\sigma^3+u(k+q)\sigma^2}{[(i\Omega_n)^2-(vq)^2][(i\omega_n+i\Omega_n)^2-\omega_{k+q}^2]} \\
&= -\lambda^2\pi K v \frac{1}{L}\sum_q q^2 \oint_{\mathcal{C}} \frac{dz}{2\pi i}\, n_B(z)\, \frac{-(i\omega_n+z)\mathbb{1}+\mu\sigma^3+u(k+q)\sigma^2}{[z^2-(vq)^2][(i\omega_n+z)^2-\omega_{k+q}^2]} \\
&= +\lambda^2\pi K v \frac{1}{L}\sum_q q^2 \sum_{\alpha=\pm1} \Bigg[n_B(\alpha v q)\, \frac{-(i\omega_n+\alpha v q)\mathbb{1}+\mu\sigma^3+u(k+q)\sigma^2}{2\alpha v q[(i\omega_n+\alpha v q)^2-\omega_{k+q}^2]} \\
&\qquad + n_B(\alpha\omega_{k+q}-i\omega_n)\, \frac{-\alpha\omega_{k+q}\mathbb{1}+\mu\sigma^3+u(k+q)\sigma^2}{2\alpha\omega_{k+q}[(\alpha\omega_{k+q}-i\omega_n)^2-(vq)^2]} \Bigg]
\end{aligned}$$

Note that for bosonic Matsubara frequencies there is no additional prefactor of -1 since the Bose occupation factor has the residue $+1$ at $z = i\Omega_n$. On the other hand, when adding a fermionic Matsubara frequency to the argument of the Bose factor it changes into a Fermi factor,

$$n_B(\epsilon - i\omega_n) = -n_F(\epsilon) \quad \text{for all} \quad \omega_n = (2n+1)\pi/\beta \tag{A.10}$$

Thus, the fermion self-energy Σ reads

$$\Sigma(k,\omega_n) = +\lambda^2\pi K v \frac{1}{L}\sum_q q^2 \sum_{\alpha=\pm 1}\Bigg[n_B(\alpha v q)\,\frac{-(i\omega_n+\alpha v q)\mathbb{1}+\mu\sigma^3+u(k+q)\sigma^2}{2\alpha v q[(i\omega_n+\alpha v q)^2-\omega_{k+q}^2]} \\ - n_F(\alpha\omega_{k+q})\,\frac{-\alpha\omega_{k+q}\mathbb{1}+\mu\sigma^3+u(k+q)\sigma^2}{2\alpha\omega_{k+q}[(\alpha\omega_{k+q}-i\omega_n)^2-(vq)^2]}\Bigg]$$

In the zero temperature limit, we can replace the Fermi and Bose occupation factors by Heaviside step functions, cf. Eq. (A.5). This yields

$$\Sigma(k,\omega_n) = -\lambda^2\pi K v \frac{1}{L}\sum_q q^2 \sum_{\alpha=\pm 1}\Bigg[\Theta(-\alpha v q)\,\frac{-(i\omega_n+\alpha v q)\mathbb{1}+\mu\sigma^3+u(k+q)\sigma^2}{2\alpha v q[(i\omega_n+\alpha v q)^2-\omega_{k+q}^2]} \\ + \Theta(-\alpha\omega_{k+q})\,\frac{-\alpha\omega_{k+q}\mathbb{1}+\mu\sigma^3+u(k+q)\sigma^2}{2\alpha\omega_{k+q}[(\alpha\omega_{k+q}-i\omega_n)^2-(vq)^2]}\Bigg]$$

In principle, the leading order correction can be obtained by carrying out a Taylor expansion for small external momentum k and frequency ω_n with respect to the momentum cutoff Λ. However, due to the structure of Σ one has to take more care in carrying out the actual Taylor expansion than for the plasmon self-energy, Π. Let us consider the two terms in the fermion self-energy separately,

$$S_1 = q^2 \sum_{\alpha=\pm 1}\Theta(-\alpha v q)\,\frac{-(i\omega_n+\alpha v q)\mathbb{1}+\mu\sigma^3+u(k+q)\sigma^2}{2\alpha v q[(i\omega_n+\alpha v q)^2-\omega_{k+q}^2]}$$
$$S_2 = q^2 \sum_{\alpha=\pm 1}\Theta(-\alpha\omega_{k+q})\,\frac{-\alpha\omega_{k+q}\mathbb{1}+\mu\sigma^3+u(k+q)\sigma^2}{2\alpha\omega_{k+q}[(\alpha\omega_{k+q}-i\omega_n)^2-(vq)^2]}$$

First, let us focus on the first term, S_1. Assuming that the plasmon velocity is positive, $v>0$, we can rewrite S_1 in a first step as

$$S_1 = q^2 \sum_{\alpha=\pm 1}\frac{-(i\omega_n - v|q|)\mathbb{1}+\mu\sigma^3+u(k-\alpha|q|)\sigma^2}{-2v|q|[(i\omega_n-v|q|)^2-\omega_{k-\alpha|q|}^2]}$$

Since we are interested in the low-energy behavior of Σ near the quantum critical point we then carry out a Taylor expansion for small momentum k, small frequency ω_n, and small chemical potential μ. Retaining only the leading order terms, this leads to

$$S_1 = \frac{-\mathbb{1}}{v^2-|u|^2} + \left[(-i\omega_n)\mathbb{1}\frac{v^2+|u|^2}{v(v^2-|u|^2)^2} - \mu\sigma^3\frac{1}{v(v^2-|u|^2)} - uk\sigma^2\frac{v^2+|u|^2}{v(v^2-|u|^2)^2}\right]\frac{1}{|q|}$$

Thus, upon integrating out the internal momenta q we obtain a logarithmic ultraviolet divergence,

$$\int_{-\Lambda}^{\Lambda}\frac{dq}{2\pi}\,S_1 = \frac{\Lambda}{\pi}\frac{-\mathbb{1}}{v^2-|u|^2} \\ + \left[(-i\omega_n)\mathbb{1}\frac{v^2+|u|^2}{v(v^2-|u|^2)^2} - \mu\sigma^3\frac{1}{v(v^2-|u|^2)} - uk\sigma^2\frac{v^2+|u|^2}{v(v^2-|u|^2)^2}\right]\frac{\ln\Lambda}{\pi}$$

where Λ is the same ultraviolet momentum cutoff as in the previous section which regularizes the divergence of the above momentum integral.

In a similar way, we can calculate the second term, S_2. In a first step, we use the fact that the fermion eigenenergies are positive, $\omega_k > 0$, and rewrite S_2 as

$$S_2 = q^2 \frac{\omega_{k+q}\mathbb{1} + \mu\sigma^3 + u(k+q)\sigma^2}{-2\omega_{k+q}[(\omega_{k+q} + i\omega_n)^2 - (vq)^2]}$$

We can then carry out a Taylor expansion for small external momentum k, small frequency ω_n, and small chemical potential μ. The leading order terms for S_2 read

$$S_2 = \frac{\mathbb{1}}{v^2 - |u|^2} + \left[(-i\omega_n)\mathbb{1}\frac{-2|u|}{(v^2-|u|^2)^2} + \mu\sigma^3\frac{1}{|u|(v^2-|u|^2)} - uk\sigma^2\frac{2|u|}{(v^2-|u|^2)^2}\right]\frac{1}{|q|}$$

Thus, the leading order divergence of S_2 is given by

$$\int_{-\Lambda}^{\Lambda}\frac{dq}{2\pi}\,S_2 = \frac{\Lambda}{\pi}\frac{\mathbb{1}}{v^2-|u|^2} + \left[(-i\omega_n)\mathbb{1}\frac{-2|u|}{(v^2-|u|^2)^2} + \mu\sigma^3\frac{1}{|u|(v^2-|u|^2)} - uk\sigma^2\frac{2|u|}{(v^2-|u|^2)^2}\right]\frac{\ln\Lambda}{\pi}$$

with Λ being the same ultraviolet momentum cutoff as above.

Finally, by summing up both contributions S_1 and S_2 we obtain the fermion self-energy Σ to leading order in k, ω_n and μ as

$$\Sigma(k,\omega_n) = -\frac{\lambda^2 K}{2(v+|u|)^2}\left[(-i\omega_n)\mathbb{1} + \frac{v+|u|}{|u|}\,\mu\sigma^3 - uk\sigma^2\right]\ln\Lambda \tag{A.11}$$

Note that the chemical potential μ obtains a correction different from the dynamical parts, ω_n and u.

A.3 Vertex Correction

Finally, let us consider the interaction between the plasmons and fermions in the lower and upper subband, as shown in Fig. A.4. In general, a vertex correction $\delta\Gamma$ is defined by the relation

$$\Gamma(q,\Omega_n;k,\omega_n) = \Gamma_0(q,\Omega_n;k,\omega_n) + \delta\Gamma(q,\Omega_n;k,\omega_n) \tag{A.12}$$

Here, k and ω_n are the external momentum and frequency dependence of the incoming fermion field, and q and Ω_n denote the momentum and frequency dependence of the incoming plasmon field. The outgoing fermion field takes momentum $k+q$ and frequency $\omega_n + \Omega_n$. Note that $\Gamma_0(q,\Omega_n;k,\omega_n) \equiv \lambda = const.$ In the strong coupling limit, i.e. for small inter-band interaction λ, the one-loop vertex correction reads

$$\delta\Gamma(q,\Omega_n;k,\omega_n) = \frac{1}{2!}\lambda^3\frac{1}{\beta L}\sum_{q',\Omega_n'} q'^2\mathcal{D}_0(q',\Omega_n') \times \mathrm{Tr}\big\{\sigma^3\mathcal{G}_0(k+q',\omega_n+\Omega_n')\sigma^3\mathcal{G}_0(k+q+q',\omega_n+\Omega_n+\Omega_n')\big\} \tag{A.13}$$

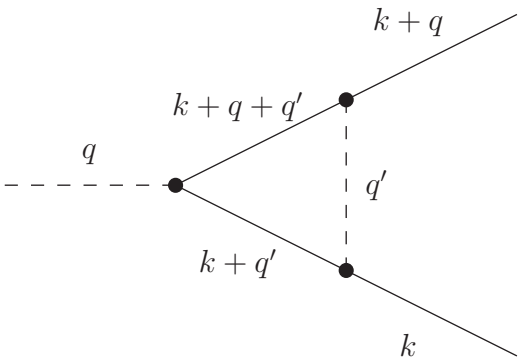

Figure A.4: Leading-order self-energy diagram for the vertex correction, $\delta\Gamma$. Fermion fields are shown as solid lines, plasmon ones as dashed lines.

where $\mathcal{D}_0$ and $\mathcal{G}_0$ are the bare plasmon and fermion propagators, respectively.

Since we are interested in the low-energy properties near the Fermi surface, all incoming and outgoing momenta k, q, and $k+q$ have to be close to the Fermi surface. Moreover, since the inter-band density-density interaction, Γ_0, is a marginal term in the Hamiltonian, it suffices to calculate the correction $\delta\Gamma$ for small external momenta and frequencies. In fact, the linear and all higher orders in a Taylor expansion result in additional terms in the Hamiltonian which are irrelevant in the renormalization group sense. Thus, to leading order we get

$$\delta\Gamma = -\lambda^3\pi K v \frac{1}{\beta L}\sum_{q',\Omega'_n} \frac{q'^2}{[(i\Omega'_n)^2-(vq')^2][(i\Omega'_n)^2-\omega_{q'}^2]}$$

In a first step, we can rewrite the summation over bosonic Matsubara frequencies by means of the residue theorem,

$$\begin{aligned}
\delta\Gamma &= -\lambda^3\pi K v \frac{1}{\beta L}\sum_{q',\Omega'_n} \frac{q'^2}{[(i\Omega'_n)^2-(vq')^2][(i\Omega'_n)^2-\omega_{q'}^2]} \\
&= -\lambda^3\pi K v \frac{1}{L}\sum_{q'} \oint_{\mathcal{C}} \frac{dz}{2\pi i}\, n_B(z)\, \frac{q'^2}{[z^2-(vq')^2][z^2-\omega_{q'}^2]} \\
&= +\lambda^3\pi K v \frac{1}{L}\sum_{q'}\sum_{\alpha=\pm1}\Bigg[n_B(\alpha v q') \frac{q'^2}{2\alpha v q'[(vq')^2-\omega_{q'}^2]} \\
&\qquad\qquad + n_B(\alpha\omega_{q'}) \frac{q'^2}{2\alpha\omega_{q'}^2[\omega_{q'}^2-(vq')^2]}\Bigg]
\end{aligned}$$

In the zero temperature limit, the Bose occupation factors can be replaced by Heaviside step functions,

$$\begin{aligned}
\delta\Gamma &= +\lambda^3\pi K v \frac{1}{L}\sum_{q'}\left[\frac{q'^2}{2v|q'|[(vq')^2-\omega_{q'}^2]} + \frac{q'^2}{2\omega_{q'}[\omega_{q'}^2-(vq')^2]}\right] \\
&= +\lambda^3\pi K v \frac{1}{L}\sum_{q'}\left[\frac{1}{2v(v^2-|u|^2)|q'|} + \frac{1}{2|u|(|u|^2-v^2)|q'|}\right]
\end{aligned}$$

The remaining momentum integral contains a logarithmic ultraviolet divergence. Using the hard momentum cutoff scheme as described in the previous sections we can extract this divergence. To leading order we obtain

$$\delta\Gamma \equiv \delta\Gamma(q, \Omega_n; k, \omega_n) = -\frac{\lambda^3 K}{2|u|(v + |u|)} \ln \Lambda \tag{A.14}$$

where Λ is the ultraviolet momentum cutoff.

Appendix B

Calculation of the Specific Heat Coefficient

B.1 Free Energy in the Non-Interacting System

The starting point of our analysis is the functional representation of the free energy per volume, $f \equiv L^{-1}F = -(\beta L)^{-1} \ln \mathcal{Z}$, through the quantum partition function $\mathcal{Z}$.

B.1.1 Free Energy of the Plasmons

Using a coherent state path integral for the plasmon field ϕ the quantum partition function of the plasmons is given by

$$\mathcal{Z}_{\mathrm{pl}} = \int \mathcal{D}(\phi) \exp\left\{ -\frac{1}{2}\frac{1}{\beta L} \sum_{q,\Omega_n} \phi^*_{q,\Omega_n} \mathcal{D}_0^{-1}(q,\Omega_n) \phi_{q,\Omega_n} \right\} = \left(\det \mathcal{D}_0^{-1}\right)^{-1/2} \tag{B.1}$$

Thus, the plasmon contribution to the free energy per volume is obtained as

$$f_{\mathrm{pl}} = -\frac{1}{\beta L} \ln \mathcal{Z}_{\mathrm{pl}} = \frac{1}{2}\frac{1}{\beta L} \ln\left\{\det \mathcal{D}_0^{-1}\right\} = \frac{1}{2}\frac{1}{\beta L} \mathrm{Tr}\left\{\ln \mathcal{D}_0^{-1}\right\} \tag{B.2}$$

where L is the one-dimensional volume of the system, and $\beta = 1/(k_B T)$ is the inverse of temperature. Note that the trace runs over momentum space and bosonic Matsubara frequencies, i.e. $\mathrm{Tr}(\cdots) \equiv \sum_{k,\Omega_n}(\cdots)$.

First, let us rewrite the sum over bosonic Matsubara frequencies, $\Omega_n = 2n\pi/\beta$, by means of the residue theorem in terms of a contour integral in complex frequency space,

$$f_{\mathrm{pl}} = \frac{1}{2L} \sum_k \oint_{\mathcal{C}} \frac{dz}{2\pi i} \frac{\beta}{2} \coth\left(\frac{\beta z}{2}\right) \ln\left[\frac{-\pi K v}{z^2 - (vk)^2}\right]$$

where $h(z) = (\beta/2)\coth(\beta z/2)$ has simple poles at $z = i\Omega_n$ with unit residue. Note that the logarithm has a branch cut along the negative real axis in the complex

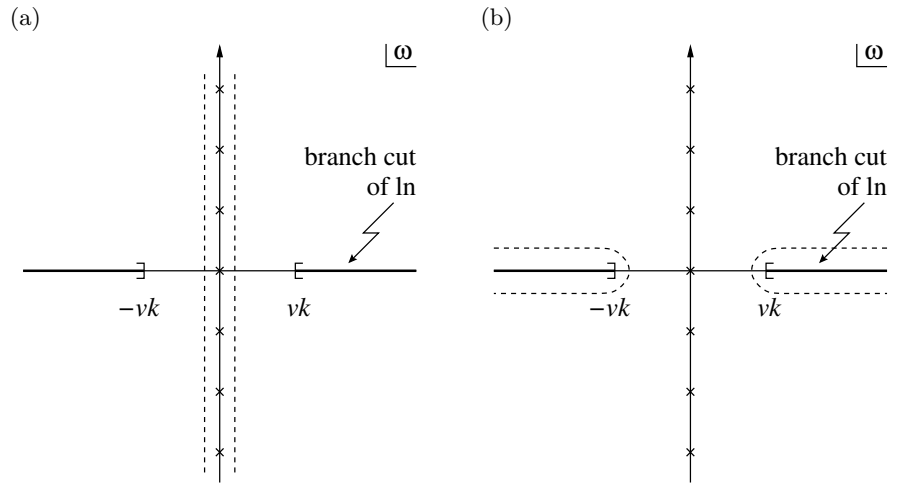

Figure B.1: Deformation of the integration contour $\mathcal{C}$ (dashed line) for the plasmon contribution to the free energy, $f_{\rm pl}$. The bosonic Matsubara frequencies $\Omega_n = 2n\pi/\beta$ are marked by crosses, and the branch cut of $\ln(vk \pm z)$ is indicated by a thick line.

plane. By deforming the integration contour $\mathcal{C}$ according to Fig. B.1 we obtain

$$\begin{aligned}
&\oint_{\mathcal{C}} \frac{dz}{2\pi i} \frac{\beta}{2} \coth\left(\frac{\beta z}{2}\right) \ln\left[\frac{-\pi K v}{z^2 - (vk)^2}\right] \\
&= -2\int_{v|k|}^{\bar{\Omega}} d\Omega \, \frac{\beta}{2} \coth\left(\frac{\beta\Omega}{2}\right) = -2\int_{v|k|}^{\bar{\Omega}} d\Omega \, \frac{d}{d\Omega} \ln\sinh\left(\frac{\beta\Omega}{2}\right) \\
&= -2\ln\sinh\left(\frac{\beta\Omega}{2}\right)\Big|_{v|k|}^{\bar{\Omega}} = 2\ln\left[2\sinh\left(\frac{\beta v|k|}{2}\right)\right] + const
\end{aligned}$$

where in the last line we have neglected the (infinite) constant which arises from the frequency cutoff $\bar{\Omega} \to \infty$. Thus, the plasmon contribution to the free energy per volume is given by

$$f_{\rm pl} = 2T \int_0^{\Lambda} \frac{dk}{2\pi} \ln\left[2\sinh\left(\frac{vk}{2T}\right)\right] \tag{B.3}$$

where Λ is the ultraviolet momentum cutoff introduced in Chapter 4 to regularize the logarithmic ultraviolet divergence of the integral.

B.1.2 Free Energy of the Ising Fermions

In a coherent state path integral representation, the quantum partition function of the Ising fermions reads

$$\mathcal{Z}_{\rm el} = \int \mathcal{D}(\psi,\psi^\dagger) \exp\left\{-\frac{1}{2}\frac{1}{\beta L}\sum_{k,\omega_n} \Psi^\dagger_{k,\omega_n} \mathcal{G}_0^{-1}(k,\omega_n) \Psi_{k,\omega_n}\right\} = \left(\det \mathcal{G}_0^{-1}\right)^{1/2} \tag{B.4}$$

where $\mathcal{G}_0$ is the bare propagator of the Ising fermions. Here, we use a Nambu spinor notation for the Ising fermions which results in the unusual exponent of $1/2$. The contribution of the Ising fermions to the free energy is thus given by

$$f_{\rm el} = -\frac{1}{\beta L}\ln \mathcal{Z}_{\rm el} = -\frac{1}{2}\frac{1}{\beta L}\ln\left\{\det \mathcal{G}_0^{-1}\right\} = -\frac{1}{2}\frac{1}{\beta L}\,\mathrm{Tr}\left\{\ln \mathcal{G}_0^{-1}\right\} \tag{B.5}$$

where L is the one-dimensional volume of the system, and $\beta = 1/(k_B T)$ is the inverse of temperature. Note that the trace not only runs over momentum space and fermionic frequencies but also contains a summation over the eigenvalues of $\mathcal{G}_0^{-1}$ due to its matrix structure, i.e. $\mathrm{Tr}(\cdots) \equiv \sum_{k,\omega_n} \sum_{\mathrm{EV}} (\cdots)$.

After diagonalizing the inverse of the fermion propagator, $\mathcal{G}_0^{-1}$, the sum over fermionic Matsubara frequencies, $\omega_n = (2n+1)\pi/\beta$, can be easily performed by means of the residue theorem. Rewriting the sum as a contour integral in complex frequency space we get

$$f_{\mathrm{el}} = -\frac{1}{2L} \sum_k \sum_{\alpha=\pm 1} \oint_{\mathcal{C}} \frac{dz}{2\pi i} \frac{\beta}{2} \tanh\left(\frac{\beta z}{2}\right) \ln(\alpha\omega_k - z)$$

where $\omega_k = \sqrt{\mu^2 + (uk)^2}$ are the eigenenergies of the Ising fermions, and u being the fermion velocity. Note that $h(z) = (\beta/2)\tanh(\beta z/2)$ has unit residue at $z = i\omega_n$. By deforming the integration contour $\mathcal{C}$ with respect to the branch cut of the logarithm (see Fig. B.2) we obtain

$$\begin{aligned}
&\oint_{\mathcal{C}} \frac{dz}{2\pi i} \frac{\beta}{2} \tanh\left(\frac{\beta z}{2}\right) \ln(\alpha\omega_k - z) \\
&= -\int_{\alpha\omega_k}^{\bar{\omega}} d\omega \, \frac{\beta}{2} \tanh\left(\frac{\beta\omega}{2}\right) = -\int_{\alpha\omega_k}^{\bar{\omega}} d\omega \, \frac{d}{d\omega} \ln\cosh\left(\frac{\beta\omega}{2}\right) \\
&= -\ln\cosh\left(\frac{\beta\omega}{2}\right)\Big|_{\alpha\omega_k}^{\bar{\omega}} = \ln\left[2\cosh\left(\frac{\alpha\beta\omega_k}{2}\right)\right] + const
\end{aligned}$$

In the last line we again have neglected an (infinite) constant due to the frequency cutoff $\bar{\omega} \to \infty$. Finally, upon performing the remaining momentum integral we get

$$f_{\mathrm{el}} = -2T \int_0^{\Lambda} \frac{dk}{2\pi} \ln\left[2\cosh\left(\frac{\omega_k}{2T}\right)\right] \quad \text{with} \quad \omega_k = \sqrt{\mu^2 + (uk)^2} \tag{B.6}$$

where Λ is the ultraviolet momentum cutoff introduced before.

B.2 Specific Heat Coefficient in the Non-Interacting System

The specific heat coefficients for both the plasmonic and fermionic excitations in the two subbands are obtained by differentiating the corresponding free energy twice with respect to temperature. In the non-interacting system, the resulting integrals can be easily solved using the following identities:

$$\int_0^{\infty} dx \, \frac{(2x)^n}{\sinh^2(x)} = 2n\,\Gamma(n)\,\zeta(n) \tag{B.7}$$

$$\int_0^{\infty} dx \, \frac{(2x)^n}{\cosh^2(x)} = 2n\,(1 - 2^{1-n})\,\Gamma(n)\,\zeta(n) \tag{B.8}$$

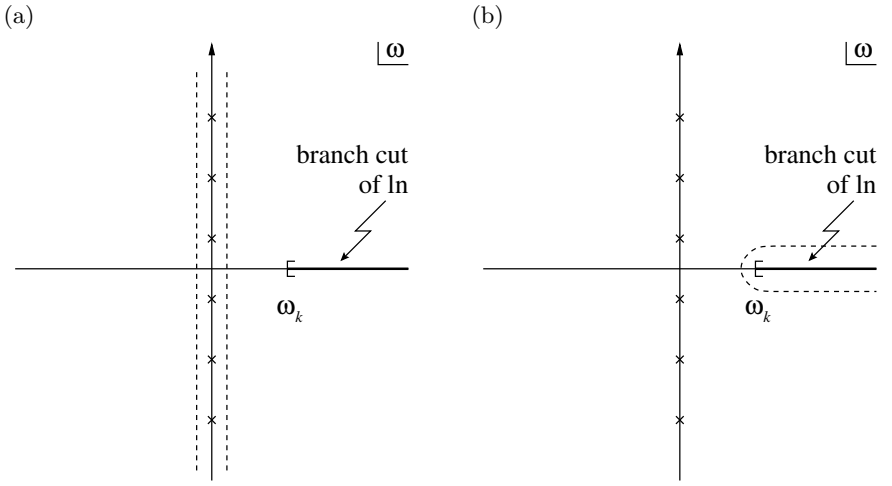

Figure B.2: Deformation of the integration contour $\mathcal{C}$ (dashed line) for the Ising fermion contribution to the free energy, $f_{\rm el}$. The fermionic Matsubara frequencies $\Omega_n = (2n+1)\pi/\beta$ are marked by crosses, and the branch cut of $\ln(\alpha\omega_k - z)$ for $\alpha = +1$ is indicated by a thick line.

where $\Gamma(n)$ is the Euler gamma function and $\zeta(n)$ is the Riemann zeta function,

$$\Gamma(z) = \int_0^\infty dt\, t^{z-1}e^{-t} \quad \text{and} \quad \zeta(s) = \sum_{k=1}^{\infty} \frac{1}{k^s} \quad \text{for} \quad \mathrm{Re}(s) > 1 \tag{B.9}$$

B.2.1 Specific Heat Coefficient of the Plasmons

The plasmon contribution to the specific heat coefficient, $\gamma_{\rm pl}$, is obtained by differentiating the free energy per volume $f_{\rm pl}$ (cf. Eq. (B.3)) twice with respect to temperature,

$$\gamma_{\rm pl} = \left.\frac{\partial^2 f_{\rm pl}}{\partial T^2}\right|_\mu = \frac{1}{2T^3}\int_0^\Lambda \frac{dk}{2\pi} \frac{(vk)^2}{\sinh^2\left[\frac{vk}{2T}\right]} \tag{B.10}$$

where Λ is the ultraviolet momentum cutoff introduced in the previous sections. As the integrand falls off exponentially for large x it is safe to set $\Lambda \to \infty$. Thus, upon substituting $x = (vk)/(2T)$ we get

$$\gamma_{\rm pl} = \frac{2}{\pi v}\int_0^\infty dx\, \frac{x^2}{\sinh^2(x)} = \frac{2}{\pi v}\,\Gamma(2)\,\zeta(2) = \frac{2}{\pi v}\frac{\pi^2}{6} = \frac{\pi}{3v} \tag{B.11}$$

B.2.2 Specific Heat Coefficient of the Ising Fermions

The specific heat coefficient of the Ising fermions, $\gamma_{\rm el}$, is obtained by differentiating the free energy per volume $f_{\rm el}$ (cf. Eq. (B.6)) twice with respect to T,

$$\gamma_{\rm el} = \left.\frac{\partial^2 f_{\rm el}}{\partial T^2}\right|_\mu = \frac{1}{2T^3}\int_0^\Lambda \frac{dk}{2\pi} \frac{\omega_k^2}{\cosh^2\left[\frac{\omega_k}{2T}\right]} \quad \text{with} \quad \omega_k = \sqrt{\mu^2 + (uk)^2} \tag{B.12}$$

Quantum Critical Regime: $|\mu| T^{-1/(\nu z)} \ll 1$

In the quantum critical regime, we can carry out a Taylor expansion in $|\mu|/T \ll 1$ and retain only leading order terms. In the limit $\Lambda \to \infty$ we get

$$\gamma_{\rm el} \approx \frac{1}{2T^3} \int_0^\infty \frac{dk}{2\pi} \frac{(|u|k)^2}{\cosh^2\left[\frac{|u|k}{2T}\right]} = \frac{2}{\pi|u|} \int_0^\infty dx \, \frac{x^2}{\cosh^2(x)} = \frac{2}{\pi|u|} \, \frac{1}{2} \, \Gamma(2) \, \zeta(2) = \frac{\pi}{6|u|} \tag{B.13}$$

where we have used the identity (B.8) to evaluate the integral.

Low-Temperature Regime: $|\mu| T^{-1/(\nu z)} \gg 1$

In the low-temperature regime, we can carry out a Taylor expansion in $T/|\mu| \ll 1$. To this end, let us first substitute $x = |u|k/|\mu|$,

$$\begin{aligned} \gamma_{\rm el} &= \frac{1}{2T^3} \int_0^\infty \frac{dk}{2\pi} \frac{\mu^2 + (uk)^2}{\cosh^2\left[\frac{1}{2T}\sqrt{\mu^2 + (uk)^2}\right]} \\ &= \frac{1}{4\pi|u|} \left(\frac{|\mu|}{T}\right)^3 \int_0^\infty dx \, \frac{1 + x^2}{\cosh^2\left[\frac{|\mu|}{2T}\sqrt{1 + x^2}\right]} \end{aligned}$$

The denominator of the integrand can be simplified by replacing the hyperbolic cosine with an exponential term,

$$\begin{aligned} \gamma_{\rm el} &\approx \frac{1}{4\pi|u|} \left(\frac{|\mu|}{T}\right)^3 \int_0^\infty dx \, \frac{1 + x^2}{\frac{1}{4}\exp\left[\frac{|\mu|}{2T}\sqrt{1 + x^2}\right]} \\ &= \frac{1}{\pi|u|} \left(\frac{|\mu|}{T}\right)^3 \int_0^\infty dx \, (1 + x^2) \exp\left[-\frac{|\mu|}{T}\sqrt{1 + x^2}\right] \\ &\approx \frac{1}{\pi|u|} \left(\frac{|\mu|}{T}\right)^3 \int_0^\infty dx \, (1 + x^2) \exp\left[-\frac{|\mu|}{T}\left(1 + \frac{x^2}{2}\right)\right] \end{aligned}$$

where in the last line we have substituted the square root by its series expansion. To leading order we thus get

$$\gamma_{\rm el} \approx \frac{1}{\sqrt{2\pi}|u|} \left(\frac{|\mu|}{T}\right)^{5/2} e^{-|\mu|/T} \tag{B.14}$$

B.3 Free Energy in the Interacting System

The starting point of our calculation of the specific heat in the interacting system is the free energy per volume, $f = -(\beta L)^{-1} \ln \mathcal{Z}$, where $\mathcal{Z}$ is the quantum partition function.

In the spirit of the momentum-shell renormalization group methods, the free energy is renormalized, and the resulting β function reads

$$\beta(f) = y_f f(b) + \delta f(b) \tag{B.15}$$

where $y_f = d + z$ is the engineering scaling dimension of f, and $\delta f(b)$ are the momentum-shell corrections due to the interactions between electrons. It is convenient to absorb the engineering scaling dimension by defining $\tilde{f} = b^{-y_f} f(b)$ which leads to

$$\beta(\tilde{f}) = b^{-y_f} \delta f(b) \tag{B.16}$$

Note that the interaction corrections consist of two contributions, $\delta f(b) = \delta f_{\mathrm{pl}}(b) + \delta f_{\mathrm{el}}(b)$ which stem from the renormalization of the plasmon velocity v, the fermion velocity u and the chemical potential μ. Upon integrating the β function, the free energy per volume is obtained as

$$f = \int_0^\infty d(\ln b)\, b^{-y_f} \delta f\big(b^z T, b^{1/\nu}\mu, v(b), u(b)\big) + const \tag{B.17}$$

where we have neglected the regular part of the free energy since this contribution scales to zero in the limit $b \to \infty$.

B.3.1 Free Energy of the Plasmons

The plasmon contribution to the free energy per volume is thus given by

$$f_{\mathrm{pl}} = \int_0^\infty d(\ln b)\, b^{-(d+z)} \delta f_{\mathrm{pl}}\big(b^z T, b^{1/\nu}\mu, v(b), u(b)\big) \tag{B.18}$$

Here, δf_{pl} denotes the leading order corrections which arises from integrating out high-energy excitations during a renormalization group transformation of the bare free energy,

$$\delta f_{\mathrm{pl}}(T, \mu, v, u) \approx \frac{T}{\pi} \ln\left[2\sinh\left(\frac{v\Lambda}{2T}\right)\right]\Lambda \tag{B.19}$$

Thus, the free energy of the plasmons reads

$$f_{\mathrm{pl}} = \int_0^\infty d(\ln b)\, b^{-(d+z)} \frac{T(b)}{\pi} \ln\left[2\sinh\left(\frac{v(b)\Lambda}{2T(b)}\right)\right]\Lambda$$

Upon substituting $b = \Lambda/k$ and $T(b) = b^z T$ we get

$$f_{\mathrm{pl}} = 2T \int_0^\Lambda \frac{dk}{2\pi} \ln\left[2\sinh\left(\frac{v\big(\frac{\Lambda}{k}\big)k}{2T}\right)\right] \tag{B.20}$$

where T is the bare (initial) temperature of the renormalization group flow. Note that the main difference between the interacting and the non-interacting system is the explicit momentum dependence of the plasmon velocity v, cf. Eq. (B.3).

B.3.2 Free Energy of the Ising Fermions

Similarly, the contribution of the Ising fermions to the free energy is given by

$$f_{\mathrm{el}} = \int_0^\infty d(\ln b)\, b^{-(d+z)} \delta f_{\mathrm{el}}\big(b^z T, b^{1/\nu}\mu, v(b), u(b)\big) \tag{B.21}$$

where $\delta f_{\rm el}$ denotes the leading order corrections from the momentum shell which is integrated out in the renormalization group transformation,

$$\delta f_{\rm el}(T,\mu,v,u) \approx -\frac{T}{\pi}\ln\left[2\cosh\left(\frac{\omega_\Lambda}{2T}\right)\right]\Lambda \tag{B.22}$$

Repeating above steps, the free energy per volume of the Ising fermions reads

$$f_{\rm el} = -2T\int_0^\Lambda \frac{dk}{2\pi}\ln\left[2\cosh\left(\frac{1}{2T}\sqrt{\Delta^2\left(\frac{\Lambda}{k}\right)+u^2\left(\frac{\Lambda}{k}\right)k^2}\right)\right] \tag{B.23}$$

Note that in the derivation of Eq. (B.23) we have substituted $\Delta(b) = b^{-1}\mu$ to absorb the engineering scaling dimension of the chemical potential.

B.4 Specific Heat Coefficient in the Interacting System

As for the specific heat coefficients in the non-interacting system, $\gamma_{\rm pl}$ and $\gamma_{\rm el}$ are obtained from the free energy per volume by differentiating twice with respect to temperature. However, the resulting momentum integrals are tedious to work out, as is shown in the following discussion.

B.4.1 Specific Heat Coefficient of the Plasmons

The specific heat coefficient of the plasmon excitations is equal to

$$\gamma_{\rm pl} = \left.\frac{\partial^2 f_{\rm pl}}{\partial T^2}\right|_\mu = \frac{1}{2T^3}\int_0^\Lambda \frac{dk}{2\pi}\frac{v^2\left(\frac{\Lambda}{k}\right)k^2}{\sinh^2\left[\frac{k}{2T}\,v\left(\frac{\Lambda}{k}\right)\right]} \tag{B.24}$$

where Λ is the ultraviolet momentum cutoff introduced in our renormalization group scheme. In the interacting case we have to consider the symmetric case, $|u| = v$, and the asymmetric case, $|u| < v$, separately.

Symmetric Case ($|u| = v$): Here, the renormalization group flow of the plasmon velocity obeys a power-law,

$$v(b) = \begin{cases} vb^{1-z} & \text{for } b < b^* \\ v^* & \text{for } b \geq b^* \end{cases}$$

with $v^* = v(b^*)$ and $z = 1 + (\lambda^2 K)/(4v^2) = const$ being the effective dynamical exponent. Note that b^* is the cutoff scale of the renormalization group flow. Thus, the plasmon specific heat coefficient reads

$$\begin{aligned}\gamma_{\rm pl} &= \frac{1}{2T^3}\int_0^\Lambda \frac{dk}{2\pi}\frac{v^2\left(\frac{\Lambda}{k}\right)k^2}{\sinh^2\left[\frac{k}{2T}\,v\left(\frac{\Lambda}{k}\right)\right]} \\ &= \frac{1}{2T^3}\int_0^{k^*} \frac{dk}{2\pi}\frac{(v^*k)^2}{\sinh^2\left[\frac{v^*k}{2T}\right]} + \frac{1}{2T^3}\int_{k^*}^\Lambda \frac{dk}{2\pi}\frac{v^2\left(\frac{\Lambda}{k}\right)k^2}{\sinh^2\left[\frac{k}{2T}\,v\left(\frac{\Lambda}{k}\right)\right]}\end{aligned}$$

where $k^* = \Lambda/b^*$. In the limit $\Lambda \to \infty$ the first term is negligible as the main contribution to $\gamma_{\rm pl}$ comes from the second term. Thus, $\gamma_{\rm pl}$ can be approximated as

$$\gamma_{\rm pl} \approx \frac{1}{2T^3}\int_0^\infty \frac{dk}{2\pi}\frac{v^2\left(\frac{\Lambda}{k}\right)k^2}{\sinh^2\left[\frac{k}{2T}\,v\left(\frac{\Lambda}{k}\right)\right]} = \frac{1}{2T^3}\int_0^\infty \frac{dk}{2\pi}\frac{\left(v\Lambda^{1-z}k^z\right)^2}{\sinh^2\left[\frac{v}{2T}\,\Lambda^{1-z}k^z\right]}$$

with $\Lambda \to \infty$. This integral can be solved by substituting $x = \frac{v}{2T}\,\Lambda^{1-z}k^z$:

$$\gamma_{\rm pl} \approx \frac{1}{2T^3}\int_0^\infty \frac{dk}{2\pi}\frac{\left(v\Lambda^{1-z}k^z\right)^2}{\sinh^2\left[\frac{v}{2T}\,\Lambda^{1-z}k^z\right]} \approx \frac{2}{\pi v}\left(\frac{\mathcal{V}\Lambda}{T}\right)^{\frac{z-1}{z}}\frac{1}{z}\int_0^\infty dx\,\frac{(2x)^{\frac{z+1}{z}}}{\sinh^2(x)}$$

Using Eq. (B.8) this yields the following result for the specific heat coefficient in the quantum critical regime:

$$\gamma_{\rm pl} \approx C_1(z)\frac{2}{\pi v}\left(\frac{\mathcal{V}\Lambda}{T}\right)^{\frac{z-1}{z}} \quad \text{with} \quad C_1(z) = \frac{z+1}{z^2}\,\Gamma\left(\frac{z+1}{z}\right)\zeta\left(\frac{z+1}{z}\right) \tag{B.25}$$

Here, $\mathcal{V}$ is some velocity scale to obtain the correct physical dimensions. In a similar way, we can calculate the specific heat coefficient in the low-temperature regime. Here we obtain

$$\gamma_{\rm pl} \approx C_1(z)\frac{2}{\pi v}\left(\frac{\mathcal{V}\Lambda}{|\mu|}\right)^{\nu(z-1)} \tag{B.26}$$

where ν is the effective correlation length exponent.

Asymmetric Case ($|u| < v$): Here, the renormalization group flow of v is dominated by a logarithmic dependence,

$$v(b) = \begin{cases} ve^{-(\mathcal{C}\ln b)^{1/5}} & \text{for } b < b^* \\ v^* & \text{for } b \geq b^* \end{cases}$$

with $v^* = v(b^*) = ve^{-(\mathcal{C}\ln b^*)^{1/5}}$, and $\mathcal{C}$ being the invariant of the renormalization group flow. As for the symmetric case, $\gamma_{\rm pl}$ is equal to

$$\begin{aligned}\gamma_{\rm pl} &= \frac{1}{2T^3}\int_0^\Lambda \frac{dk}{2\pi}\frac{v^2\left(\frac{\Lambda}{k}\right)k^2}{\sinh^2\left[\frac{k}{2T}\left(\frac{\Lambda}{k}\right)\right]} \\ &= \frac{1}{2T^3}\int_0^{k^*} \frac{dk}{2\pi}\frac{(v^*k)^2}{\sinh^2\left[\frac{v^*k}{2T}\right]} + \frac{1}{2T^3}\int_{k^*}^\Lambda \frac{dk}{2\pi}\frac{v^2\left(\frac{\Lambda}{k}\right)k^2}{\sinh^2\left[\frac{k}{2T}\left(\frac{\Lambda}{k}\right)\right]}\end{aligned}$$

with $k^* = \Lambda/b^*$. In the limit $\Lambda \to \infty$ the dominant contribution to $\gamma_{\rm pl}$ again comes from the second term. Thus,

$$\gamma_{\rm pl} \approx \frac{1}{2T^3}\int_0^\infty \frac{dk}{2\pi}\frac{v^2\left(\frac{\Lambda}{k}\right)k^2}{\sinh^2\left[\frac{k}{2T}\left(\frac{\Lambda}{k}\right)\right]} = \frac{1}{2T^3}\int_0^\infty \frac{dk}{2\pi}\frac{\left[vke^{-(\mathcal{C}\ln(\Lambda/k))^{1/5}}\right]^2}{\sinh^2\left[\frac{v}{2T}\,ke^{-(\mathcal{C}\ln(\Lambda/k))^{1/5}}\right]}$$

First, let us rewrite the integrand by introducing the expansion parameter $\Xi = (\mathcal{V}\Lambda/T)^{1/z} \gg 1$. Re-exponentiating the terms linear in k we get

$$\begin{aligned}\gamma_{\rm pl} &\approx \frac{2}{T}\int_0^\infty \frac{dk}{2\pi}\frac{\left[e^{z^{-1}\ln\Xi - \ln(\Lambda/k) - (\mathcal{C}\ln(\Lambda/k))^{1/5}}\right]^2}{\sinh^2\left[e^{z^{-1}\ln\Xi - \ln(\Lambda/k) - (\mathcal{C}\ln(\Lambda/k))^{1/5}}\right]} \\ &\approx \frac{2}{\pi v}\int_{-z^{-1}\ln\Xi}^\infty dx\,e^{-x}\,\frac{\left[e^{-x-(\mathcal{C}(x+z^{-1}\ln\Xi))^{1/5}}\right]^2}{\sinh^2\left[e^{-x-(\mathcal{C}(x+z^{-1}\ln\Xi))^{1/5}}\right]}\end{aligned}$$

In the last line we we have substituted $x = \ln(\Lambda/k) - z^{-1}\ln\Xi$. Since $\Xi \gg 1$ we can carry out a Taylor expansion in $x/\Xi \ll 1$. Keeping only leading order terms we get

$$\gamma_{\mathrm{pl}} \approx \frac{2}{\pi v}\int_{-z^{-1}\ln\Xi}^{\infty} dx\, e^{-x}\, \frac{\left[e^{-x-(\mathcal{C}z^{-1}\ln\Xi)^{1/5}}\right]^2}{\sinh^2\left[e^{-x-(\mathcal{C}z^{-1}\ln\Xi)^{1/5}}\right]}$$

Finally, let us revert above substitution by setting $y = e^{-x-(\mathcal{C}z^{-1}\ln\Xi)^{1/5}}$. The remaining integral

$$\gamma_{\mathrm{pl}} \approx \frac{2}{\pi v}\, e^{(\mathcal{C}z^{-1}\ln\Xi)^{1/5}} \int_0^{\infty} dy\, \frac{y^2}{\sinh^2(y)}$$

is then solved easily. We obtain in the quantum critical regime the specific heat coefficient

$$\gamma_{\mathrm{pl}} \approx \frac{\pi}{3v}\, e^{(\mathcal{C}z^{-1}\ln\frac{\mathcal{V}\Lambda}{T})^{1/5}} = \frac{\pi}{3v^*} \tag{B.27}$$

where v^* is the plasmon velocity at the cutoff scale b^* in the quantum critical regime.

A similar calculation is performed in the low-temperature regime. However, in this regime the expansion parameter Ξ has to be defined as $\Xi = (\mathcal{V}\Lambda/|\mu|)^{\nu}$, and a subsequent Taylor expansion shows that in the low-temperature regime the specific heat coefficient is given by

$$\gamma_{\mathrm{pl}} \approx \frac{\pi}{3v}\, e^{(\mathcal{C}\nu\ln\frac{\mathcal{V}\Lambda}{|\mu|})^{1/5}} = \frac{\pi}{3v^*} \tag{B.28}$$

with v^* being the plasmon velocity at the cutoff scale in the low-temperature regime.

B.4.2 Specific Heat Coefficient of the Ising Fermions

The specific heat coefficient of the Ising fermions is in general given by

$$\gamma_{\mathrm{el}} = \left.\frac{\partial^2 f_{\mathrm{el}}}{\partial^2 T}\right|_{\mu} = \frac{1}{2T^3}\int_0^{\Lambda}\frac{dk}{2\pi}\frac{\Delta^2\left(\frac{\Lambda}{k}\right) + u^2\left(\frac{\Lambda}{k}\right)k^2}{\cosh^2\left[\frac{1}{2T}\sqrt{\Delta^2\left(\frac{\Lambda}{k}\right) + u^2\left(\frac{\Lambda}{k}\right)k^2}\right]} \tag{B.29}$$

where $\Delta(b) = b^{-1}\mu$ is a convenient choice to absorb the engineering scaling dimension of the chemical potential, and u is the fermion velocity.

Quantum Critical Regime: $|\mu|T^{-1/(\nu z)} \ll 1$

In the quantum critical regime we can carry out a Taylor expansion in $|\mu|/T \ll 1$, independent from the actual renormalization group flow of the fermion velocity u and the gap function Δ,

$$\gamma_{\mathrm{el}} \approx \frac{1}{2T^3}\int_0^{\Lambda}\frac{dk}{2\pi}\frac{\left[u\left(\frac{\Lambda}{k}\right)k\right]^2}{\cosh^2\left[\frac{1}{2T}u\left(\frac{\Lambda}{k}\right)k\right]}$$

Symmetric Case ($|u| = v$): In the symmetric case, the renormaliation group flow of the fermion velocity follows a power-law behavior:

$$u(b) = \begin{cases} ub^{1-z} & \text{for } b < b^* \\ u^* & \text{for } b \geq b^* \end{cases} \quad \text{and} \quad \Delta(b) = \begin{cases} \mu b^{\frac{3}{2}(1-z)} & \text{for } b < b^* \\ \Delta^* & \text{for } b \geq b^* \end{cases}$$

with $u^* = u(b^*)$ and $z = 1 + (\lambda^2 K)/(4v^2) = const$ the effective dynamical exponent. Note that the renormalization group flow of u stops at the cutoff scale b^*. In the quantum critical regime, γ_{el} is given by

$$\begin{aligned} \gamma_{\text{el}} &\approx \frac{1}{2T^3} \int_0^\Lambda \frac{dk}{2\pi} \frac{u^2\big(\frac{\Lambda}{k}\big)k^2}{\cosh^2\big[\frac{1}{2T}\, u\big(\frac{\Lambda}{k}\big)k\big]} \\ &= \frac{1}{2T^3} \int_0^{k^*} \frac{dk}{2\pi} \frac{(u^*k)^2}{\cosh^2\big[\frac{u^*k}{2T}\big]} + \frac{1}{2T^3} \int_{k^*}^\Lambda \frac{dk}{2\pi} \frac{u^2\big(\frac{\Lambda}{k}\big)k^2}{\cosh^2\big[\frac{1}{2T} u\big(\frac{\Lambda}{k}\big)k\big]} \end{aligned}$$

with $k^* = \Lambda/b^*$. Again, in the limit $\Lambda \to \infty$ the main contribution to γ_{el} comes from the second term. This integral is solved in very much the same way as in Sec. B.4.1. Thus,

$$\gamma_{\text{el}} \approx C_2(z) \frac{1}{\pi |u|} \left(\frac{\mathcal{V}\Lambda}{T}\right)^{\frac{z-1}{z}} \quad \text{with} \quad C_2(z) = 2(1 - 2^{-1/z}) C_1(z) \tag{B.30}$$

Note that $\mathcal{V}$ is some velocity scale which gives the correct physical dimensions.

Asymmetric Case ($|u| < v$): In the asymmetric case, the renormalization group flow of the fermion velocity and the gap function is given by a logarithmic decrease,

$$u(b) = \begin{cases} ue^{-(\mathcal{C}\ln b)^{1/5}} & \text{for } b < b^* \\ u^* & \text{for } b \geq b^* \end{cases} \quad \text{and} \quad \Delta(b) = \begin{cases} \mu e^{-\frac{3}{2}(\mathcal{C}\ln b)^{1/5}} & \text{for } b < b^* \\ \Delta^* & \text{for } b \geq b^* \end{cases}$$

with $u^* = u(b^*)$ and $\Delta^* = \Delta(b^*)$. Similar to the symmetric case the main contribution to the specific heat coefficient arises from the following integral:

$$\gamma_{\text{el}} \approx \frac{1}{2T^3} \int_0^\infty \frac{dk}{2\pi} \frac{\big[uke^{-(\mathcal{C}\ln(\Lambda/k))^{1/5}}\big]^2}{\cosh^2\big[\frac{uk}{2T} e^{-(\mathcal{C}\ln(\Lambda/k))^{1/5}}\big]}$$

Note that we have calculated this type of integral in Sec. B.4.1. Thus,

$$\gamma_{\text{el}} \approx \frac{\pi}{6|u|}\, e^{(\mathcal{C}z^{-1}\ln\frac{\mathcal{V}\Lambda}{T})^{1/5}} = \frac{\pi}{6|u^*|} \tag{B.31}$$

with u^* being the fermion velocity at the cutoff scale of the renormalization group flow.

Low-Temperature Regime: $|\mu| T^{-1/(\nu z)} \gg 1$

In the low-temperature regime we can carry out a Taylor expansion in $T/|\mu| \ll 1$ which yields

$$\gamma_{\text{el}} \approx \frac{1}{2T^3} \int_0^\Lambda \frac{dk}{2\pi} \frac{\big[\Delta\big(\frac{\Lambda}{k}\big)\big]^2}{\cosh^2\big[\frac{1}{2T}\Delta\big(\frac{\Lambda}{k}\big)\big]}$$

Symmetric Case ($|u| = v$): Here, the fermion velocity u and the gap function Δ again obey a power-law behavior under renormalization group transformations,

$$u(b) = \begin{cases} ub^{1-z} & \text{for } b < b^* \\ u^* & \text{for } b \geq b^* \end{cases} \quad \text{and} \quad \Delta(b) = \begin{cases} \mu b^{\frac{3}{2}(1-z)} & \text{for } b < b^* \\ \Delta^* & \text{for } b \geq b^* \end{cases}$$

with $u^* = u(b^*)$ and $\Delta^* = \Delta(b^*)$, and z being the effective dynamical exponent. Due to the cutoff scale b^*, the above integral for γ_{el} splits up into two parts,

$$\begin{aligned} \gamma_{\text{el}} &\approx \frac{1}{2T^3} \int_0^{\Lambda} \frac{dk}{2\pi} \frac{\left[\Delta\left(\frac{\Lambda}{k}\right)\right]^2}{\cosh^2\left[\frac{1}{2T}\Delta\left(\frac{\Lambda}{k}\right)\right]} \\ &= \frac{1}{2T^3} \int_0^{k^*} \frac{dk}{2\pi} \frac{(\Delta^*)^2}{\cosh^2\left[\frac{\Delta^*}{2T}\right]} + \frac{1}{2T^3} \int_{k^*}^{\Lambda} \frac{dk}{2\pi} \frac{\left[\Delta\left(\frac{\Lambda}{k}\right)\right]^2}{\cosh^2\left[\frac{1}{2T}\Delta\left(\frac{\Lambda}{k}\right)\right]} \end{aligned}$$

Here, the main contribution to γ_{el} comes from the second term:

$$\gamma_{\text{el}} \approx \frac{1}{2T^3} \int_0^{\infty} \frac{dk}{2\pi} \frac{\left[|\mu|\Lambda^{\frac{3}{2}(1-z)}k^{-\frac{3}{2}(1-z)}\right]^2}{\cosh^2\left[\frac{|\mu|}{2T}\Lambda^{\frac{3}{2}(1-z)}k^{-\frac{3}{2}(1-z)}\right]}$$

Upon substituting $x = |\mu|\Lambda^{\frac{3}{2}(1-z)}k^{-\frac{3}{2}(1-z)}$ we can easily calculate the remaining integral by using the identity (B.8). As a result,

$$\gamma_{\text{el}} \approx C_2\left(\frac{\nu z - 1}{\nu}\right) \frac{1}{\pi|u|} \left(\frac{\mathcal{V}\Lambda}{|\mu|}\right)^{\frac{\nu}{\nu z-1}} \left(\frac{\mathcal{V}\Lambda}{T}\right)^{\frac{\nu}{\nu z-1}-1} \tag{B.32}$$

where $C_2(z) = 2(1 - 2^{-1/z})C_1(z)$, and $C_1(z) = \frac{z+1}{z^2}\,\Gamma\left(\frac{z+1}{z}\right)\zeta\left(\frac{z+1}{z}\right)$ as been defined above.

Asymmetric Case ($|u| < v$): In the asymmetric case, the renormalization group flow of u and Δ is given by

$$u(b) = \begin{cases} ue^{-(\mathcal{C}\ln b)^{1/5}} & \text{for } b < b^* \\ u^* & \text{for } b \geq b^* \end{cases} \quad \text{and} \quad \Delta(b) = \begin{cases} \mu e^{-\frac{3}{2}(\mathcal{C}\ln b)^{1/5}} & \text{for } b < b^* \\ \Delta^* & \text{for } b \geq b^* \end{cases}$$

with $u^* = u(b^*)$ and $\Delta^* = \Delta(b^*)$. The main contribution to the specific heat coefficient γ_{el} can be obtained by performing a Taylor expansion of γ_{el} in $|\mu|/T \ll 1$. Combining the expansion from Sec. B.2.2 and the results for the low-temperature regimes in the interacting system, we finally get the relation

$$\gamma_{\text{el}} \approx \frac{1}{\sqrt{2\pi}|u^*|} \left(\frac{|\Delta^*|}{T}\right)^{5/2} e^{-|\Delta^*|/T} \tag{B.33}$$

for the specific heat coefficient. Note that u^* and Δ^* are the fermion velocity and the gap at the cutoff scale, respectively.

Deutsche Zusammenfassung

Stark korrelierte Elektronensysteme sind ein bedeutender Schwerpunkt in der modernen Festkörperphysik. Viele Experimente weisen auf die Existenz starker Korrelationen in ein-, zwei- und dreidimensionalen Systemen hin, aber die theoretische Beschreibung vieler der beobachteten Phänomene ist unklar oder diskutabel. Insbesondere werden viele bislang unerklärte Phänomene mit den außergewöhnlichen Eigenschaften von sogenannten Quantenphasenübergängen in Verbindung gebracht. Quantenphasenübergänge finden streng genommen nur am absoluten Temperaturnullpunkt durch Variation eines externen Kontrollparameter wie zum Beispiel des Drucks statt. Trotz dieser Einschränkung beeinflussen quantenkritische Punkte im Phasendiagramm wesentlich die thermodynamischen Eigenschaften des zugrundeliegenden Modells auch bei endlichen Temperaturen. Die Untersuchung dieser Quantenphasenübergänge und ihrer Eigenschaften ist daher Gegenstand aktueller Forschung.

Diese Diplomarbeit beschäftigt sich mit einem solchen Quantenphasenübergang. Als theoretisches Modell wird ein eindimensionaler Quantendraht spinpolarisierter Elektronen betrachtet, in dem die Elektronen zwei Bänder besetzen können. Durch Variation des chemischen Potentials wird der Quantenphasenübergang kontrolliert, bei dem Elektronen das obere Band besetzen. Aufgrund der eindimensionalen Struktur ist es angemessen, das untere Band im Niederenergiesektor durch eine Luttinger-Flüssigkeit zu beschreiben, während das obere Band durch Ising-Fermionen beschrieben werden kann. Kapitel 2 führt zunächst in die theoretische Beschreibung eindimensionaler wechselwirkender Elektronensysteme ein und beschreibt ausführlich die Herleitung und Lösung des Tomonaga-Luttinger Modells, welches die Eigenschaften eindimensionaler Elektronensysteme im Niederenergiesektor beschreibt.

Neben der gewöhnlichen Coulomb-Wechselwirkung zwischen den Elektronen existiert in diesem Modell eines Quantendrahtes darüber hinaus die Möglichkeit, dass Elektronen paarweise vom unteren Band ins obere Band wechseln, und umgekehrt. Es ist gerade dieser Prozess, der interessante Phänomene im betrachteten Modell ermöglicht. Es wird in Kapitel 3 gezeigt, dass im Limes starker Wechselwirkung zwischen den Bändern dieser Elektronen-Paartransfer relevant für die Niederenergiephysik ist.

In Kapitel 4 wird die Renormierungsgruppen-Theorie eingeführt, die auf das vorliegende Modell angewandt wird, um dessen Eigenschaften zu untersuchen. Zunächst werden dabei im Limes schwacher Wechselwirkung perturbativ die Selbstenergien und Vertexkorrekturen bestimmt, mit dem Ergebnis, dass diese Korrekturen von logarithmischer Größenordnung sind. Die anschließende Renormierungsanalyse zeigt, dass die Geschwindigkeiten der Anregungen in beiden Bändern logarithmisch verschwinden, und zwar auf unterschiedliche Weise in Abhängigkeit von den physikalischen Anfangsparametern. Im Fall, dass die Plasmonen schneller sind als die Fermionen finden wir, dass der Fluß in den Bereich schwacher Wechselwirkung zeigt, während im entgegengesetzten Fall der Fluß zu starker Wechselwirkung zwischen den Bändern und gleichzeitig zum Verschwinden der Plasmon-Geschwindigkeit führt. Interessant ist hier insbesondere der Grenzfall, in dem beide Geschwindigkeiten gleich groß sind. Hier finden wir, dass die Wechselwirkung einen effektiven dynamischen Exponenten z und einen effektiven Exponenten ν für die Korrelationslänge definiert, der invariant unter Renormierungsgruppen-Transformationen ist. Dies ist ein mögliches Indiz für die Existenz eines interessanten quantenkritischen Punktes.

Im Vergleich zu klassischen Phasenübergängen, die bei endlicher Temperatur stattfinden, sind Quantenphasenübergänge streng genommen experimentell nicht zugänglich sind. Im sogenannten quantenkritischen Bereich kann man aber erwarten, dass der Quantenphasenübergang auch bei endlichen Temperaturen physikalische Eigenschaften beeinflusst. Daher sind thermodynamische Größen wie beispielsweise die spezifische Wärme ein wichtiges Hilfsmittel, um Quantenphasenübergänge zu charakterisieren. Durch eine Skalenanalyse wird in Kapitel 5 gezeigt, dass der Koeffizient γ der spezifischen Wärme am Quantenphasenübergang in unserem Modell divergiert und dass die Divergenz durch den dynamischen Exponenten z und den Exponenten ν der Korrelationslänge charakterisiert wird. Die Vorhersagen der Skalenanalyse werden schließlich anhand des vorliegenden Modells durch analytische Rechnungen überprüft.

Acknowledgements

First of all, I would like to thank my supervisor *Achim Rosch* for his enlightening discussions on physics and for being a great teacher. I would also like to express my deepest gratitude to *Markus Garst* for his great support and encouragement in my work. I would also like to thank *Julia S. Meyer* for her collaboration on this subject.

My special thanks to my friends *Fabrizio Anfuso* and *Mario Zacharias* for proof-reading this thesis and for suggesting numerous improvements.

I would like to thank all, present and former, members of our research group: *Matthias Vojta*, *Tanja Rindler-Daller*, *Benedikt Binz*, *Ricardo Doretto*, *Rolf Helmes*, *Peter Jung*, *Oliver Rösch*, *Heidrun Weber*, *Andreas Hackl*, *David Rasch*, *Lukas Hollender*, and *Alexander Wollny* for making the group a nice place to work. I would also like to thank all the other members of the Institute of Theoretical Physics for creating a nice and friendly atmosphere.

Finally, I would like to thank my parents and my brother and sister for their endless support and for their patience.

Erklärung

Hiermit versichere ich, die vorliegende Arbeit selbstständig und ohne fremde Hilfe angefertigt zu haben. Verwendete Literatur und andere Unterlagen sind jeweils im Text vermerkt und im Anhang aufgelistet.

Köln, den 20. Juni 2008

Matthias Sitte

Bibliography

[1] O. M. Auslaender *et al.*, Science **308**, 88 (2005).

[2] R. Saito, G. Dresselhaus, and M. S. Dresselhaus, *Physical Properties of Carbon Nanotubes*, Imperial College Press, London (1998).

[3] S. M. Girvin, arXiv:cond-mat/9907002v1

[4] X. G. Wen, Phys. Rev. Lett. **64**, 2206 (1990).

[5] X. G. Wen, Phys. Rev. B **43**, 11025 (1991).

[6] J. S. Meyer, K. A. Matveev, and A. I. Larkin, Phys. Rev. Lett. **98**, 126404 (2007).

[7] L. Landau, Sov. Phys. JETP **3**, 920 (1957).

[8] L. Landau, Sov. Phys. JETP **5**, 101 (1957).

[9] L. Landau, Sov. Phys. JETP **8**, 70 (1958).

[10] D. Pines and P. Nozières, *The Theory of Quantum Liquids: Volume I*, W. A. Benjamin Inc., New York (1966).

[11] J. W. Negele and H. Orland, *Quantum Many-Particle Systems*, Westview Press, Boulder (1988).

[12] G. D. Mahan, *Many-Particle Physics*. Kluwer Academic/Plenum Publishers, New York (2000).

[13] J. M. Luttinger, J. Math. Phys. **4**, 1154 (1963).

[14] S. Tomonaga, Prog. Theor. Phys. **5**, 544 (1950).

[15] D. C. Mattis and E. H. Lieb, J. Math. Phys. **6**, 304 (1963).

[16] F. D. M. Haldane, J. Phys. C **14**, 2585 (1981).

[17] T. Giamarchi, *Quantum Physics in One Dimension*, Oxford University Press Inc., New York (2004).

[18] J. von Delft and H. Schoeller, Ann. Phys. **7**, 225 (1998).

[19] J. Voit, Rep. Prog. Phys. **58**, 977 (1995).

[20] H. Schulz, Phys. Rev. Lett. **71**, 1864 (1993).

[21] G. Piacente *et al.*, Phys. Rev. B **69**, 045324 (2004).

[22] R. Shankar, Rev. Mod. Phys. **66**, 129 (1994).

[23] M. E. Peskin and D. V. Schroeder, *An Introduction to Quantum Field Theory*, Perseus Books Publishing, Reading (1995).

[24] M. Garst, *Aspects of Quantum Phase Transitions: Grüneisen Parameter, Dimensional Crossover and Coupled Impurities*, Shaker Verlag, Aachen (2004).

[25] N. Goldenfeld, *Lectures on Phase Transitions and the Renormalization Group*, Westview Press, Boulder (1992).

[26] S. Sachdev, *Quantum Phase Transitions*, Cambridge University Press, Cambridge (2001).

[27] T. Vojta, Ann. Phys. **9**, 403 (2000).

[28] M. Vojta, Rep. Prog. Phys. **66**, 2069 (2003).

[29] H. von Löhneysen, A. Rosch, M. Vojta, and P. Wölfle, Rev. Mod. Phys. **79**, 1015 (2007).

[30] J. Cardy, *Scaling and Renormalization in Statistical Physics*, Cambridge University Press, Cambridge (1996).

[31] M. E. Fisher, Rev. Mod. Phys. **70**, 653 (1998).